Structural System Identification by Dynamic Observability Technique

DoctoralThesis

Doctoral thesis performed by:
Tian Peng

Directors:
Prof. Dr. José Turmo
Prof. Dr. Joan Ramon Casas

Doctoral program:
Construction Engineering

Barcelona, Spain
April, 2021

UNIVERSITAT POLITÈCNICA DE CATALUNYA
BARCELONATECH
Departamento de Ingeniería Civil y Ambiental

UNIVERSITAT POLITÈCNICA DE CATALUNYA BARCELONATECH

Structural system identification by dynamic observability technique

Tian Peng

PhD program in Construction Engineering

Structural System Identification by Dynamic Observability Technique

Doctoral thesis by:

Tian Peng

Thesis advisor:

José Turmo, Joan Ramon Casas

Department of Civil and Environmental Engineering

Barcelona, April, 2021

Dedication

致 我的父母和妹妹

To my parents and sister

Jun Peng, Fujian Guo, Xiaoxue Peng

“Do not go where the path may lead, go instead where there is no path and leave a trail”

--Ralph Waldo Emerson

Acknowledgments

The author thanks its support to the Spanish Ministry of Economy and Competitiveness for the funding provided through the research projects BIA2013-47290-R and BIA2017-86811-C2-1-R. It is also to be noted that the part of this work was done included an exchange of faculty financed by the Chinese government to Miss. Peng thorough the program (No. 201808390083).

First and foremost, I would like to thank my supervisors, **Prof. Jose Turmo**, **Prof. Joan Ramon Casas, and Prof. Maria Nogal** for their patient guidance, continuous support, and motivation during my Ph.D. study. Their hard-working and rigorous academic attitude towards research is worth learning and is what I always admire. They have spent so much time on inspiring me, discussing with me and cultivating my academic critical thinking, and training me with strict requirements. Their roles are deeply imprinted in my heart as models not only in the field of research but also in daily life. It is my honour to work with them during my Ph.D. stage, and all of my Ph.D. time will be the most memorable life experience.

I spent almost four years at Universitat Politècnica de Catalunya (UPC), Barcelona. I love this university who gives me the chance to study in a foreign country and teaches me how to be a qualified Ph.D. I want to thanks all the professors and members of UPC, especially Dña. Rosa Maria Olea, who is being helpful and supportive all the time, and Prof. Alberto De La Fuente Antequera, who gave me a sincere opinion on my research proposal presentation. And I want to thank Prof. Gonzalo Ramos for the research method proposed and Lei Jun, Irene Josa for their help in my research. And thanks to my colleagues and friends in UPC, Seyyed Behrad Emadi, Milad Komary, Behnam Mobaraki, David Requejo, Olga Ortega, Heng Yang, Fei Song, Junhui Zhang. And also, to my roommates in Barcelona, Boyi Ye, Lang Zhou, thanks for your companionship.

And I stayed at Delft University of Technology, Delft, Netherlands, as an academic exchange student for seven months. Thanks to **Prof. Maria Nogal**'s guidance, both in life and research. During this covid-19 period, I learned how to get along with myself. I want to thanks my friends in TUD, Xinglin Gao, Zengfu Wang, Xinyue Yang, for their warm companionship and selfless help. Thanks to everyone who warms and encourages me in my life.

Thanks to my boyfriend, **Chongfeng Liu**, for our ten years of friendship and sincere love. Thanks for your support, encouragement and accompany for more than ten years.

Last, my profound gratitude goes to my beloved mother, **Fujian Guo**, and my precious father, **Jun Peng**. Your countless contributions and support are always my driving force. Thank you for supporting and understanding my decision to study aboard. No matter where I go in the future and what job I work on, your love will always be with me. And thanks my dear sister **Xiaoxue**

Peng, for being with parents when I'm not at home, taking on family responsibilities and unwavering belief in me. Your love is the most precious treasure in my life.

Abstract

The degradation of structures and their component materials is irreversible due to many factors, such as the change of temperature, humidity, corroding agents, the effect of wind, and accidental collision. Thus, the concern of structure health has increased for the occurrence of some engineering accidents, and structural health monitoring (SHM) has become a powerful tool to help decision making during the structure's life cycle. Structure system identification (SSI) is a key component of SHM, whose aim is to identify the integrity and the state of the structure using non-destructive techniques.

SSI can be classified as static and dynamic depending on the type of excitation. SSI by Observability Method (OM) using static tests was proposed and analyzed to address the observability of the estimated parameters. This mathematical approach has been used in other fields such as hydraulics, electrical, and power networks or transportation. Usually, the structural behavior of engineering structures can be identified according to dynamic characteristics such as mode shapes, natural frequencies, and damping ratios. However, the analysis of SSI by dynamic Observability Method using dynamic information is lacking.

This Ph.D. thesis developed the dynamic Observability Method using masses, modal frequencies, modal deflections based on the static OM to obtain the geometrical and mechanical parameters of the structure. This thesis mainly contains three aspects of work.

Firstly, in Chapter 3, the development, for the first time, of constrained observability techniques (COM) for parametric estimation of structures using dynamic information such as frequencies and mode-shapes was proposed. New algorithms are introduced based on the dynamic eigenvalue equation. Two step by step examples are used to illustrate the functioning of these. Parametric expressions for the observed variables are successfully obtained，which will allow the study of the sensitivity of each of the variables in the problem and the error distribution, which is an advantage with respect to non-parametric SSI techniques. A large structure is used to validate this new application, whose structural properties can be obtained satisfactorily in either the whole or local analysis, and the results show that the required measurement set is smaller than the required for a static analysis. Chapters 4 and 5 are the applications of COM to fill the shortcomings of current research, such as the optimal SHM+SSI strategy and uncertainty quantification.

Secondly, in Chapter 4, the role of the SHM strategy and the SSI analysis based on the Constrained Observability Method (COM), which aims at reducing the estimation error, is discussed. A machine learning decision tool to help building the best-combined strategy of SHM and SSI that can result in the most accurate estimations of the structural properties is proposed, and the combination of COM and decision tree algorithm is used for the first time. The machine

learning algorithm is based on the theory of Decision Trees. Decision trees are firstly presented to investigate the influence of the variables (layout of bridge, span length, measurement set, and weight factor in the objective function of the COM) involved in the SHM+SSI process on the error estimation in a general structure. The verification of the method with a real bridge with different levels of damage shows that the method is robust even for a high damage level, showing the SHM+SSI strategy that yields the most accurate estimation.

Finally, an analysis of uncertainty quantification (UQ) is necessary to assess the effect of uncertainties on the estimated parameters and to provide a way to evaluate these uncertainties. This work is carried out in Chapter 5. There are a large number of UQ approaches in science and engineering. It is identified that the proposed dynamic Constrained Observability Method (COM) can make up for some of the shortcomings of existing methods. After that, the COM is used to analyze a real bridge. A result is compared with a method based on a Bayesian approach demonstrating its applicability and correct performance through the analysis of a reinforced concrete beam. In addition, during the bridge system identification by COM, it is found that the best measurement set will depend whether the epistemic uncertainty (model error) is involved or not. As the epistemic uncertainty can be decreased as the knowledge of the structure´s performance increases it is concluded that the optimum sensor placement will be achieved considering not only the sensors accuracy, but also the location of unknown parameters.

Keywords: structure system identification, dynamic Observability Method, decision trees, uncertainty analysis, sensors

Resumen de la Tesis

La degradación de las estructura y de las propiedades de sus materiales es irreversible debido a muchos factores, como el cambio de temperatura, el efecto del viento, agentes externos y la colisión accidental. Por lo tanto, la preocupación por el estado de conservación de las estructuras ha aumentado debido también a la ocurrencia de algunos accidentes. La monitorización de la salud estructural (SHM) se ha convertido en una herramienta poderosa para ayudar a la toma de decisiones durante el ciclo de vida de la estructura. La identificación del sistema estructural (SSI) es un componente clave de SHM, cuyo objetivo es identificar la integridad y el estado de la estructura utilizando técnicas no destructivas.

SSI puede clasificarse como estático y dinámico según el tipo de excitación. Recientemente, se ha propuesto y analizado SSI mediante el Método de Observabilidad (OM) utilizando medidas experimentales de pruebas estáticas para abordar la observabilidad de los parámetros estimados. Este enfoque matemático se ha utilizado en otros campos como la hidráulica, la electricidad y las redes de energía o transporte. Por lo general, el comportamiento de las estructuras de ingeniería se puede identificar de acuerdo con características dinámicas como formas modales, frecuencias naturales y amortiguamiento. Sin embargo, hasta la fecha, no se han propuesto análisis de SSI por el método de observabilidad utilizando información dinámica.

Esta tesis desarrolla el Método de Observabilidad Dinámico usando masas, frecuencias propias y modos de vibración para identificar los parámetros mecánicos de los elementos de una estructura. A tal fin, se desarrollan tres líneas de trabajo.

En primer lugar, se propone la primera aplicación de técnicas de observabilidad restringida para la estimación paramétrica de estructuras utilizando información dinámica como frecuencias y modos de vibración. Se introducen nuevos algoritmos basados en la ecuación dinámica de valores propios. Se utilizan dos ejemplos paso a paso para ilustrar su l funcionamiento. Se obtienen con éxito expresiones paramétricas para las variables observadas, lo que permite estudiar la sensibilidad de cada una de las variables en el problema y la distribución del error, lo cual es una ventaja respecto a las técnicas SSI no paramétricas. Para la validación de esta nueva aplicación se utiliza una estructura compleja, cuyas propiedades estructurales se pueden obtener satisfactoriamente en el análisis total o local, y los resultados muestran que el conjunto de medidas requerido es menor que en el caso del análisis estático. Los capítulos 4 y 5 son las aplicaciones de COM para subsanar las deficiencias de la investigación actual, como la estrategia óptima de SHM + SSI y la cuantificación de la incertidumbre.

En segundo lugar, se discute el papel que juega la estrategia SHM y el análisis SSI basado en el Método de Observabilidad Restringido (COM), con el objetivo reducir el error de estimación. Se propone una herramienta de decisión de aprendizaje automático para ayudar a construir la mejor estrategia combinada de SHM y SSI que puede resultar en estimaciones más precisas de las

propiedades estructurales. Para ello, se utiliza la combinación de algoritmo COM dinámico y el método de los árboles de decisión por primera vez. Los árboles de decisión se presentan, en primer lugar, como una herramienta útil para investigar la influencia de las variables (tipología estructural del puente, longitud del vano, conjunto de medidas experimentales y pesos en la función objetivo) involucradas en el proceso SHM + SSI con el objetivo de minimizar el error en la identificación de la estructura . La verificación del método con un puente real con diferentes niveles de daño muestra que el método es robusto incluso para un nivel de daño importante , resultando en la estrategia SHM + SSI que arroja la estimación más precisa.

Por último, es necesario un análisis de cuantificación de la incertidumbre (UQ) para evaluar el efecto de las incertidumbres sobre los parámetros estimados y proporcionar una forma de evaluar las incertidumbres en los parámetros identificados. Hay una gran cantidad de enfoques de UQ en ciencia e ingeniería. En primer lugar, se identifica que el Método de Observabilidad Restringido (COM) dinámico propuesto puede compensar algunas de las deficiencias de los métodos existentes. Posteriormente, el COM se utiliza para analizar un puente real. Se compara el resultado con un método existente basado, demostrando su aplicabilidad y correcto desempeño mediante la aplicación a una viga de hormigón armado. Además, se obtiene como resultado que el mejor conjunto de puntos de medición experimental dependerá de la incertidumbre epistémica incorporada en el modelo. Dado que la incertidumbre epistémica se puede eliminar a medida que aumenta el conocimiento de la estructura, la ubicación óptima de los sensores debe lograrse considerando no sólo la precisión de los mismos, sino también los modos de vibración de la estructura.

Palabras clave: identificación de sistemas estructurales, observabilidad dinámica, árboles de decisión, análisis de incertidumbre, , sensores

TABLE OF CONTENTS

LIST OF TABLES

LIST OF FIGURES

Chapter 1: Introduction

1.1. Motivation

With the rapid development of the construction industry in the past few decades, many buildings, bridges, and infrastructure are used in our daily life, which gives us a lot of convenience in transportation, experience, and other aspects. These permanent structures or building facilities are designed for a service life in between 50 to 120 years, depending on the country and the built asset.

However, existing structures are inevitably exposed to the natural environment (wind, earthquake, temperature, or even some extreme climate) and human operation (traffic, impact, daily degradation by use). Thus, the material properties are degraded, such as bending stiffness, axial stiffness, and mass. In this case, the durability of the structures may be affected, leading them into a dangerous condition instead of the initially safe state.

According to US data, there are over 600,000 bridges that ensure network continuity across all 50 states. According to the American Society of Civil Engineers (ASCE), one out of every nine bridges in the United States has a structural flaw (ASCE, 2013, Ghonima, O. et al. 2018). The average lifespan of a structurally deficient bridge is less than 75 years. The average age of structurally defective bridges in the US National Bridge Inventory is 69 for concrete bridges, 67 for steel bridges, 48 for pre-stressed concrete bridges, and 65 for all bridges (Farhey, D et al. 2018). According to the Federal Highway Administration (FHWA, 2018), two billion dollars were spent annually on concrete bridge deck upkeep and capital costs (ASCE, 2013).

Figure 1-1. Some examples of bridge collapse

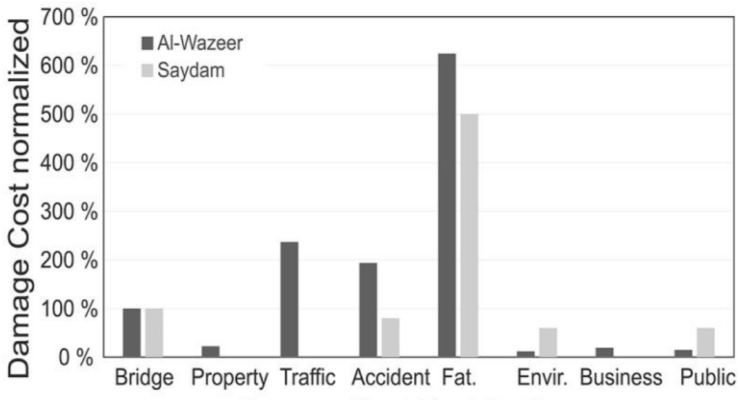

Figure 1-2. Damage cost contribution (Proske, D. 2020)

Some cases of extreme damage in bridges are shown in Figure 1-1, which will make a significant impact on the regional economy or even public safety. Figure 1-2 shows the allocation of various damage costs (relative to the damage of the bridge), such as damage to the bridge itself, to other property, traffic restrictions, additional accidents, damage to life and limb (Fat.), damage to the environment (Envir.), impairment of business activities, and negative effects on the public for bridge collapses and damages based on the work of Saydam, D (2013) and Al-Wazeer, A (2007). The possibility of decreasing the risks associated with structural damage is based on the feasibility of assessing the actual performance. This can be achieved by visual inspection or non-destructive testing. A continuous monitoring is the optimal strategy, as presented by the Structural Health Monitoring (SHM). Thus, structural health monitoring (SHM) and structural system identification (SSI) become powerful tools to help engineer decision making during the life cycle of civil and infrastructure systems in order to decrease the failure risk. In most cases, the actual characteristics of the structures are unknown due to damage and uncertainties in the

construction methods or stress state. Actually, to derive the actual value of the unknown property is the target of SSI.

1.2. Objectives

The global objective of this work is to propose an SSI method based on the constrained observability method, using the measured natural frequencies and mode shapes of the structure as input, and to deal with the error propagation in the identification process taking into account the errors/uncertainties in the measurement input. To serve this purpose, the detailed objectives of this thesis can be presented as follows.

Objective 1: To obtain a method based on the observability method and to deal with the effect of measurement error in the vibration data.

Objective 2： To apply the proposed COM method into several examples and a large frame, which verifies the feasibility of COM.

Objective 3: To propose the combination of COM and CART algorithm to define the best strategy combining SHM and SSI, as well as to investigate the influence of the variables (structural layout of the bridge, span length, measurement set, and weight factor in the objective function).

Objective 4: To enhance a quantitative recognition of how the uncertainty inherent to model parameters and measured variables propagates across dynamic COM and to analyze the obtained uncertainty in the identified parameters.

1.3. Methodology

To achieve the proposed objectives, the following works were organized to be done.

Step 1: Literature review on SSI methods and understanding the state of the static and dynamic SSI.

Step 2: Learning the method of static OM, static COM, static NOM (numerical observability method), static EMOM (error-minizing observability method) and their corresponding codes, deepen the understanding of observability method.

Step 3: Based on results from step 2, developing the dynamic COM, using the measured frequencies and mode shapes as input, and application to several examples to check its feasibility and reliability.

Step 4: Learning the skill of decision tree (DT) techniques and the relative knowledge of Machine Learning and exploring the combination of COM and DT. Application to the bridge Hollandse Brug, building the FEM model, considering different impact factors and model parameters,

Step 5: Application of the uncertainty analysis to the Hollandse Brug.

1.4. Thesis organization

Based on the proposed objectives and the corresponding methodology, this thesis is organized into six chapters. Each chapter is thought to deal with particular topics: state of the art, the development of Dynamic Constrained Observability Method (D-COM), the combination of D-COM and DT, the uncertainty analysis. The summary content of each chapter is as follows.

Chapter 2 is the state of the art. Firstly, the state of structural health monitoring and structure system identification is gathered. Secondly, the static SSI by observability method is summarized, and the main idea of static observability method is illustrated. Lastly, three gaps are detected according to the relate literature review.

Chapters 3 proposes the first application of constrained observability techniques for parametric estimation of structures using dynamic information such as frequencies and mode shapes. After that, the step by step process and the merit of COM are illustrated by an academic example. To verify the feasibility of this method, two examples using experimental data are used as a proof of concept, whose estimated results are compared with other SSI methods. Aftermost a large structure is identified to reveal the potential applicability of the dynamic COM method.

Chapter 4 analyzes the combination of COM with a machine learning decision tool. The aim is to help building the best-combined strategy of SHM and SSI, resulting in the most accurate estimations of the structural properties. In this chapter, the variables (the layout, measurement set, and frequency-related weighting factor) are studied to analyze their effect when applying the

observability method with COM. The verification of this method with a real bridge with different levels of damage shows that the combination is robust even for a high damage degree.

In Chapter 5 the uncertainty analysis to a real bridge is analyzed using the COM method. This part aims at understanding how the uncertainty regarding epistemic and aleatory uncertainties affects the uncertainty of the output variables (how the uncertainty propagates). Through the uncertainty analysis, the robustness of COM can be verified

Finally, in Chapter 6, the conclusions are given based on the above chapter analysis. In addition, the major contributions of this thesis and possible future research works are presented.

1.5. Activities

To develop this work, the following activities have been carried out:

1. Literature review (in the first year).
2. Learn the knowledge of the static OM (in the first year) .
3. Learn the basic principle of dynamic OM (in the first year).
4. Program Matlab code using dynamic OM (in the first and the second years).
5. Update COM to enable SSI achieve fully observability (in the second and the second years).
6. International stay (in the third year).
7. Use COM to work with SHM+SSI strategy (in the third years).
8. Use COM to do the uncertainty quantitative analysis (in the fourth year).
9. Conclusions (in the fourth year).
10. Writing conference and SCI papers (in the third and fourth years).

Chapter 2: State of the art

2.1 Structural system identification

The up-dated knowledge of the integrity of in-service structures through its lifetime is a very important objective for owners, end-users and both, construction and maintenance teams, to whom this information might help in decision making (Castillo, E. et al 2006, Castillo, E. et al 2013, Pimentel, M. et al 2017 & Xiong, H.B. et al 2019), as mentioned in Chapter 1.1. For this reason, SSI has attracted research's massive interest in recent years.

Simplified Finite Element Models (FEMs) are often used to simulate the response of civil structures (Bentz, E.C. et al 2017). When this structural response is modeled through computer simulations, mechanical and geometrical properties of the structural elements, such as the Young's modulus and the cross-section area are assumed to be known. Nevertheless, in most of the cases, the actual characteristics are unknown due to damage and uncertainties in the construction methods or stress state. System identification is the process of developing or improving a mathematical model of a physical system using experimental data to describe the input, output or response, and noise relationship (Juang, J. et al 1994). The range of possible uses of system identification is wide. When performed in order to model a structural system, system identification allows the identification of structural parameters, such as stiffness, mass or stress and strain (Li, S. et al 2013 & Maes, K. et al 2013).

Structural System Identification (SSI) methods can be classified according to the relationship between inputs and outputs used to calibrate the model. On the one hand, non-parametric methods link outputs and inputs creating a mathematical model to characterize the system. Hence, the established relationship has no explicit physical meaning. Examples of non-parametric SSI methods might be found in references (Abdeljaber, O. et al 2017, Stutz, L.T. et al 2015 & Torres Cedillo, S. et al 2016). On the other hand, parametric methods relate inputs to outputs on the basis of an actual physical meaning; due to this physical basis, this type of methods drive to a better understanding of the problem and of the sensitivity to certain parameters. Examples of these methods might be found in references (Spiridonakos, M. et al 2009 & Viola, E. et al 2013).

Besides the non-parametric/parametric classification, SSI might be classified depending on the nature of the excitation test used for the calibration; this is, dynamic and static ones, according to whether or not they engage inertial effects. Examples of different techniques involving static identification can be found in references (Hajela, P. et al 1990, Hjelmstad, K.D. et al 1997). On the other hand, examples of dynamic identification methods can be found in references (Kijewski, T. et al 2003, Huang, C.S. et al 2005, Tarinejad, R. et al 2014 & Zhou, Z. et al 2003). There have also been attempts to combine dynamic and static data in the SSI (Hajela, P. et al 1990, Perera, R. et al 2013 & Sanayei, M. et al 2001).

2.2 Observability method

The observability Method (OM) has recently been implemented as a SSI method in the static scenario (Maes, K. et al 2013). The basis of the observability analysis lies on the problem of identifying if a set of available measurements is sufficient to uniquely estimate the state of a system or of a part of it. The application of this technique has the advantage of providing, for the first time in the literature, symbolic equations of the estimates.

The OM has demonstrated its efficiency in the structural engineering field in a number of structural typologies (such as trusses, columns, frame systems, and cable-stayed bridges) (see e.g. Lozano-Galant, J.A. et al 2014, Nogal, M. et al 2015, Castillo, E. et al 2008, Castillo, E. et al 2015, Lozano-Galant, J.A. et al 2015, Lei, J. et al 2016, Lei, J. et al 2017, Lei, J. et al 2019). Table 2.1 summarizes the various works in the literature that deal with the application of observability techniques to SSI. The following characteristics are described in this table: (1) Test: A kind of test used on-site to track structural reaction. S is for static. (2) Computation: This is a kind of analysis that is used to solve a system of equations. Symbolic: P, or Numerical, N, (3) Numerical optimization tool: If a numerical optimization tool was used to describe the parameter values, and (4) Shear: Whether or not the shear deformations are taken into account in the scheme of equations.

The analysis of Table 2.1 shows that up to now, all studies in the literature are based on the monitored response on static tests. This table also evidences an evolution in the analysis methods. In fact, to enable the application of the OM to real structures the parametric simulation introduced into the first applications has been successively changed to a numerical one. To deal

with the numerical errors in the system of equations, most of the latter studies use the optimization tool named Constrained Observality Method, COM introduced by Lei, J. et al. (2017). A more detailed explanation of this method is presented in Section 2.3.

Table 2-1: Characteristics of the observability methods presented in the literature: P: Symbolic, and N: Numerical.

	Test	**Analysis**	**Optimization**	**Shear**
Lozano-Galant et, J.A. et al (2013)	S	P		
Lozano-Galant et, J.A. et al (2014)	S	P		
Castillo, E. et al (2015)	S	P		
Nogal, M. et al (2015)	S	P		
Castillo, E. et al (2016)	S	N		
Lei, J. et al (2016)	S	N		
Lei, J. et al (2017)	S	P+N	[redacted]	
Tomás, D. et al (2018)	S	P+N		[redacted]
Emadi, E. et al (2019)	S	N	[redacted]	[redacted]
Lei, J. et al (2019)	S	N	[redacted]	

However, there are researchers (Lozano-Galant, J.A. et al 2013) that argue that from a practical point of view, estimation of parameters from static response is less appealing than doing it from modal or dynamic response. This is so because it is much easier to dynamically excite a large structure than statically, especially in large scale structures. Moreover, it is easier to measure accelerations than displacements because of the simplicity of establishing an inertial reference frame for measuring accelerations (Hjelmstad, K. et al 1995). Hence, within the framework of observability, the problem of dynamic identification from vibration modes and frequencies can be also addressed, with a mathematical approach similar to the problem of static identification (Lozano-Galant, J.A. 2013).

As indicated this method is blank to deal with dynamic SSI. To fill this gap, a first paper (Peng, T. et al 2020) was published proposing a new methodology on how to use vibration data in system identification by observability techniques. The method is based on the idea of static COM. A detailed review of this work is presented in Chapter 3.

2.3 Static SSI by COM

It is said that a subset of variables is observable when the system of equations derived from a set of experimental measurements implies a unique solution for this subset, even though the remaining variables remain undetermined. When the system is observable, it might be relevant to identify critical measurements; this is, those measurements that, if unknown, render the state of the system unobservable. Conversely, if the system is unobservable, it is relevant to identify observable islands; this is, those areas of the system whose respective states can be estimated. It is also important to identify the minimum set of additional measurements that renders the whole system observable. Therefore, observability analysis is the previous step to the identification of the system. It addresses the question of stating whether enough measurements to estimate the state of a system are available. The static approach of the SSI by OM is based on the stiffness matrix method. It will be briefly introduced as it may be interesting to the reader for the sake of comparison with the dynamic observability, which is the basis of the present doctoral thesis.

The equations corresponding to this method when static measurements are used, are written in terms of nodal forces and displacements. For a certain structure, the following matrix equation can be written:

$$[K]^{(3N_N \times 3N_N)}\{\delta\}^{(3N_N \times 1)} = \{f\}^{(3N_N \times 1)} \tag{2.1}$$

where $[K]$ stands for the stiffness matrix, $\{\delta\}$ for the vector of displacements and $\{f\}$ for the vector of forces; the sizes of the matrices are indicated by its superscripts, in which N_N denotes the number of nodes. To solve this system of equations, where unknowns appear in K (bending and axial stiffnesses); δ (displacements) and f (reactions); once the boundary conditions and applied forces at nodes are introduced in Eq. (2.1), the terms of K and δ can be rearranged as shown in Eq. (2.2), by extracting the unknown bending or axial sfiffness from $[K]$ to $\{\delta\}$ and removing the measured variables from $\{\delta\}$, in such a way that K^* is a matrix of known coefficients and δ^* is a vector of knowns and unknowns, either bending or axial stiffness, unknown displacements or a product of both.

The subset $\delta_1^*$of δ^* and the subset f_1^* of f^* are known, and the remaining subsets δ_0^* of δ^* and a subset f_0^* of f^* are not.

$$[K^*]\{\delta^*\} = \begin{bmatrix} K_{00}^{*pxr} & K_{01}^{*pxs} \\ K_{10}^{*qxr} & K_{11}^{*qxs} \end{bmatrix} \begin{Bmatrix} \delta_0^{*rx1} \\ \delta_1^{*sx1} \end{Bmatrix} = \begin{Bmatrix} f_0^{*px1} \\ f_1^{*qx1} \end{Bmatrix} = \{f^*\} \tag{2.2}$$

$K_{00}^{*pxr}, K_{01}^{*pxs}, K_{10}^{*qxr}, K_{11}^{*qxs}$,are the partitioned matrices of $[K^*]$ and $\delta_0^{*rx1}, \delta_1^{*sx1}$, f_0^{*px1}, f_1^{*qx1} are the partitioned vectors of $\{\delta^*\}$ and $\{f^*\}$ respectively. The dimensions of each of the elements are given by their superscripts.

In order to apply the OM, it is necessary to join together all the known variables in one side to form a vector $\{D\}$ of known parameters and all the unknowns to the other side, forming a vector $\{z\}$ of unknown parameters; this is done by rearranging the system in an equivalent form, which in this case yields into:

$$[B]\{z\} = \begin{bmatrix} K_{10}^{qxr} & 0 \\ K_{00}^{pxr} & -I^{pxq} \end{bmatrix} \begin{Bmatrix} \delta_0^{rx1} \\ f_0^{px1} \end{Bmatrix} = \begin{Bmatrix} f_1^{qx1} - K_{11}^{qxs}\delta_1^{sx1} \\ -K_{01}^{pxs}\delta_1^{sx1} \end{Bmatrix} = \{D\} \tag{2.3}$$

In (2.3), taking the product of unknowns in z as a new single variable, then $[B]\{z\} = \{D\}$ is a system of linear equations and its general solution can be written in terms of the particular solution z_p, and the homogeneous one, z_{nh}, which will correspond to the case $[B]\{z\} = 0$. Therefore, $z_p + z_{nh}$ will also be a solution of the system of equations. This general solution is given by:

$$\{z\} = \begin{Bmatrix} \delta_{00}^{rx1} \\ f_{00}^{px1} \end{Bmatrix} + [V]\{\tau\} \tag{2.4}$$

where $\begin{Bmatrix} \delta_{00}^{rx1} \\ f_{00}^{px1} \end{Bmatrix}$ is the particular solution of the system and $[V]\{\tau\}$ is the homogeneous one and represents a generic vector in the null space. In this vector, $[V]$ is a basis of the space and $\{\tau\}$ are arbitrary real values that represent the coefficients of all possible linear combinations. For the system of equations to have a unique solution vector, $[V]$ has to either be null or have some null rows. However, even if the system of equations does not have a unique solution, any unknown associated with a null row in the null space $[V]$ is observable. In this case, the general solution equals the particular one and it can be computed by calculating the pseudo inverse of matrix $[B]$. If there are observed parameters, the input is updated by incorporating observed variables and the previous procedure repeated until no new variables are observable. If some variables remain non-observed, the equation of the last recursive step is recorded as the form $B_{om}z_{om} = D_{om}$.

However, it should be noted that in static SSI by OM, the vector $\{z\}$ in Eq. (2.3) might contain two types of unknowns: (a) monomials of degree one, for example, axial and flexural stiffness, horizontal and vertical displacements, and the rotations, $\{EA_j, EI_j, u_{ik}, v_{ik}, w_{ik}\}$, and (b) monomials of degree two, for example,$\{EA_j u_{ik}, EI_j v_{ik}, EI_j w_{ik}\}$ and they are all regarded as simple variables in $\{z\}$. In fact, there is a relation between some monomials of degree one $\{EA_j, EI_j, u_{ik}, v_{ik}, w_{ik}\}$ and monomials of degree two $\{EA_j u_{ik}, EI_j v_{ik}, EI_j w_{ik}\}$, that is, $EA_j u_{ik} = EA_j * u_{ik}$, $EI_j v_{ik} = EI_j * v_{ik}$, $EI_j w_{ik} = EI_j * w_{ik}$. As these constrains cannot be imposed in SSI by OM because it is a linear method, the variables may not be successfully detected in some cases (i.e., it might happen that full observability is not achieved). Constrained Observability Method (COM) (Lei, J. et al 2018) is proposed to overcome the drawback of OM to continue the identification of unknown parameters by defining the residual values:

$$\epsilon = B_{om} z_{om} - D_{om} \tag{2.5}$$

The unknown variables in z_{om} are identified by minimizing the squared sum of the residual.

2.4 Gaps detected and solutions proposed

Based on the previous state of the art, where the problems detected in the parametric SSI and the available observability techniques using static data are emphasized, this thesis elaborates a framework for their solution as presented in the following chapters.

2.4.1 Dynamic OM

1) Gaps: a fully observability by dynamic OM

Sections 2.2 and Table 2.1 show the evolution in static SSI by OM. However, the dynamic data (frequencies and mode-shapes) is easier to obtain compared with the data for the static OM analysis. The dynamic observability method (OM) (Josa, I. 2017) has great limitations for complex structure and might not be able to detect any parameter. Even for a simple structure, a fully observability is hard to achieve by a dynamic OM.

2) Strategies in this thesis: dynamic COM

The dynamic COM (Chapter 3) is proposed to achieve a fully observability, which is evolved based on the static COM (Section 2.3).

The aim of Chapter 3 is to propose a new constrained dynamic SSI methodology; namely, a technique that allows the identification of a subset of characteristics of a structure, such as axial or flexural stiffnesses that might be uniquely defined when a subset of natural frequencies and modal shapes is obtained from an experimental modal analysis. Two examples (Lam, HF. 1998 & Haralampidis, Y. 2010 Simoent, E. et al 2015) are used as a proof of concept of the dynamic COM proposed in Chapter 3. A fully observability can be obtained, as well as the successful application to a complex structure.

2.4.2 SHM+SSI strategy

1) Gaps: Current SHM+SSI strategy

The dynamic COM in Chapter 3 addresses the nonlinearity of the SSI methods by using subsets of natural frequencies and/or modal shapes. Obtaining natural frequencies and mode shapes is limited to the case when no traffic is present on the bridge (Li, H. 2020), and the effect of environmental changes (mainly temperature) in the recorded sensor data can be easily processed and removed by a Principal Component Analysis (PCA) (Nie, Z. 2020) or similar, before the application of the method. The dynamic COM combines the unknown parameters including the theoretical frequencies and mode shapes into an optimization process that minimizes the objective function obtained as the squared sum of the frequencies- and mode shape-related errors.

The selection of the objective function to minimize in the optimization process has a profound impact on the problem output. It does not only affect the interpretation of the best correlation between the unknown parameters but also influences the performance of the selected optimization algorithm. Normally, eigenvalue residual and consideration of the modal assurance criterion MAC related function are used, as well as the residual vector of the deviation from the orthogonality of the experimental mode shapes to the analytical ones (Teughels, A. et al. 2001). Most of the sensitivity-based approaches reported for FE updating of real case studies have considered only the eigenvalue or frequency residual (Brownjohn, J. M. W. et al. 2000 & Zhao, J. et al 2002). Additionally, some papers are concentrated on the multi-objective identification method by dividing the frequencies or eigenvalue residual (Christodoulou, K. & Papadimitriou, C. 2007) and

mode shape-related residual as two parts to estimate the structural parameters (Farhat, C. et al 1993 &Mares, C. et al 2002). On the other hand, some researchers establish weighted multi-objective functions considering frequency residual, mode shape-related residual, and modal flexibility residual together (Jaishi, B. & Ren, W., 2005), the majority of them giving equal weights to each residual (Zarate, B., & Caicedo, J. 2008). The dynamic SSI in this thesis is using the optimization process of dynamic COM, thus defining an objective function of eigenvalue residual and MAC related residual. In order to get a better accuracy, different values of weighting factors affecting the eigenvalue and MAC residual are proposed. However, a clear methodology on the selection of the optimum weight factors to consider is not fully available in the existing literature.

A major goal of conducting SHM and the subsequent SSI is to derive conclusions about the real state of a given structure (Hasni, H. et al 2019 & Park, H. et al 2018). Whereas the SHM focuses on collecting the structural system response, SSI aims at determining the actual mechanical properties of the structure based on the observed response. Both the monitoring strategy and SSI analysis play an essential role in the uncertainty level of the estimated features. However, this combined approach is not common in the literature. For instance, Guo, Y. et al. (2016), Brimacombe, J. et al. (2008) and Han, L. et al (2014) show how the sensors' accuracy, the optimal placement of sensors, and how they are combined highly influence the quality of the estimation. However, these analyses do not consider both the monitoring setting and the characteristics of the method used for SSI as design variables at the same time. Improving one of the sides, i.e., either the conditions of monitoring or the definition of the model used for SSI, does not guarantee the most accurate estimation, which can be obtained if both of them are combined.

2) Strategies in this thesis: an optimal SHM+SSI strategy

An adequate combination of the monitoring strategy and SSI analysis can yield an accurate estimation of the structural parameters. Making the right decisions when designing a strategy that combines both SHM and SSI can result in significant time and cost savings, avoiding estimations that cannot be trusted due to their large uncertainty. With this aim, an optimal SHM+SSI strategy is proposed in Chapter 4. This strategy is the combination of COM and decision tree (DT) analysis, considering several factors that

may influence the final result as the structural layout (boundary conditions), geometrical dimensions (for instance the span length in case of bridges), the measurement set (optimal sensor deployment). Also the weighting factors to be used in the objective function are considered.

The approach is based on decision tree analysis. Decision tree algorithms are one of the most common techniques of inductive learning, especially in the field of Machine Learning (ML) (Chandra, B. & Varghese, P. P, 2008 and Salzberg, S. 1995). The decision tree algorithm can be used for solving regression and classification problems. For its powerful capability to combine numerical with categorical data, its application in the area of civil engineering is gaining relevance (Salazar, F. et al 2007). A fuzzy group decision making (FGDM) approach offered a flexible, practical, and effective way of modeling bridge risks (Wang, Y., & Elhag, T., 2007). A decision support system for bridge maintenance was developed by extensive literature review, interviews with bridge maintenance experts, and a national survey (Yehia, S. et al, 2008). The decision tree algorithm is used to analyze the deterioration of the health index of a set of concrete bridge decks (Melhem, H. G. et al 2003). A decision tree learning algorithm is adopted to train the model of a full-scale long-span suspension bridge using six recent years' database (Li, S. et al 2018). However, the analysis of the decision tree algorithm on the most critical factors to reduce the error of the estimated parameters is still insufficient. Decision trees dealing with the selection of the optimal measurement sets or model parameters do not appear in the literature. In Chapter 4, the new application of decision trees combined with SHM+SSI provides a new insight into the problem of structural identification and damage detection.

Chapter 4 represents an optimal SHM+SSI strategy that helps:

i) To select an adequate combined SHM+SSI strategy that minimizes the uncertainty of the estimations;
ii) To determine to which extent the decisions on the SHM process influence the final error in the estimation;
iii) To assess the contribution of the SSI-COM in this final error.

2.4.3 Uncertainty quantification (UQ)

1) Background of UQ analysis

Most research works focus on the deterministic SSI and probabilistic approach (Raich, A.et al 2011, Eskew, E. et al 2016, & Jang, J. et al 2017), which aims to find the structural parameters of a numerical model that guarantees the best possible fit between the model output and the observed data. Nevertheless, considering the uncertainties related to the structure model and observed data, uncertainty quantification (UQ) is necessary for assessing the effect of uncertainty, as well as the estimated accuracy (Simoen, E. et al 2015).

As described in Section 2.2, the Observability Method (OM) has been used in many fields. However, OM identification needs to be robust in terms of variations of systematic modeling uncertainty introduced when modeling complex systems and measurement uncertainty caused by the quality of test equipment and the accuracy of the sensors (Zhou, S. et al 2017). The uncertainty analysis is necessary to conduct OM efficiently and with required reliability.

UQ analysis seems to be highly probability-independent from optimal sensor placement. In contrast, the sensors need to be installed on the most informative position, that is, the location that provides the least uncertainty in the bridge parameter evaluations (Liu, W. et al. 2008). One of the most known and commonly adopted approaches for optimal sensor placement was developed by Kammer (Kammer, D. 1991). Since then, several variants of this approach have been suggested to resolve the positioning of SSI sensors (Song, J. et al. 2021, Lei, J. et al. 2019, Liu, W et al. 2008 & Meo, M. et al. 2005). However, no research works have noticed that the choice in the best position of the sensors might change when different sources of uncertainty are considered in the uncertainty analysis.

The uncertainty could be divided into two types: epistemic uncertainty and aleatory uncertainty. Epistemic uncertainty refers to the type of uncertainty caused by the lack of knowledge, thus, with more data acquisition, this type of uncertainty can be reduced. On the other hand, the aleatory uncertainty refers to the intrinsic uncertainty that depends on the random nature of the observed property or variable, thus it cannot be removed no

matter the amount of data is used (Der Kiureghian, A. et al 2009) as the noise of measurement sensors always exist.

From the practical point of view, determining the level of uncertainty of the estimated parameters through the dynamic observability method is of interest to determine the accuracy and robustness of the method. Moreover, an informed decision-making process requires not only of a punctual estimation of the variables, but also the level of confidence of the estimation. The knowledge of the uncertainty level of the identified structural parameters will allow a more accurate reliability analysis of the structure. It is also essential to compare the advantages and disadvantages of the dynamic COM with the existing methods regarding the error propagation in order to show the applicability of COM.

2) Gaps: drawback of existing UQ method

The ill-posedness of the inverse SSI problem occurs frequently and is extremely susceptible to errors, or, in more general terminology, to uncertainties. Uncertainty quantification is a tool to explore and improve the robustness of the SSI methods. In general, methods for quantifying uncertainty can be divided into two major categories: probabilistic and non-probabilistic approaches. Probabilistic approaches reflect the traditional approach to modeling uncertainty, set on the firm foundations of probability theory, where uncertainty is modeled by appointing unknown quantities to probability density functions (PDFs); these PDFs are then propagated to probabilistic output descriptions. Non-probabilistic methods use random matrix theory to construct an uncertain output of the prediction model operator (Soize, C. 2000 & Simoen, E. et al., 2015).

Non-probabilistic approaches, such as interval methods (Moens, D.et al 2011, Wang, C. et al. 2017, Garc á, O. et al. 2008), fuzzy theory (Jena, S. et al. 2020) and convex model theory (Cao, L. 2021), and probabilistic methods, such as maximum likelihood estimation method (Sankararaman, S. et al 2011), Bayesian method (Zhang, F. et al 2016 & Cao, J. et al. 2020), stochastic inverse method (Choi, C. et al 2016), non-parametric minimum power method (Chee, C. 2017) and probabilistic neural networks (Cao, M. et al. 2015) have been presented in the existing literature.

In the management of uncertainty, probabilistic Bayesian theory is an attractive framework. It has been widely applied, such as in the identification of material parameters in a cable-stayed bridge (Ni, Y. et al. 2021), plate structures (Huang, T. et al. 2021) and steel tower (Lam, H. et al. 2015). Although the probabilistic method is commonly seen as the most rigorous methodology for dealing with uncertainties effectively and is exceptionally robust to sensors errors (Lei, J. 2019), it is not especially suitable for epistemic uncertainty modeling (Möller, B. et al. 2008, Oberkampf, W. et al. 2002, & Baudrit, C. et al. 2008). The argumentation behind this relates to the definition of the (joint) PDFs explaining the unknown quantities: it is argued that adequate qualitative knowledge for constituting a truthful and representative probabilistic model is hardly available. However, model uncertainty has a major effect on estimating structural reliability (Hu, Z. et al., 2017).

To respond to some obvious disadvantages/limitations of the probabilistic approach related to the construction of PDFs and the modeling of epistemic uncertainty, the last few decades have seen an increase in non-probabilistic techniques for uncertainty modeling. It was developed by Soize (Soize, C. 2000, 2003, 2005 & 2009), based on the principle of maximum entropy. Most non-probabilistic methods are generated based on interval analysis. Interval methods are useful to consider the crisp bounds on the non-deterministic values (Moens, D.et al 2011). The non-probabilistic fuzzy approach, an extension of the interval method, was introduced in 1965 by Zadeh (Zadeh, L.A. 1965), aiming to evaluate the response membership function with different confidence degrees (Hanss M, 2005 & Haag, T. 2012). Ben-Haim developed the convex model method for evaluating the model usability based on the robustness to uncertainties (Ben-Haim, Y. et al. 1998). Interval approaches, however, are not capable of distinguishing dependency between various model responses by themselves, which may make them severely over-conservative with regard to the real complexity in the responses to the model. Most of the non-probabilistic methods are somehow based on a hypercubic approximation of the result of the interval numerical model, and therefore neglect possible dependence between the output parameters (Legault, J. et al. 2012， & Faes, M. et al. 2019).

3) Strategies in this thesis: UQ analysis by COM

A probabilistic UQ approach is proposed in Chapter 5 to analyze the error propagation through the SSI by the dynamic Constrained Observability Method, by considering both the epistemic and aleatory uncertainty. To overcome some of the drawbacks mentioned above (the need for a definition of the (joint) PDFs; the neglect of possible dependence between the output parameters), different modal orders are considered separately, after that, all involved mode orders are put together to estimate the output parameters in an objective function. The method of simultaneous evaluation can appropriately take into account the dependence between various parameters.

Chapter 3 Dynamic constrained observability techniques

3.1 Introduction

According to the state of the art analysis of dynamic OM in Chapter 2.4.1., the previous research of dynamic OM has great limitations for complex structure and might not be able to identify actual structural parameters. Thus a new constrained dynamic SSI methodology which can achieve the fully observability is needed.

The application of the OM to dynamic analysis proposed in this chapter is based on the dynamic equation of motion of a system with no damping and no external applied forces (Josa, I. 2017). The equation can be expressed for a two-dimensional structure with N_N nodes, N_B boundary conditions and R vibration modes as:

$$\mathbf{K}^{[(3N_N-N_B)\times(3N_N-N_B)]}\emptyset_i{}^{[(3N_N-N_B)\times 1]} = \lambda_i \mathbf{M}^{[(3N_N-N_B)\times(3N_N-N_B)]}\emptyset_i{}^{[(3N_N-N_B)\times 1]]} \quad (i = 1,2,3\ldots,R) \qquad (3.1)$$

where **K** and **M** stand for the stiffness matrix and the mass matrix, respectively. Besides, $\emptyset_i$ represents the vector of modal displacements, for a 2D model with beam elements, this vector includes the deformation in the x-direction (u_{ik}), y-direction (v_{ik}) and rotation (w_{ik}) at each node k for each vibration mode i. And λ_i stand for the squared frequency for i^{th} vibration mode.

As done with the static approach (Lei, J. et al 2017 & 2018, Lozano-Galant, J.A. et al 2014), the previous Eq. (3.1) might be written in terms of its known and unknown parameters in modal vector, these being indicated by subscripts 1 and 0, respectively. These operations generate the modified stiffness and mass matrices $\mathbf{K}_i^*$and $\mathbf{M}_i^*$ and the modified modal shapes $\emptyset_{Ki}^*$ and $\emptyset_{Mi}^*$ as shown in Eq. (3.2).

$$\mathbf{K}_i^*\emptyset_{Ki}^* = \begin{bmatrix} K_{i,0}^{*(3N_N-N_B)\times rx} & K_{i,1}^{*(3N_N-N_B)\times sx} \end{bmatrix} \begin{Bmatrix} \emptyset_{Ki,0}^{*rx\times 1} \\ \emptyset_{Ki,1}^{*sx\times 1} \end{Bmatrix} = \begin{bmatrix} M_{i,0}^{*(3N_N-N_B)\times mx} & M_{i,1}^{*(3N_N-N_B)\times nx} \end{bmatrix} \begin{Bmatrix} \emptyset_{Mi,0}^{*mx\times 1} \\ \emptyset_{Mi,1}^{*nx\times 1} \end{Bmatrix} = \mathbf{M}_i^*\emptyset_{Mi}^* \quad (i = 1,2,3\ldots,R) \qquad (3.2)$$

Note that now the squared frequencies are included in the right-hand side of the equation $\mathbf{M}_i^*$ and from this step on product variables might be obtained from coupling the target unknowns with other unknowns. Examples of these product variables are $EA_j u_{ik}$, $EA_j v_{ik}$, $EI_j u_{ik}$, $EI_j v_{ik}$ and $EI_j w_{ik}$ on the left-hand side of the equation, in $\emptyset_{Ki,0}^{*rx\times 1}$, and $\lambda_i m_j u_{ik}$, $\lambda_i m_j v_{ik}$ and $\lambda_i m_j w_{ik}$ on the right-hand side, in $\emptyset_{Mi,0}^{*mx\times 1}$, where j represents the j^{th} element and k represents k^{th} node. $\emptyset_{Mi,0}^{*mx\times 1}$ might content the simple variables u_{ik}, v_{ik}, w_{ik} once the value of $\lambda_i m_j$ is known.

As a consequence of these product variables, nonlinear parameters appear and the system of equations becomes a non-linear one. Due to the fact that the observability technique requires linear equations in order to properly determine the observed parameters, this is solved by treating product variables as single linear variables, which linearizes the system.

The final step is to rearrange all the system in order to have all the unknowns of the system in one column vector. By doing so, it is possible to obtain the system of equations in the form Eq. (3.3)

$$\mathbf{B}_i\mathbf{z}_i = \begin{bmatrix} K_{i,0}^{*(3N_N-N_B)\times rx} & -M_{i,0}^{*(3N_N-N_B)\times mx} \end{bmatrix} \begin{Bmatrix} \emptyset_{Ki,0}^{*rx\times 1} \\ \emptyset_{Mi,0}^{*mx\times 1} \end{Bmatrix} = \left\{ M_{i,1}^{*(3N_N-N_B)\times nx} \emptyset_{Mi,1}^{*nx\times 1} - K_{i,1}^{*(3N_N-N_B)\times sx} \emptyset_{Ki,1}^{*sx\times 1} \right\} = \mathbf{D}_i \quad (i = 1,2,3 \dots, R) \qquad (3.3)$$

When multiple modal frequencies are considered together, the equation will be built by combining information of several models. For example, the first R modal information is given by $\mathbf{Bz} = \mathbf{D}$ shown as follows:

$$\mathbf{Bz} = \begin{bmatrix} B_1 & 0 & 0 & 0 \\ 0 & B_2 & 0 & 0 \\ 0 & 0 & \ddots & 0 \\ 0 & 0 & 0 & B_R \end{bmatrix} \begin{Bmatrix} z_1 \\ z_2 \\ \vdots \\ z_R \end{Bmatrix} = \begin{bmatrix} D_1 & 0 & 0 & 0 \\ 0 & D_2 & 0 & 0 \\ 0 & 0 & \ddots & 0 \\ 0 & 0 & 0 & D_R \end{bmatrix} = \mathbf{D} \qquad (3.4)$$

Expression in which **B** is a matrix of constant coefficients, **D** is a fully known vector and $\mathbf{z}_i$ contains the full set of unknown variables. This system can be solved obtaining the solution of the coupled variables as presented in Eq. (2.4). Thus, the identified coupled variables (e.g., $EI_j w_{ik}$) are referred as observed variables. In other to uncouple the observed variables, e.g.,

$EI_j w_{ik} = EI_j * w_{ik}$, the dynamic COM is here proposed based in a similar way as in the static case. However, in this case, the objective function is defined as:

$$J = W_\lambda \sum_{i=1}^{R} \left(\frac{\Delta\lambda_i}{\widetilde{\lambda_\iota}} \right)^2 + W_\emptyset \sum_{i=1}^{R} (1 - MAC_i)^2 \tag{3.5}$$

$$MAC_i\ (\emptyset_{mi}, \widetilde{\emptyset_{m\iota}}) = \frac{[\emptyset_{mi}^T \widetilde{\emptyset_{m\iota}}]^2}{(\emptyset_{mi}^T \emptyset_{mi})(\widetilde{\emptyset_{m\iota}}^T \widetilde{\emptyset_{m\iota}})} \tag{3.6}$$

The modal assurance criterion (MAC_i) (Simoen, E. et al 2015) is used in Eq. (3.5), which consists of computing the so-called MAC values as a measure for the correspondence between the calculated mode shape $\emptyset_{mi}$, obtained from the inverse analysis using the estimated stiffnesses and areas and the measured shape $\widetilde{\emptyset_{m\iota}}$ as shown in Eq. (3.6). Besides, $\Delta\lambda_i$ are the differences between the measured, $\widetilde{\lambda_\iota}$, and the estimated. W_λ and $W_\emptyset$ represent the weighting factors of frequencies and mode-shapes respectively. In this study, W_λ and $W_\emptyset$ are assumed to be equal (Boris Zárate, A. et al 2008).

The solution is obtained by minimizing Eq. (3.5) with the imposed constraints of the form: $EA_j u_{ik} = EA_j * u_{ik}$, $EI_j v_{ik} = EI_j * v_{ik}$, $EI_j w_{ik} = EI_j * w_{ik}$ present in Eq. (3.4).

The proposed approach addresses the possibility of ill-conditioning by means of two actions. First, the unknowns are normalized by the a-priori best estimate, such as designer parameters (see Section 3.4.1), which can make the condition number of coefficient matrix smaller. Second, the range of some normalized unknowns is given when the optimization process is conducted according to Eq. (3.5) to capture the fact that they have a physical meaning and their values cannot be either negative or extremely high (see Section 3.5), which helps to accelerate optimization and limit value range. These two actions reduce the effect of a potential ill-conditioned equation. If the result does not make sense, then the process will be repeated with a new initial guess.

The functioning of COM will be explained step by step in the next section with a simple numerical example, which, additionally, fully demonstrates the excellence of COM compared to OM in the dynamic case.

3.2 The dynamic COM method

3.2.1 Algorithm of dynamic COM

The proposed algorithm takes as inputs the topology of the structure, node connectivity and the subset of measured variables, which are the mode shapes (fully or partially known) and natural frequencies obtained from the modal analysis. On the other hand, the outputs obtained from the known data are the subset of observable variables along with their estimations.

The algorithm for the structure system identification by COM is depicted in Figure 3-1 and detailed as follows:

Step 1. Build stiffness and mass matrices of the structure, K and M.

The stiffness matrix **K** and the mass matrix **M** are built based on the 2D analysis using beam elements. Every single mode inverse analysis will use the same **K** and **M** matrix since the structure itself will not change.

Step 2. Modify stiffness and mass matrices K and M in order to have matrices made out of monomial terms.

Those terms in the matrices that are made up of summands are separated and arranged in different columns. Modal displacements vectors $\emptyset_{Ki}$ and $\emptyset_{Mi}$ are transformed accordingly.

Step 3. Generate the list of product variables.

The list of product variables is obtained by moving all the unknown variables from the matrices to its corresponding vectors of modal displacements. After this step, the terms of matrices **K** and **M** are known values.

Step 4. Remove measured variables from vectors and update vectors and matrices.

The columns of matrices associated with measured values are multiplied by their corresponding values. Non-null factors are removed from the vectors of modal displacements and introduced in the matrices. As a consequence of this, duplicated unknowns might appear in the rows of the vectors.

Step 5. Eliminate duplicated variables.

The duplicated unknowns in the vectors are identified and combined together in the same row and the matrices are modified accordingly. At the end of this step the matrices are made out of coefficients $\mathbf{K}_i^*$ and $\mathbf{M}_i^*$ and the vectors are made out of unrepeated unknowns $\emptyset_{Ki}^*$ and $\emptyset_{Mi}^*$.

Step 6. Build Bz = D equation.

Matrix $\mathbf{B}_i$ is assembled using matrices $\mathbf{K}_i^*$ and $\mathbf{M}_i^*$ and vector $\boldsymbol{z}_i$ is formed by joining all the unknown information of the system as presented in Equation (3.3). Matrix $\mathbf{B}_i$ and vector $\mathbf{D}_i$ are built up by the completely known terms. The overall equation is established by combining several single modal information, like Eq. (3.4). If there are repeated product variables in $\boldsymbol{z}$, they are identified and grouped together by summing up the corresponding columns of **B**.

Step 7. Obtain null space of matrix B.

In order to obtain the set of observable variables the null space $[V]$ of matrix **B** is obtained, which can be done by using internal functions of programming codes such as the backslash in Matlab.

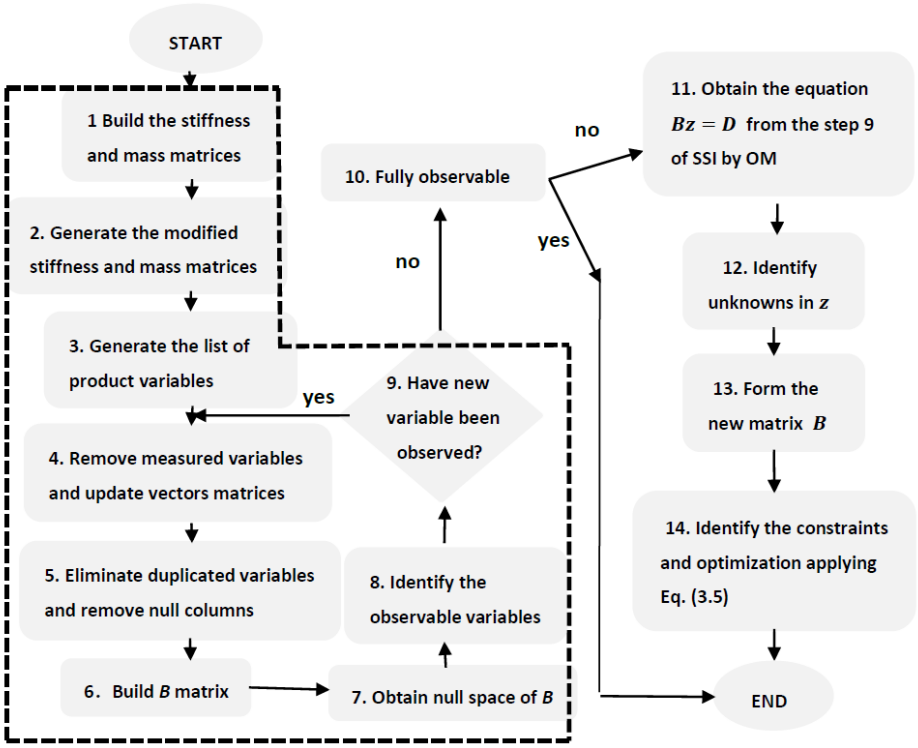

Figure 3-1. The flow-chart of COM

Step 8. Identify observable variables.

The observable variables are identified by examining the null rows of the null space $[V]$ of matrix **B**. The associated product variables with these rows are the observable ones.

Step 9. Recursive processes.

For the measured variables available, it is possible that no all the parameters can be observed. In these cases, the output of the problem can be incorporated to the original input, so that the range of final observed parameters for a given data set is increased. Therefore, if new parameters are observed in the previous step, the process is repeated from step 3 onwards again.

Step 10. Check whether the full observability is achieved or not.

If full observability is achieved at the end of step 9, there is no need to perform following steps. Otherwise, go to step 11 by using the constrained condition.

Step 11. Updated B$\boldsymbol{z} = \mathbf{D}$.

Extract the updated system of equations $\mathbf{B}_{om}\mathbf{z}_{om} = \mathbf{D}_{om}$ from step 9, obtain the unknown variables $\boldsymbol{z}$.

Step 12. Identify whether there are hidden unknowns in $\boldsymbol{z}$ or not.

Divide $\mathbf{z}_{om}$ into two sets: (a) single variables z_s, for example, EA_j, EI_j, u_{ik}, v_{ik}, w_{ik}, and (b) coupled variables z_c, for example, $EA_j u_{ik}$, $EI_j v_{ik}, EI_j w_{ik}$. Split the coupled variables of z_c into single ones, and those which are not in z_s yet (let the subset of new identified singles variable be z_n) have to be added to $\mathbf{z}_{om}$, obtaining $\mathbf{z}^* = \{\mathbf{z}_{om}, z_n\}^T$. For instance, under a specific given set obtained $\mathbf{z}_{om} = \{EI_1 w_{11}, EI_1 w_{12}, EI_1 w_{13}\}$, then $\mathbf{z}^* = \{EI_1 w_{11}, EI_1 w_{12}\ EI_1 w_{13}, EI_1,$ $w_{11}, w_{12}, w_{13}\}$.

Step 13. Form the new matrix $\mathbf{B}^*$

In order to link vector $\mathbf{z}^*$ with $\mathbf{D}_{om}$, a new matrix $\mathbf{B}^*$ is required. Matrix $\mathbf{B}_{om}$ should be transformed into $\mathbf{B}^*$ adding the null matrix, which can be shown in Eq. (3.7).

$$\mathbf{B}^*\,\mathbf{z}^* = [\mathbf{B}^* \quad \Omega]\begin{Bmatrix}\mathbf{z}_{om}\\ z_n\end{Bmatrix} = \mathbf{D}_{om} \tag{3.7}$$

Step 14. Identify the constraints and optimization.

Establish the nonlinear constraints between z_c , z_s and z_n , then, chooses the initial values of $\mathbf{z}^*$ and set upper and lower bounds for the solution (inertia and area). In this step, the nonlinear constraints are imposed to ensure the equality between the coupled known z_c and the single unknowns z_s and z_n. The optimization function, Eq. (3.5), is used to minimize the square sum of the residual vector of frequencies and MAC with the considered constraints.

The algorithm for the structure system identification by COM is also depicted in Table 3-1.For the sake of illustration, Section 3.3 shows its application to an academic example.

Table 3-1. Algorithm of Constrained Observability Method

Input: Geometric information (*Geom*), boundary conditions (*Bound*), measured partial mode shapes and frequecies ($\emptyset_{mi,1}$, and $\lambda_{i,1}$), known structural parameters ($EI_{j,1}$, $EA_{j,1}$ and $m_{j,1}$) and number of modes to consider (R).

Output: Observable variables $\{EI_{,0}, EA_{,0}\}$

1: $(\mathbf{K}, \emptyset_i)$ ← BuildStiffnessMatrix (*Geom*, *Bound*)

2: $(\mathbf{M}, \lambda_i)$ ← BuildMassMatrix (*Geom*)

3: $(\mathbf{K}_i^*, \mathbf{M}_i^*, \emptyset_{Ki}^*, \emptyset_{Mi}^*)$ ← RearrangeMatrices $(\mathbf{K}, \mathbf{M}, \emptyset_i, \lambda_i)$

4: $([B_i], \{z_i\}, \{D_i\})$ ← ObservabilityEquation ($\mathbf{K}_i^*, \mathbf{M}_i^*, \emptyset_{Ki}^*, \emptyset_{Mi}^*, \lambda_{i,1}, \emptyset_{mi,1}, EI_{j,1}, EA_{j,1}$)

5: ($\mathbf{B}, \mathbf{z}, \mathbf{D}$ ←CombineModalFreq ($\mathbf{B}_i, \mathbf{z}_i, \mathbf{D}_i, R$)

6: $\{Identified\}$ ← 1

7: **While** $\{Identified\}$ is not empty

8: $[V]$ ← ObtainNullSpace ($\mathbf{B}$)

9: $\{Identified\}$ ← IdentifyObservableVariables ($[V]$)

10: **If** $\{Identified\}$ is not empty

11: $\{ValueIdentified\}$ ← GetParticularSolution ($\mathbf{B}, \mathbf{z}, \mathbf{D}$,$\{Identified\}$)

12: ($\mathbf{B}, \mathbf{z}, \mathbf{D}$) ← UpdateEquation ($\mathbf{B}, \mathbf{z}, \mathbf{D}$,$\{Identified\}$, $\{ValueIdentified\}$)

13: $\{Estimated\}$ ← Collect ($\{Identified\}$)

---

14 **end if**

15: **end while** %OM end

16: ($\mathbf{B}_{om}, \mathbf{z}_{om}, \mathbf{D}_{om}$) ← ExtractEquations ($\mathbf{B}, \mathbf{z}, \mathbf{D}$)

17: **If** $\mathbf{z}_{om}$ is not empty

18: $\mathbf{z_n}$ ← GetHiddenUnknowns ($\mathbf{z}_{om}$)

19: ($\mathbf{B}^*, \mathbf{z}^*, \mathbf{D}_{om}$)←DefineEquations ($\mathbf{B}_{om}, \mathbf{z}_{om}, \mathbf{D}_{om}$, $\mathbf{z_n}$)

20: Constraints ← GetNonlinearConstraints ($\mathbf{z}^*$)

21: $\mathbf{z}^*$ ← Optimization ($\mathbf{B}^*, \mathbf{z}^*, \mathbf{D}_{om}$, Constraints)

22: **end** %COM end

23: $\{EI_{,0}, EA_{,0}\}$ ← Findresult ({*Estimated*}, $\mathbf{z}^*$)

Note: Known and unknown are being indicated by subscripts 1 and 0.

3.2.2 An example by dynamic COM

In this part, the academic example presented in Figure 3-2 is analyzed symbolically step by step with the objective of achieving a better understanding of the proposed methodology. The structure is composed of 2 elements and 3 nodes. One single mode of vibration is studied, although the technique can be applied to multiple vibration modes. Therefore, the size of the matrix of coefficients of the system of equations is $(3N_N - N_B) \times (3N_N - N_B)$. The structure has the vertical and horizontal displacements restrained at nodes 1 and 3, that is, $N_B = 4$. In this structure, the consistent mass matrix formulation has been used. Then, for each structural element *j* the mass matrix depends on the total mass of the element m_j and on its length L_j.

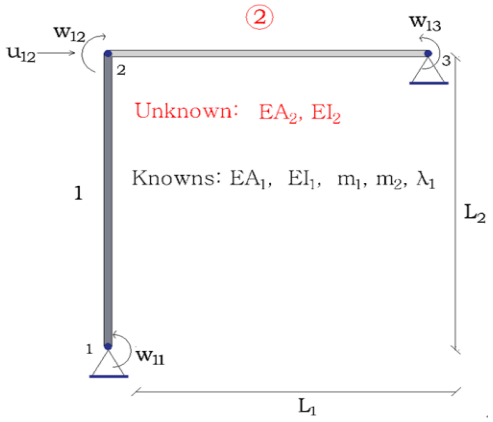

Figure 3-2. Frame studied in Example 1 and degrees of freedom with positive value

For the problem in Figure 3-2, the axial and flexural stiffness of elements 1, EA_1, EI_1, the squared value of the first natural frequency, λ_1, the length of the elements, L_1=$L_2 = L$, and their masses per unit length, m_1 and m_2, are assumed to be known. Besides, to show the application, three known parameters are introduced: the first natural frequency and the horizontal displacement and rotation at node 2 of the first mode shape (u_{12}, w_{12}). The known and unknowns properties are shown in the Figure 3-2. Thus， the input includes geometric information, boundary conditions, measured partial mode shapes and squared frequency (u_{12}, w_{12} and λ_1), known structural parameters (EA_1, EI_1 and m_1, m_2) and number of modes to consider ($R = 1$). The goal output of this analysis is EA_2 and EI_2.

If the example was experimentally analysed, the modal frequency and the components of the vibration mode would be obtained by performing a modal analysis of measured vibrations of the real structure. In order to identify the observable variables (namely, set of variables that can be estimated on the basis of the mentioned measured data) the following steps are considered according to Table 3-1.

Step 1. First, the characteristic equation of the system is written by building the stiffness **K** matrix of the structure, its mass matrix **M** and the modal displacements vector (line 1 and line 2 in Table 3-1). This is shown in Figure 3-3.

Steps 2 and 3. To generate the modified stiffness and mass matrices, those parameters made up of several summands are separated and all the possible unknown parameters are moved to the column vectors as shown in Figure 3-4 (line 3 in Table 3-1). With this, new variables appear as a result of having stiffnesses (EA_j, EI_j) coupled with modal displacements (u_{1k}, v_{1k}, w_{1k}).

Step 4 and 5. The stiffness and mass matrices are updated by introducing the known variables (line 4 in Table 3-1). This is done by multiplying the columns associated with known variables by its corresponding values and by removing the associated factors from the vectors. Note that a new column vector appears after carrying out this step; this is a vector of independent terms, which is built by all those terms that become fully known after introducing measured variables. Since there are terms in the modified vectors of modal displacements that appear more than once, these are joined by adding together their corresponding columns resulting in $\mathbf{K}_1^*$ and $\mathbf{M}_1^*$. Besides, if there are null columns in the matrices, they can be removed together with their corresponding

variable giving us vectors $\emptyset_{K1}^{*}$ and $\emptyset_{M1}^{*}$. The resulting system of equations can be seen in Figure 3-5. Matrix $\mathbf{B}_i$ is assembled using matrices $\mathbf{K}_i^{*}$ and $\mathbf{M}_i^{*}$ and vector $\mathbf{z}_i$ is formed by joining all the unknown information of the system as presented in Eq. (3.3) as shown in Figure 3-6.

$$\begin{bmatrix} \frac{4EI_1}{L_1} & \frac{-6EI_1}{L_1^2} & 0 & \frac{2EI_1}{L_1} & 0 \\ \frac{-6EI_1}{L_1^2} & \frac{12EI_1}{L_1^3}+\frac{EA_2}{L_2} & 0 & \frac{-6EI_1}{L_1^2} & 0 \\ 0 & 0 & \frac{EA_1}{L_1}+\frac{12EI_2}{L_2^3} & \frac{6EI_2}{L_2^2} & \frac{6EI_2}{L_2^2} \\ \frac{2EI_1}{L_1} & \frac{-6EI_1}{L_1^2} & \frac{6EI_2}{L_2^2} & \frac{4EI_1}{L_1}+\frac{4EI_2}{L_2} & \frac{2EI_2}{L_2} \\ 0 & 0 & \frac{6EI_2}{L_2^2} & \frac{2EI_2}{L_2} & \frac{4EI_2}{L_2} \end{bmatrix} \begin{Bmatrix} w_{11} \\ u_{12} \\ v_{12} \\ w_{12} \\ w_{13} \end{Bmatrix} =$$

$$\lambda_1 \begin{bmatrix} \frac{m_1L_1^3}{105} & \frac{13m_1L_1^2}{420} & 0 & \frac{-m_1L_1^3}{140} & 0 \\ \frac{13m_1L_1^2}{420} & \frac{13m_1L_1}{35}+\frac{m_2L_2}{3} & 0 & \frac{-11m_1L_1^2}{210} & 0 \\ 0 & 0 & \frac{m_1L_1}{3}+\frac{13m_2L_2}{35} & \frac{11m_2L_2^2}{210} & \frac{-13m_2L_2^2}{420} \\ \frac{-m_1L_1^3}{140} & \frac{-11m_1L_1^2}{210} & \frac{11m_2L_2^2}{210} & \frac{m_1L_1^3}{105}+\frac{m_2L_2^3}{105} & \frac{-m_2L_2^3}{140} \\ 0 & 0 & \frac{-13m_2L_2^2}{420} & \frac{-m_2L_2^3}{140} & \frac{m_2L_2^3}{105} \end{bmatrix} \begin{Bmatrix} w_{11} \\ u_{12} \\ v_{12} \\ w_{12} \\ w_{13} \end{Bmatrix}$$

Figure 3-3. Example 1. Characteristic equation of the structure in Figure 3-2.

$$\begin{bmatrix} \frac{4}{L_1} & \frac{-6}{L_1^2} & 0 & 0 & 0 & \frac{2}{L_1} & 0 & 0 \\ \frac{-6}{L_1^2} & \frac{-12}{L_1^3} & \frac{1}{L_2} & 0 & 0 & \frac{-6}{L_1^2} & 0 & 0 \\ 0 & 0 & 0 & \frac{1}{L_1} & \frac{12}{L_2^3} & 0 & \frac{6}{L_2^2} & \frac{6}{L_2^2} \\ \frac{2}{L_1} & \frac{-6}{L_1^2} & 0 & 0 & \frac{6}{L_2^2} & \frac{4}{L_1} & \frac{4}{L_2} & \frac{2}{L_2} \\ 0 & 0 & 0 & 0 & \frac{6}{L_2^2} & 0 & \frac{2}{L_2} & \frac{4}{L_2} \end{bmatrix} \begin{Bmatrix} EI_1w_{11} \\ EI_1u_{12} \\ EA_2u_{12} \\ EA_1v_{12} \\ EI_2v_{12} \\ EI_1w_{12} \\ EI_2w_{12} \\ EI_2w_{13} \end{Bmatrix} =$$

$$\lambda_1 \begin{bmatrix} \frac{L_1^3}{105} & \frac{13L_1^2}{420} & 0 & 0 & 0 & \frac{-L_1^3}{140} & 0 & 0 \\ \frac{13L_1^2}{420} & \frac{13L_1}{35} & \frac{L_2}{3} & 0 & 0 & \frac{-11L_1^2}{210} & 0 & 0 \\ 0 & 0 & 0 & \frac{L_1}{3} & \frac{13L_2}{35} & 0 & \frac{11L_2^2}{210} & \frac{-13L_2^2}{420} \\ \frac{-L_1^3}{140} & \frac{-11L_1^2}{210} & 0 & 0 & \frac{11L_2^2}{210} & \frac{L_1^3}{105} & \frac{L_2^3}{105} & \frac{-L_2^3}{140} \\ 0 & 0 & 0 & 0 & \frac{-13L_2^2}{420} & 0 & \frac{-L_2^3}{140} & \frac{L_2^3}{105} \end{bmatrix} \begin{Bmatrix} m_1 w_{11} \\ m_1 u_{12} \\ m_2 u_{12} \\ m_1 v_{12} \\ m_2 v_{12} \\ m_1 w_{12} \\ m_2 w_{12} \\ m_2 w_{13} \end{Bmatrix}$$

Figure 3-4. Example 1. Modified stiffness and mass matrices from Figure 3-3.

$$\mathbf{K}_{i,0}^{*(3N_N-N_B)\times rx} \quad \emptyset_{Ki,0}^{*rx\times 1} \quad \mathbf{K}_{i,1}^{*(3N_N-N_B)\times sx} \emptyset_{Ki,1}^{*sx\times 1}$$

$$\begin{bmatrix} \frac{4EI_1}{L_1} & 0 & 0 & 0 & 0 & 0 \\ \frac{-6EI_1}{L_1^2} & \frac{u_{12}}{L_2} & 0 & 0 & 0 & 0 \\ 0 & 0 & \frac{EA_1}{L_1} & \frac{12}{L_2^3} & \frac{6w_{12}}{L_2^2} & \frac{6}{L_2^2} \\ \frac{2EI_1}{L_1} & 0 & 0 & \frac{6}{L_2^2} & \frac{4w_{12}}{L_2} & \frac{2}{L_2} \\ 0 & 0 & 0 & \frac{6}{L_2^2} & \frac{2w_{12}}{L_2} & \frac{4}{L_2} \end{bmatrix} \begin{Bmatrix} w_{11} \\ EA_2 \\ v_{12} \\ EI_2 v_{12} \\ EI_2 \\ EI_2 w_{13} \end{Bmatrix} + \begin{Bmatrix} \frac{2EI_1 w_{12}}{L_1} + \frac{-6EI_1 u_{12}}{L_1^2} \\ \frac{-6EI_1 w_{12}}{L_1^2} + \frac{12EI_1 u_{12}}{L_1^3} \\ 0 \\ \frac{4EI_1 w_{12}}{L_1} + \frac{-6EI_1 u_{12}}{L_1^2} \\ 0 \end{Bmatrix} =$$

$$\lambda_1 \begin{bmatrix} \frac{m_1 L_1^3}{105} & 0 & 0 \\ \frac{13m_1 L_1^2}{420} & 0 & 0 \\ 0 & \frac{m_1 L_1}{3} + \frac{13m_2 L_2}{35} & \frac{-13m_2 L_2^2}{420} \\ \frac{-m_1 L_1^3}{140} & \frac{11m_2 L_2^2}{210} & \frac{-m_2 L_2^3}{140} \\ 0 & \frac{-13m_2 L_2^2}{420} & +\frac{m_2 L_2^3}{105} \end{bmatrix} \begin{Bmatrix} w_{11} \\ v_{12} \\ w_{13} \end{Bmatrix} + \lambda_1 \begin{Bmatrix} \frac{-m_1 w_{12} L_1^3}{140} + \frac{13m_1 L_1^2 u_{12}}{420} \\ \frac{-11m_1 w_{12} L_1^2}{210} + \frac{13m_1 L_1 u_{12}}{35} + \frac{m_2 L_2 u_{12}}{3} \\ \frac{11m_2 w_{12} L_2^2}{210} \\ \frac{m_1 w_{12} L_1^3}{105} + \frac{m_2 w_{12} L_2^3}{105} + \frac{-11m_1 L_1^2 u_{12}}{210} \\ \frac{-m_2 w_{12} L_2^3}{140} \end{Bmatrix}$$

$$\mathbf{M}_{i,0}^{*(3N_N-N_B)\times mx} \quad \emptyset_{Mi,0}^{*mx\times 1} \quad \mathbf{M}_{i,1}^{*(3N_N-N_B)\times nx} \emptyset_{Mi,1}^{*nx\times 1}$$

Figure 3-5. Example 1. Modified stiffness and mass matrices of the structure in Figure 3-4 after upating them with measured variables and summing up the columns with common terms.

$$\begin{bmatrix} \frac{4EI_1}{L_1}-\frac{\lambda_1 m_1 L_1^3}{105} & 0 & 0 & 0 & 0 & 0 & 0 \\ \frac{-6EI_1}{L_1^2}-\frac{13\lambda_1 m_1 L_1^2}{420} & \frac{u_{12}}{L_2} & 0 & 0 & 0 & 0 & 0 \\ 0 & 0 & \frac{12}{L_2^3} & \frac{EA_1}{L_1}-\frac{\lambda_1 m_1 L_1}{3}-\frac{13\lambda_1 m_2 L_2}{35} & \frac{6w_{12}}{L_2^2} & \frac{6}{L_2^2} & \frac{13\lambda_1 m_2 L_2^2}{420} \\ \frac{2EI_1}{L_1}+\frac{\lambda_1 m_1 L_1^3}{140} & 0 & \frac{6}{L_2^2} & -\frac{11\lambda_1 m_2 L_2^2}{210} & \frac{4w_{12}}{L_2} & \frac{2}{L_2} & \frac{\lambda_1 m_2 L_2^3}{140} \\ 0 & 0 & \frac{6}{L_2^2} & \frac{13\lambda_1 m_2 L_2^2}{420} & \frac{2w_{12}}{L_2} & \frac{4}{L_2} & -\frac{\lambda_1 m_2 L_2^3}{105} \end{bmatrix} \begin{Bmatrix} w_{11} \\ EA_2 \\ EI_2 v_{12} \\ v_{12} \\ EI_2 \\ EI_2 w_{13} \\ w_{13} \end{Bmatrix} =$$

$$\begin{Bmatrix} \frac{13\lambda_1 m_1 L_1^2 u_{12}}{420}+\frac{-m_1 L_1^3 w_{12}}{140}+\frac{6EI_1 u_{12}}{L_1^2}-\frac{2EI_1 w_{12}}{L_1} \\ \frac{13\lambda_1 m_1 L_1 u_{12}}{35}+\frac{\lambda_1 m_2 L_2 u_{12}}{3}+\frac{-11 m_1 L_1^2 w_{12}}{210}-\frac{12EI_1 u_{12}}{L_1^3}+\frac{6EI_1 w_{12}}{L_1^2} \\ \frac{11 m_2 L_2^2 w_{12}}{210} \\ \frac{-11\lambda_1 m_1 L_1^2 u_{12}}{210}+\frac{m_1 L_1^3 w_{12}}{105}+\frac{m_2 L_2^3 w_{12}}{105}+\frac{6EI_1 u_{12}}{L_1^2}-\frac{4EI_1 w_{12}}{L_1} \\ \frac{-m_2 L_2^3 w_{12}}{140} \end{Bmatrix}$$

Figure 3-6. Example 1. System of equations in the form of Eq. (3.4) for structure in Figure 3-2.

Step 6. When multiple modal frequencies are considered together, the equation will be built by combining information of several models $\mathbf{B}_i\mathbf{z}_i = \mathbf{D}_i$ (line 5 in Table 3-1). In this example, $R = 1$, thus $\mathbf{Bz} = \mathbf{D}$ is same as Figure 3-6.

Steps 7 and 8. Afterwards, the null space $[V]$ of matrix **B** is obtained (line 8 in Table 3-1). This allows the identification of the null rows of the null space, which corresponds to the observable parameters.

From the expression of **z**, the EA_2 and w_{11} can be uniquely specified (line 9 in Table 3-1) and observable as the associated rows in $[V]$ are null and their values will not be affected by $\rho_{1.1}$, $\rho_{1.2}$ (line 11 in Table 3-1). Because it is a parametric method, the proposed technique allows the parametric expressions of the variables in this case. However, because of the complexity of these expressions they are not shown here due to space limitations.

Step 9. New variables are obtained in step 8. The unknowns obtained here in previous step, EA_2 and w_{11} are merged into the initial inputs by OM. Therefore, the new set of variables, that is,

$\{\lambda_1, w_{11}, u_{12}, EA_2$ and $w_{12}\}$ are considered as known for the next iteration to renew the $\boldsymbol{Bz} = \boldsymbol{D}$ (line 12 in Table 3-1).

$$\mathbf{z} = \boldsymbol{z}_p + [V]\{\tau\} = \begin{Bmatrix} w_{11} \\ EA_2 \\ EI_2 v_{12} \\ v_{12} \\ EI_2 \\ EI_2 w_{13} \\ w_{13} \end{Bmatrix}_p + \begin{bmatrix} 0 & 0 \\ 0 & 0 \\ -L & -\dfrac{132EA_1L^5\lambda_1 m_2 - 44L^7\lambda_1^2 m_1 m_2 - 27L^7\lambda_1 m_2^2}{504(-60EA_1 + 20L^2\lambda_1 m_1 + 21L^2\lambda_1 m_2)} \\ 0 & \dfrac{2L^3\lambda_1 m_2}{-60EA_1 + 20L^2\lambda_1 m_1 + 21L^2\lambda_1 m_2} \\ -1/w_{12} & -\dfrac{L^4(60EA_1\lambda_1 m_2 - 20L^2\lambda_1^2 m_1 m_2 - 11L^2\lambda_1 m_2^2)}{120w_{12}(60EA_1 - 20L^2\lambda_1 m_1 - 21L^2\lambda_1 m_2)} \\ 1 & 0 \\ 0 & 1 \end{bmatrix} \begin{Bmatrix} \tau_{1.1} \\ \tau_{1.2} \end{Bmatrix}$$

Figure 3-7. Example 1. Solution given by the particular and the homogeneous solution.

$$\mathbf{Bz} = \begin{bmatrix} 0 & 0 & 0 & 0 & 0 \\ 0 & 0 & 0 & 0 & 0 \\ \dfrac{12}{L_2^3} & \dfrac{6w_{12}}{L_2^2} & \dfrac{6}{L_2^2} & \dfrac{EA_1}{L_1} - \dfrac{\lambda_1 m_1 L_1}{3} - \dfrac{13\lambda_1 m_2 L_2}{35} & \dfrac{13\lambda_1 m_2 L_2^2}{420} \\ \dfrac{6}{L_2^2} & \dfrac{4w_{12}}{L_2} & \dfrac{2}{L_2} & -\dfrac{11\lambda_1 m_2 L_2^2}{210} & \dfrac{\lambda_1 m_2 L_2^3}{140} \\ \dfrac{6}{L_2^2} & \dfrac{2w_{12}}{L_2} & \dfrac{4}{L_2} & \dfrac{13\lambda_1 m_2 L_2^2}{420} & -\dfrac{\lambda_1 m_2 L_2^3}{105} \end{bmatrix} \begin{Bmatrix} EI_2 v_{12} \\ EI_2 \\ EI_2 w_{13} \\ v_{12} \\ w_{13} \end{Bmatrix} =$$

$$\begin{Bmatrix} -\dfrac{4EI_1 w_{11}}{L_1} + \dfrac{6EI_1 u_{12}}{L_1^2} + \dfrac{\lambda_1 m_1 w_{11} L_1^3}{105} + \dfrac{13\lambda_1 m_1 u_{12} L_1^2}{420} - \dfrac{2EI_1 w_{12}}{L_1} - \dfrac{\lambda_1 m_1 L_1^3 w_{12}}{140} \\ \dfrac{6EI_1 w_{11}}{L_1^2} + \dfrac{12EI_1 u_{12}}{L_1^3} + \dfrac{13\lambda_1 m_1 w_{11} L_1^2}{420} + \dfrac{13\lambda_1 m_1 u_{12} L_1}{35} + \dfrac{\lambda_1 m_2 u_{12} L_2}{3} - \dfrac{EA_2 u_{12}}{L_2} + \dfrac{6EI_1 w_{12}}{L_1^2} - \dfrac{11\lambda_1 m_1 L_1^2 w_{12}}{210} \\ \dfrac{11\lambda_1 m_2 L_2^2}{210} \\ -\dfrac{2EI_1 w_{11}}{L_1} + \dfrac{6EI_1 u_{12}}{L_1^2} - \dfrac{\lambda_1 m_1 w_{11} L_1^3}{140} - \dfrac{11\lambda_1 m_2 L_2^2 u_{12}}{210} - \dfrac{4EI_1 w_{12}}{L_1} + \dfrac{\lambda_1 m_1 L_1^3 w_{12}}{105} - \dfrac{\lambda_1 m_2 L_2^3 w_{12}}{105} \\ -\dfrac{\lambda_1 m_2 L_2^3 w_{12}}{140} \end{Bmatrix} = \mathbf{D}$$

Figure 3-8. Example 1. System of equations in the form of Eq. (3.4) for structure in Figure 3-2.

EA_2 and w_{11} are collected into the list of estimated item (line 13 in Table 3-1). Given that some variables were identified in the previous iteration, a next iteration starts. The null space, $[V]$ and the general solution of Figure 3-8 (line 8 in Table 3-1), are given as*:*

$$\mathbf{z}_2 = \mathbf{z}_{p2} + [V]_2\{\tau\}_2 = \begin{Bmatrix} EI_2 v_{12} \\ EI_2 \\ EI_2 w_{13} \\ v_{12} \\ w_{13} \end{Bmatrix}_p + \begin{Bmatrix} -L & \frac{L^5\lambda_1 m_2(44L^2\lambda_1 m_1 - 132E_1A_1 + 27L^2\lambda_1 m_2)}{504(20L^2\lambda_1 m_1 - 60E_1A_1 + 21L^2\lambda_1 m_2)} \\ \frac{1}{w_{12}} & \frac{L^2(11L^4\lambda_1^2 m_2^2 + 20m_1L^4\lambda_1^2 m_2 - 60E_1A_1L^3\lambda_1 m_2)}{120w_2(20L^2\lambda_1 m_1 - 60E_1A_1 + 21L^2\lambda_1 m_2)} \\ 1 & 0 \\ 0 & \frac{(2L^3\lambda_1 m_2)}{20L^2\lambda_1 m_1 - 60E_1A_1 + 21L^2\lambda_1 m_2} \\ 0 & 1 \end{Bmatrix} \begin{Bmatrix} \tau_{2.1} \\ \tau_{2.2} \end{Bmatrix}$$

Figure 3-9. Example 1. Solution given by the particular and the homogeneous solution.

Step 10. It is obvious that no new variable is observable as no null row exists in the null space of [V] (line 9 in Table 3-1). Therefore, no new yielded variable can be identified through the OM (line 10 in Table 3-1), thus, the iterative process of line 7 stops (line 14 in Table 3-1).

Steps 11-13. Extract the equation $\mathbf{B}_{om}\mathbf{z}_{om} = \mathbf{D}_{om}$ from OM, Figure 3-8 (line 16 in Table 3-1). Only partial observability is achieved and still 3 unknowns remain, especially the stiffness EI_2. Hence, the full observability is not achieved, triggering the execution of COM (from line 17 in Table 3-1). and check if hidden unknowns exist or not (line 18 in Table 3-1). First split the complex variables $\mathbf{z}_c = \{EI_2 v_{12}, EI_2 w_{13}\}$ into single ones $\{EI_2, v_{12}, w_{13}\}$, which are included in single variables $\mathbf{z}_s = \{EI_2, v_{12}, w_{13}\}$. Thus $\mathbf{z}^* = \{EI_2 v_{12}, EI_2 w_{13}, EI_2, v_{12}, w_{13}\}$, $\mathbf{B}^*\mathbf{z}^* = \mathbf{B}_{om}\mathbf{z}_{om} = \mathbf{D}_{om}$ (line 19 in Table 3-1).

Steps 14. Identify the nonlinear constraints in $\mathbf{z}^*$ (line 20 in Table 3-1). Establish the constraints $EI_2 v_{12} = EI_2 * v_{12}$, $EI_2 w_{13} = EI_2 * w_{13}$.Then an optimization routine, is used to achieve the fully exploitation of the information in measurements with the acquired nonlinear constraints and all the parameters observed (line 21 in Table 3-1). In the optimization process,

the nonlinear constraints are imposed by ensuring the equality between the coupled unknowns and the product of corresponding single unknowns. Thus, all the unknowns are obtained successfully.

As shown, just using OM (step 1 to step 10) to solve the problem, the structural parameter, EI_2, cannot be identified, and the recursive process will end at step 10. Although $\rho_{2.1}$ and $\rho_{2.2}$in Figure 3-9 play the essential role to make the establishment of constraints $EI_2 v_{12} = EI_2 * v_{12}$, $EI_2 w_{13} = EI_2 * w_{13}$ and to make sure the identification of $EI_2 v_{12}$, $EI_2 w_{13}, EI_2, v_{12}, w_{13}$, the value of $\rho_{2.1}$ and $\rho_{2.2}$ cannot be uniquely determined by OM. Hence, the main idea of COM is to introduce the nonlinear constraint relationship between the coupled unknowns and single unknowns of OM. After that, the optimization is performed to achieve fully observability by the objective function in Eq. (3.5).

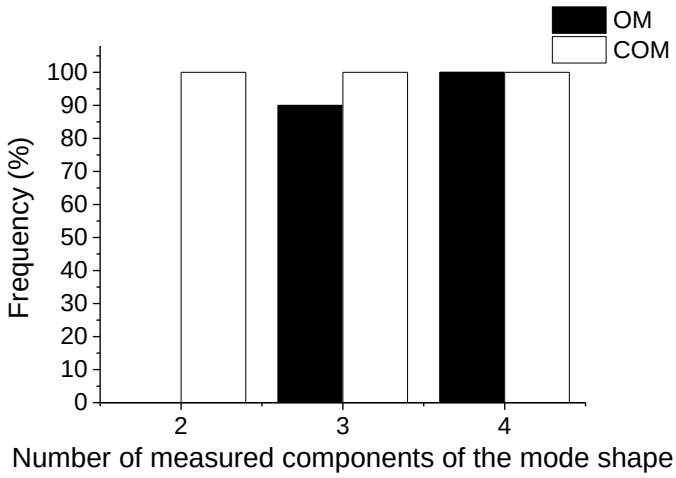

Figure 3-10. Frequency of the occurrence of fully observability by OM and COM in the first mode

Figure 3-10 shows the comparison of fully observability obtained by OM and by COM for this simple structure. It can be seen that COM, as an extended version of OM, enhances the performance of OM. Especially, the frequency of fully observability soars from 0 to 100% when the number of measured components of the first mode shape is equal to 2. The larger the number of measured components, the larger the likelihood of fully observability, nevertheless, the restriction of the feasible number of sensors in real structures should be considered. Because the values of the mode-shapes are normalized by a reference value, considering just one single measure of each vibration mode does not provide meaningful information, therefore single

measures can be ignored. Hence, COM has demonstrated great superiority when compared to OM even in this simple case with numerical and non-experimental values. Therefore, COM should be strongly recommended in the following examples where real experimental data is used.

3.3 The verification of dynamic COM

In the previous chapter the good performance of the dynamic COM was demonstrated in a numerical example. The next step is to check the performance when real experimental data is used.

3.3.1 Two dof by dynamic COM

In this example, taken from reference (Haralampidis, Y et al, 2010), the reliability of the proposed dynamic COM method is checked when experimental data is considered. Whereas a simple academic example was used in the previous section for the sake of illustration, this example allows the comparison of the method with existing results.

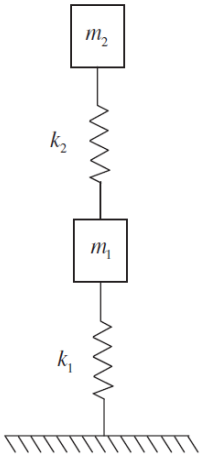

a)

Experimental modal frequencies and mode-shapes of the two-story aluminum building model.

		Mode 1	Mode 2
Modal frequencies (Hz)		17.2	50.4
Modeshapes	1st Floor	0.48	−1.23
	2nd Floor	1.00	1.00

b)

Figure 3-11. a) Two DOF lumped mass model; b) experimental modal frequencies and mode-shapes

The dynamic COM is applied to identify the stiffness properties of two floors. For this, the structure is modeled by a two-DOF linear lumped mass shear building model as schematically shown in Figure 3-11 a). In the modelling, the masses are treated as deterministic, while the model parameters are chosen to be the two interstory stiffness of the two-story building. According to Reference (Haralampidis, Y et al, 2010), the model masses were estimated from

the structural drawings to be m_1=3.9562 kg and m_2 =4.4482 kg. The a priori best estimate of the interstory stiffness calculated from the structural drawings is the same for both stories and equal to $k_0 = 2.3694 \times 10^5$ Nm^{-1}. The following parameterization of the two- DOF model shown in Figure 3-11 is used: $k_i = x_i k_0, i = 1,2$, which can avoid the ill-posed problems since the unknowns x_i were normalized by the a-priori best estimate and it can reduce the morbidity of the matrix. The purpose of the identification is to update the values of the stiffness parameters x_1 and x_2 using the measured modal data reported in Figure 3-11 b).

Through the COM analysis, the results are displayed in the Table 3-2, and compared with the two reference results (Haralampidis, Y et al, 2010). Here, the measured data in Figure 3-11 b) are assumed as true values.

Table 3-2. Observed properties in Figure 3-11

Method	**Fully Observability**	x=[x_1 x_2]	Δf_1(%)	Δf_2(%)	$MAC(\emptyset_i, \overline{\emptyset_j})$
COM	YES	[0.517 0.709]	0.32	-0.42	$\begin{bmatrix} 0.976 & 0.0063 \\ 0.010 & 0.982 \end{bmatrix}$
Reference results 1	YES	[0.546 0.648]	1.384	-3.174	$\begin{bmatrix} 0.983 & 0.011 \\ 0.006 & 0.976 \end{bmatrix}$
Reference results 2	YES	[0.511 0.718]	0.025	-0.057	$\begin{bmatrix} 0.974 & 0.0057 \\ 0.011 & 0.983 \end{bmatrix}$

From Table 3-2, the results of frequencies from COM are between Reference results 1 and 2. The total errors of frequencies and MAC of the results are calculated by the sum of squares of the difference between the obtained and the theoretical values obtaining, $E_{f-com} = 2.75 \times 10^{-5}$, $E_{MAC-com} = 1.039 \times 10^{-3}$ and $E_{f-Re2} = 3.874 \times 10^{-7}$, $E_{MAC-Re2} = 1.12 \times 10^{-3}$. Reference results 2, x =[0.511 0.718], fit very well the frequency properties to values as low as $E_{f-Re2} = 3.874 \times 10^{-7}$ at the expense of deteriorating significantly the fit of modal properties to the values as high $E_{MAC-Re2} = 1.12 \times 10^{-3}$ compared with the COM results. This could suggest that if the tiny sacrifice in the fit of frequencies is not of concern in the identification to preserve the accuracy of modal information, the results of COM x =[0.5167 0.7091] are the most representative of this structure.

3.3.2 Reinforced concrete beam by dynamic COM

The dynamic COM is applied to the damage assessment of a reinforced concrete beam with a length of 6 m and dimensions as shown in Figure 3-12 (Simoen， E et al 2014). The transverse mode shape displacements are observed at 31 point equidistant locations along the beam, and the resulting mode shape measurements are shown with their corresponding natural frequencies in Figure 3-13. Initially, all bending stiffness parameters are assumed to be equal $EI_{\text{int}} = 7.23 \times 10^6\ \text{Nm}^{-2}$. The beam is divided into 10 substructures with a uniform stiffness value or Young's modulus in Figure 3-12 a). The following parameterization of the 10 bending stiffness model shown in Figure 3-12 is used: $EI_i = x_i EI_{\text{int}}, i = 1\sim10$. The purpose of the identification is to update the values of the stiffness parameters $x_1\sim x_{10}$ using the measured modal data reported in Figure 3-13.

The estimated yielded by COM analysis are [1.153 1.031 0.860 0.903 0.799 0.511 0.563 0.717 0.864]. Here, the measured data in Figure 3-13 are assumed as true values, which come from the original data shown in Reference (Simoen, E et al 2014). This result gives the engineer the best approximation, as justified below, and determines the location of damage; the most serious damage is located in substructure 6 and 7. The comparison of frequencies and MAC are shown in Table 3-3 where these are provided with high precision. All the errors between the estimated frequencies and the experimental ones are lower than 5%. This value is the maximum precision that can be expected according to the results presented in Reference (Murat, G et al, 2018) for a reinforced concrete structure. In addition, MAC is very close to 1, that is to say, the estimated mode shapes fit well with the data from Figure 3-13. Regarding the comparison between these estimated stiffnesses and the values from Reference (Murat, G et al, 2018) and from Figure 3-14, it is to highlight that the largest difference between two outcomes is 1.2%.

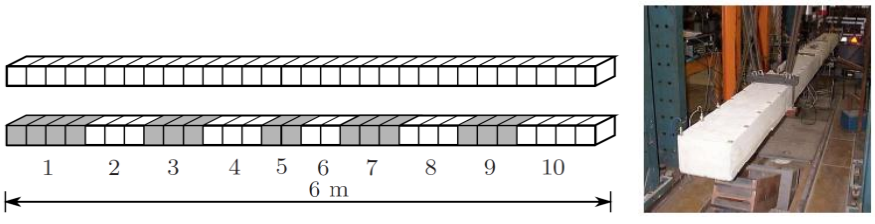

a) b)

Figure 3-12. a) set-up of static loading; b) image of vibration testing (E Simoen. Et al 2014)

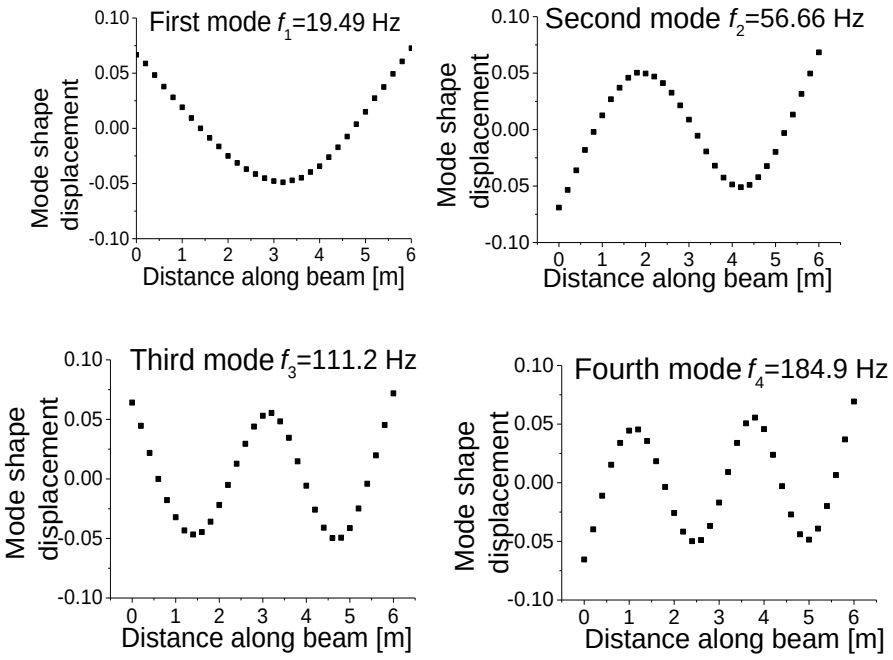

Figure 3-13. The first four experimental bending mode and the corresponding frequencies

Table 3-3. Observed properties in Figure 3-12

Method	Fully Observability	$x=[x_1 \sim x_{10}]$	Mode	Δf(%)	$MAC(\emptyset_i, \bar{\emptyset}_i)$
COM	YES	[1.154 1.029 0.856 0.902 0.797 0.544 0.508 0.560 0.713 0.864]	1	-1.05	0.996
			2	-0.76	0.999
			3	-0.04	0.999
			4	1.68	0.999

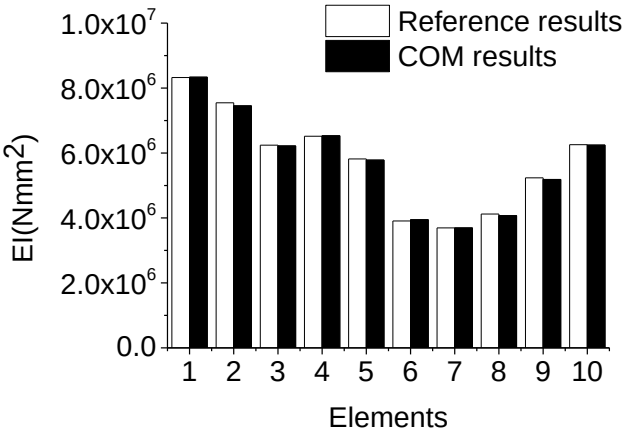

Figure 3-14. Bending stiffness of COM method and Reference results (G. Murat. et al, 2018)

3.4 Potential application

In order to show the possible applications and potential of the proposed methodology to real world structures, a more complex structure is presented in this example. The 13-story building shown in Figure 3-15 is taken under study. This structure was already considered in Reference (Lei, J et al 2018).

This frame is modelled using a total of 226 nodes and 273 elements and it is composed of a set of 8 different sections described in Figure 3-15 and Table 3-4. Therefore, the size of the system of equations is 678×678. In this study, all these 16 mechanical parameters are perturbed by random numbers in order to simulate measurement errors. To illustrate the robustness of the dynamic COM, four sets of the 16 mechanical parameters are synthesized by the product of the intact values and random numbers evenly distributed in the interval [0.8, 1.2], referred as perturbation factors later. The first mode shape of this frame calculated by SAP200 using these four parameter sets and shown in Figure 3-15 c) is used as the input of dynamic SSI by COM.

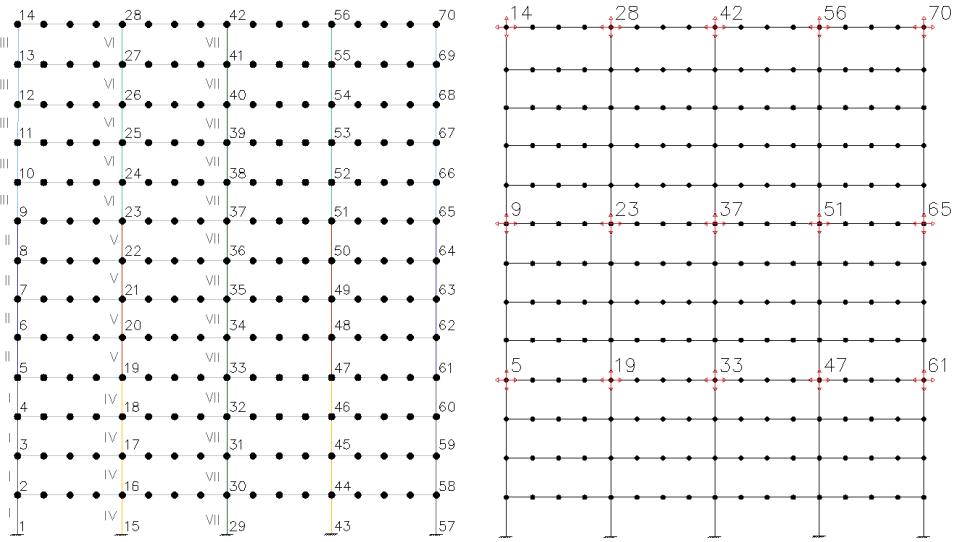

a) b)

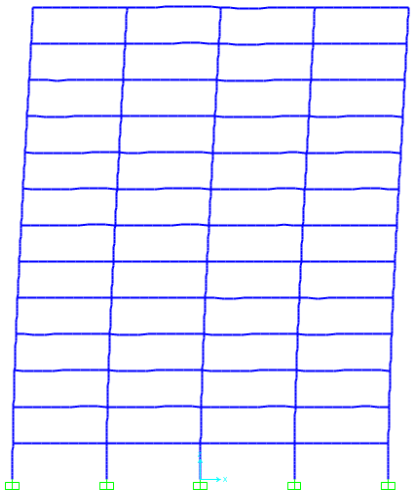

c)

Figure 3-15. Illustration of the 13-floor frame studied in Example 3. a) The members with different characteristics are represented with different colours; b) Sets of measurements used in the global analysis; c) First mode shape.

Performing a global study is of interest whenever it might be necessary to know the state of the whole structure or when the damage location is unknown. One study is carried out in order to check the effectiveness of the method, considering a set of known measurements. These sets of known measurements are measured at nodes 5, 9, 14, 19, 23, 28, 33, 37, 42, 47, 51, 56, 61, 65, 70 consisting on the vertical and horizontal displacements in the first mode at each of the mentioned nodes as seen in Figure 3-15 b) and Figure 3-15 c). The unknown parameters are bending stiffness, EI, of elements I to VIII and the displacements of the nodes that are not measured. The areas of elements are assumed to take the theoretical values. For this purpose, the estimated values of the structural parameters in four different sets affected by random perturbed factors of mechanical parameters are provided in Figure 3-16. The values of flexural stiffness are bounded as they have a physical meaning; their values cannot be neither negative or extremely high. Hence, the range for estimated normalized values should be in the range [0, 1.5]. From the observed ratio between the estimate and the true value, the error is within 8%, which is acceptable. It should be noted that no inertia (bending stiffness) can be identified by OM, while all these parameters are yielded by COM using only the first-mode information.

Table 3-4. Properties of the frame shown in Figure 3-16.

Section	*Elements*	$A(\mathrm{m}^2)$	$I(\mathrm{m}^4)$

Ⅰ: Outer Bottom Columns	1 to 4 and 53 to 56	0.563	0.026
Ⅱ: Outer Intermediate Columns	5 to 8 and 57 to 60	0.360	0.011
Ⅲ: OuterUpper Columns	9 to 13 and 61 to 65	0.250	0.005
Ⅳ: Interior Bottom Columns	14 to 17and 40 to 43	0.360	0.011
Ⅴ: Interior Intermediate Columns	18 to 21and 44 to 47	0.250	0.011
Ⅵ: Interior Upper Columns	22 to 26 and 48 to 52	0.160	0.002
Ⅶ: Central Core	27 to 39	1.800	5.400
Ⅷ: Beams	66 to 273	0.180	0.005

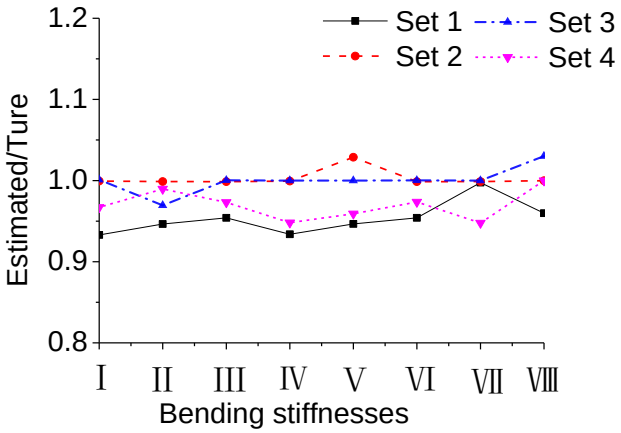

Figure 3-16. Estimated bending stiffnesses in four random perturbation factors sets

3.5 Conclusions

This chapter proposes, for the first time, the application of constrained observability techniques for parametric estimation of structures using dynamic information such as frequencies and mode-shapes.

The nonlinearity of the system obtained when observability is applied, can be properly treated to identify the unknown variables by rearranging the matrix expression and moving the parameters to the modified vectors of mode-shapes and by considering the coupled variables as single variables. After that, the nonlinear constraints between the unknowns are added to tackle the issue of partial observability, as can be seen in Section 3.3.1 and the example in Section 3.3.2. Besides, the merit of the dynamic COM is demonstrated as a good solution to the fully observability which OM cannot achieve. In order to verify the feasibility of this method, two

examples using experimental data are used as a proof of concept. In both examples, the dynamic COM shows acceptable errors of frequencies and MAC, providing similar or sometimes higher accuracy compared to the reference data. The identified frequencies are approved with less than 2 % error with respect to the experimental ones. At the same time, the errors in the MAC values are less than 3% in the first example and 0.5% in the second example. However, a main advantage is obtained by using dynamic COM compared to other SSI methods. This is the possibility to identify if a set of available measurements is sufficient or not to uniquely estimate the state of the structure or a part of it.

To test the performance of the proposed method in real world scenarios, a large structure is used whose real mechanical parameters are perturbed by random numbers in order to simulate measurement errors. It can be seen that the flexural stiffness of all elements can be estimated within acceptable errors. These may allow the application by choosing the most adequate sets of measurements according to the supposed particular condition of the structure.

CHAPTER 4 Combined SHM+SSI strategy by COM

4.1 Introduction

This chapter aims to discuss the role that the SHM strategy and further SSI analysis have in reducing the estimation error, in response to the gap identified in Section 2.4.2. The objective is to define the optimal strategy of parameter estimation by the intelligent combination of SHM plus SSI by dynamic COM. A decision support tool based on machine learning is proposed to help engineers to establish the best SHM+COM strategy yielding the most accurate estimations, and then to determine to which extent the decisions on the SHM process influence the final error in the estimation, and to assess the contribution of the SSI-COM in this final error.

4.2 Methodology

4.2.1 Constrained observability method

The methodology followed to obtain the optimum sensor locations (the SHM that provides the lowest estimation error) and the best choice of the weighting factors in the objective function is the combination of COM and decision tree (DT) analysis.

The dynamic SSI by COM is explained in previous chapter, highlighting the differences with the OM. Dynamic SSI by COM (Peng, T. et al, 2020) is used by imposing constraints on variables when no more parameters can be observed using SSI by OM (Josa, I. 2017).

The new approach from the previous chapter is that the influence of the weighting factor (W_λ, W_δ in Eq. (3.5)) on the accuracy of the identified parameters will be considered, always keeping their relation as illustrated in Eq. (4.1).

$$W_\lambda + W_\delta = 1 \tag{4.1}$$

In the following analysis, the weighting factor for the frequency error part is the value of W_λ, and the corresponding value for mode-shapes is equal to 1-W_λ. The displacements and rotations mentioned in this COM method refer to the mode shape displacements and rotations. This means that displacements and rotations are not directly measured, but obtained from the mode shape.

In order to compare the evaluation effect of all parameters, an error index γ, associated with the final estimation by Eq. (4.2) is proposed. The error index is calculated as the mean squared error of the *n* estimated parameters $\tilde{\theta}$, that is,

$$\gamma = \frac{\sqrt{\sum_{i=1}^{n} \tilde{\theta}_i^2}}{n} \tag{4.2}$$

4.2.2 Decision tree algorithm

The complex interactions between several factors involved in the SSI (structural layout, length, measurement set and weight factor) make the identification of the best SHM+SSI strategy challenging. In order to tackle that problem, decision trees are proposed (Quinlan, J. 1986).

A decision tree learning algorithm is employed in this study to establish a regression model to assess the effect of each input factor on the error-index γ of the estimation. The algorithm starts from a root node, and then many child nodes gradually grow, forming a tree structure. The merits of decision trees are that they are computationally cheap to use, the learned results are easy to understand, the results can be obta ined even if some values are missing, and they can deal with irrelevant features (Harrington, P. et al 2012).

To build a decision tree successfully, the decision about which factor is used to split the data should be made based on an established splitting criterion. To make sure which factors are adequate, every factor needs to be considered and its effect on the splitting results measured. Then, the best factor is chosen. A binary decision tree is proposed in this chapter, thus, at each node, the data is split into two subsets. If the data of the subset on the branches are of the same class, there is no need of continuing to split the data, stopping the branch at this point. Otherwise, the splitting process on this subset should continue. Some stopping criteria can be imposed to stop the splitting process, such as a minimum number of data points belonging to a subset and a maximum depth of the tree.

The process uses the CART (classification and regression tree) algorithm (Bel, L. et al, 2009), which is an effective method of decision tree learning algorithm. The CART algorithm builds

binary trees and can handle discrete as well as continuous split values. Given that the response variable is the error-index γ, regression trees are used, and the splitting criterion is the variance reduction. The variance reduction of a node is defined as the total reduction of the variance of the response variable x due to the split at this node (Breiman, L et al, 1984), which is calculated as follows:

$$VR = \frac{1}{|S|^2}\sum_{i\in S}\sum_{j\in S}\frac{1}{2}\left(x_i - x_j\right)^2 - \left(\frac{1}{|S_t|^2}\sum_{i\in S_t}\sum_{j\in S_t}\frac{1}{2}\left(x_i - x_j\right)^2 + \frac{1}{|S_f|^2}\sum_{i\in S_f}\sum_{j\in S_f}\frac{1}{2}\left(x_i - x_j\right)^2\right) \quad (4.3)$$

where S, S_t and S_f are the set of sample indices before splitting, set of sample indices for which the split test is true, and set of sample indices for which the split test is false, respectively. Note that the concept of variance underlies in each summand of Eq. (4.3).

4.2.3 Method of optimal SHM+SSI

In a general case, the application of the DT in combination with the COM method to plan an optimal SHM+SSI is summarized as follows; (1) the undamaged structure is considered, assuming the design layout and the original mechanical properties. Its dynamic behavior is obtained (direct analysis), that is, the displacement in the *x*- and *y*- direction and rotation at each node for each considered vibration mode and their corresponding frequencies; (2) different measurement sets (i.e., number, type, and location of sensors) are defined along with the accuracy of the devices. The sensors should be located aiming at determining the unknown (target) parameters; (3) measured records given by the SHM are simulated by considering, for each combination of measurement devices, the theoretical (undamaged) values of deformation and rotation distorted by a random error consistent with the corresponding sensor accuracy. In this way, the dynamic behavior of an undamaged structure recorded by inaccurate devices is simulated. The number of simulations related to each measurement set should be large enough to capture the stochastic nature of the process; (4) the observability-based SSI using the COM is conducted (inverse analysis) to obtain the unknown (target) parameters for each simulated

measurement record. Different values of the weighting factor W_λ are used to conduct this analysis; (5) the error-index γ is obtained by comparing the values of the target parameters obtained through the direct and inverse analyses; (6) the decision tree is built using the measurement sets and values of the weighting factors as explanatory variables, and the error-index as the response variable; (7) The information provided by the decision tree will support the decision on the best measurement set and the weighting factors to be used in further system identification processes aimed to identify damage.

For the sake of illustration, Figure 4-1 shows a roadmap of the steps to follow.

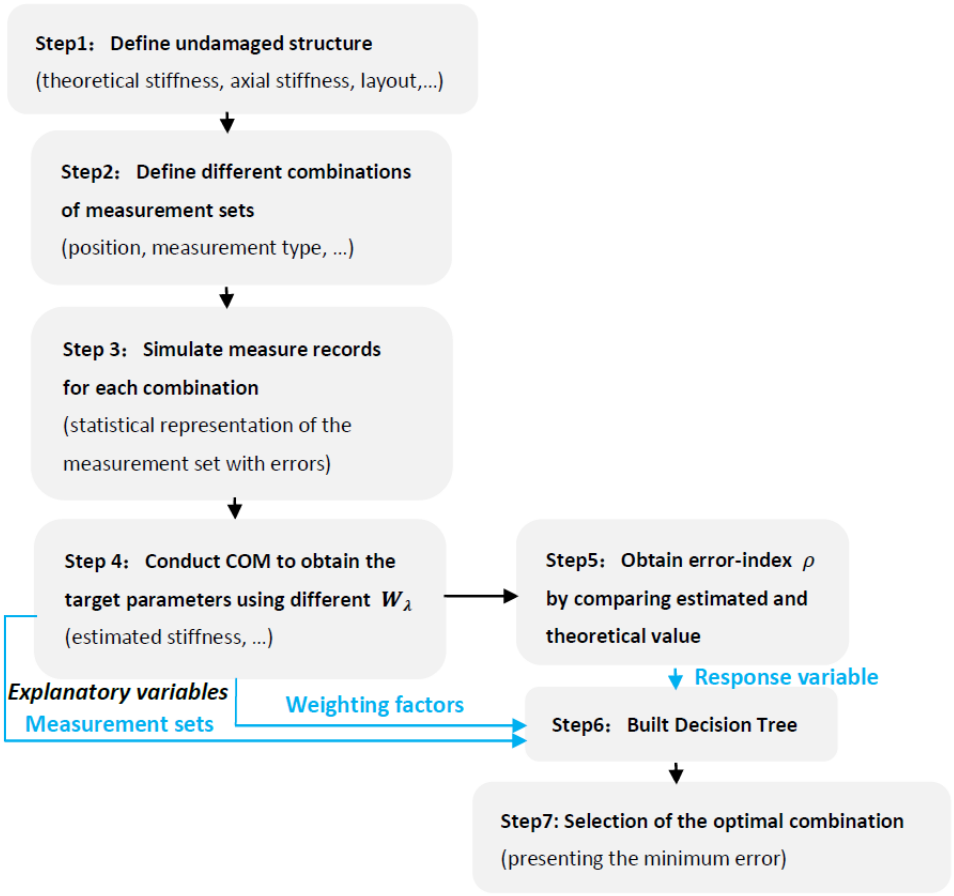

Figure 4-1. Roadmap for the application of SHM+SSI decision tool for a general case

4.3 Example of application: single-span bridge

This section provides a theoretical framework to clarify the method and illustrates the utility of this technique regarding structural behavior by performing an initial descriptive analysis of the most important variables influencing the estimation accuracy of a SHM+SSI strategy.

4.3.1 Bridge configurations

In this part, an academic example with different factors (layout or boundary conditions, span length, measurement sets, and weighting factors) is introduced in detail under the COM framework with the objective of (i) achieving a better understanding of the influence of these factors on the output uncertainty and (ii) showing the need for more sophisticated tools able to capture the joint effect of these factors and (iii) defining the best SHM strategy. Four bridge layouts are assumed according to different boundary conditions: 1|Pinned-pinned, 2|Pinned-clamped, 3|Clamped-pinned, 4|Clamped-clamped, which are shown in Figure 4-2. The FEMs of the four bridge types are defined by 7 nodes and 6 beam elements. Three types of sections are considered：①, ②, ③. The bending stiffness EI_2 and EI_3 indicated in Figure 4-2 are assumed to be unknown. For these layouts, the mass information m_1, m_2, m_3, the length of each element $L/6$, and the bending stiffness of Section 1 EI_1, are assumed as known. Considering that the horizontal displacement of the bridge is small, the influence of the horizontal direction can be ignored. The first two vibration modes are used in this study. The monitored points are studied for three scenarios that differ in the measurement sets considered, as shown in Figure 4-3. These three measurement sets include the vertical and rotational modal displacement at nodes (4, 5, 7), (4-7) and (1-7), respectively. The nodes are given in Figure 4-2. The reason for choosing these three sets is representative (obtain fully observability by OM) for illustrate the theoretical analysis of the proposed method.

A variable span length is also considered, that is, 50m, 55m, 60m, and five cases of weighting factors W_λ, that is, 0.5, 0.6, 0.7, 0.8, 0.9. The collection of all scenarios is illustrated in Table 4-1. The reason for choosing $W_\lambda \geq 0.5$ is that the frequencies are more sensitive to small changes of stiffnesses compared to mode-shape (Simoen. E et al 2015). Besides, for each scenario combining layout, measurement set, span length, and weighting factor, the frequencies, vertical displacement, and rotational modal coordinates are introduced with a given error level. The error

is assumed to follow a uniform distribution between 1~3%, 2%~6% and 10%~30%, respectively. The frequency error range was chosen checking the frequency accuracy of several dynamic tests (Li, Z et al 2016, Hou, R. et al 2019, Chen, J.G. et al 2015) where different analytical methods were used for identification. The vertical displacement error range were chosen from reference (Li, Z et al 2016), who identifies the vertical displacement with accuracies of about 2%- 6%. As accuracy of rotation is lower than the accuracy of vertical displacement (Mares, C. et al, 2002), a range of 10-30% was chosen for that purpose. In experiments or field measurements under free/ambient vibration, modal analysis was originally used for Experimental Modal Analysis (EMA).While for the drawback of EMA which needs the input forces, some Operational Modal Analysis (OMA) method were developed (Brincker, R. et al 2015), including Peak-Picking method, the Auto Regressive-Moving Average Vector model, the Natural Excitation Technique, the Random Decrement Technique, the Frequency Domain Decomposition and the Stochastic Subspace Identification. The Frequency Domain Decomposition (translational frequency response function (Ewins, D. et al 2001) and rotational frequency response function (Hosoya, N. et al 2019)) is verified to yield the value of vertical and rotational mode displacements with acceptable accuracy.

A total of 1000 samples are used to analyze each measurement set. In one sample there is one model response of frequencies and mode-shape displacement. For both, clamped and pinned supports, their vertical displacements are set to 0. For the clamped supports, the rotations of the corresponding nodes are set equal to 0. The total combination of influence factors is presented in Table 4-1.

Table 4-1. Combination of influence factors

Factors	Cases	Number
Layout	1|Pinned-pinned, 2|Pinned-clamped, 3|Clamped-pinned, 4|Clamped-Clamped	4
Measurement Set	Set 1, Set 2, Set 3	3
Span Length	50m, 55m, 60m	3
Weighting factor, W_λ	0.5, 0.6, 0.7, 0.8, 0.9	5
Total scenarios		180

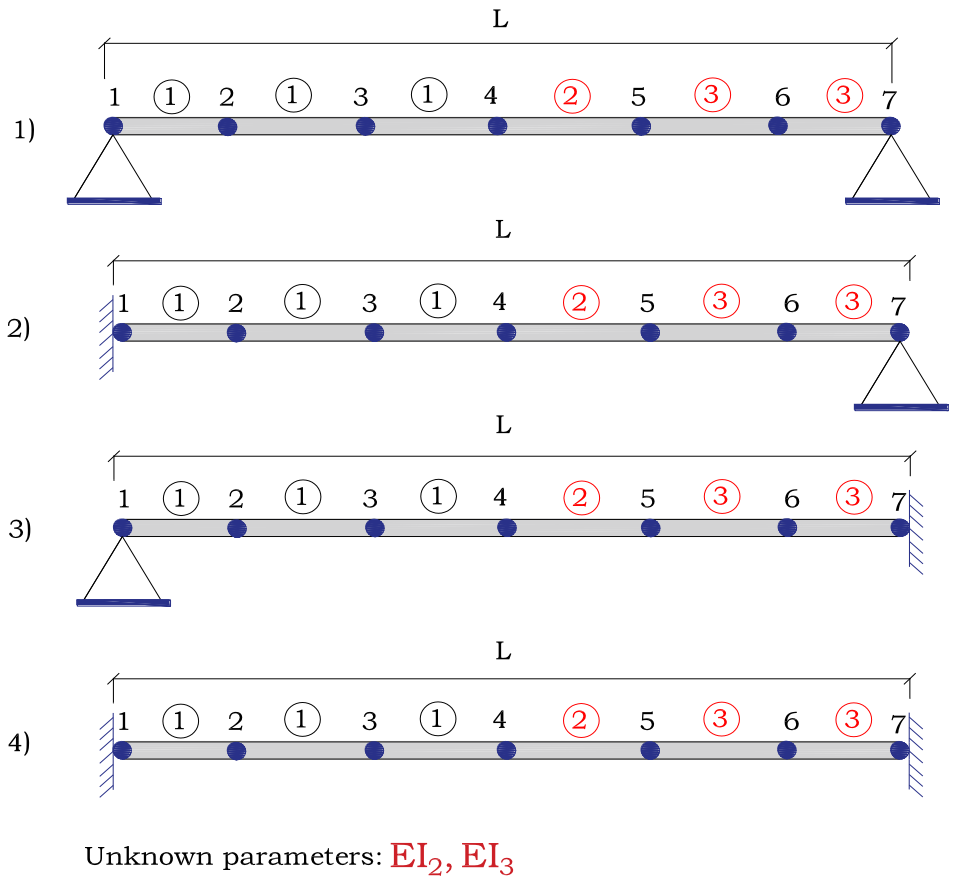

Figure 4-2. Layout of four bridge types (The numbers in circles indicate the cross-section type)

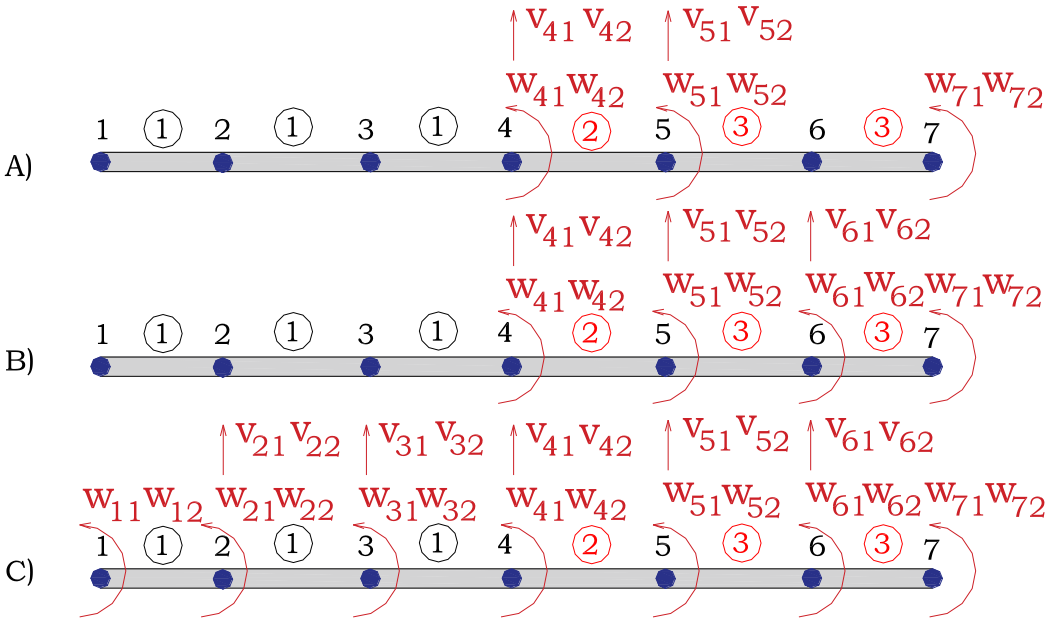

Figure 4-3. Measurement sets

4.3.2 Results

The error index γ,calculated by Eq. (4.2) results in the following expression when applied to the analyzed case

$$\gamma = \frac{1}{2}\sqrt{\left(\widetilde{EI_2} - 1\right)^2 + \left(\widetilde{EI_3} - 1\right)^2} \tag{4.4}$$

where $\widetilde{EI_2}$ and $\widetilde{EI_3}$ are the estimated stiffnesses normalized by the actual value, i.e., a value of 1 denotes a perfect estimation of the parameter. The larger the value of γ , the lower the overall accuracy of the estimated parameters.

For each of the 180 scenarios, an average value of the stiffnesses is obtained from the 1000 samples assuming different random errors in the measurements. The results are depicted in Figures 4-4, 4-5, and 4-6. From these figures, it can be seen that the span length has a minor contribution to the error-index γ, whereas the bridge layout presents the larger influence. It is also noted that the results obtained for the pinned-clamped and clamped-pinned layouts are sensibly similar. The influence of the weighting factor W_λ, varies with the measurement set, that is, its influence is very small for Set 1, especially for the layouts of pinned-clamped and clamped-pinned; for Set 2, the weighting factor displays the largest influence, which is exhibited in the case of pinned-pinned support conditions; and for Set 3, the larger influence of the weighting factor occurs with the pinned-clamped and clamped-pinned layouts.

The worst results are given in the case of clamped-clamped support conditions and measurement Set 1, with values of the error-index γ close to 12%, whereas the best results (error index around 1.8%) correspond to the same support conditions, clamped-clamped, and measurement Set 3. These values are acceptable for SSI. These two results highlight the complexity of designing an optimal SHM+SSI strategy, given the joint influence of the involved variables on the quality of the estimation.

To facilitate the understanding of these interactions, the following section presents the decision trees that will allow the organization of the scenarios according to the resulting error-indices γ.

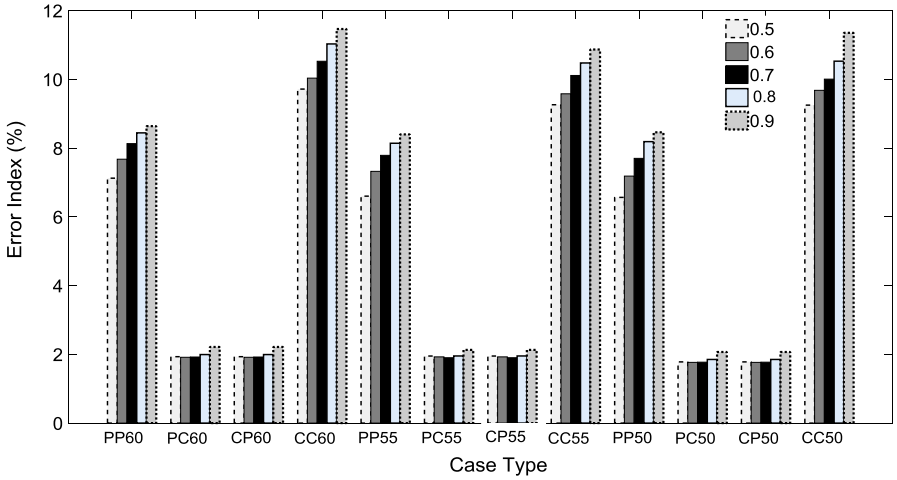

Figure 4-4. Set 1 under different weighting factors. PP, PC, CP, and CC denote pinned-pinned, pinned-clamped, clamped-pinned and clamped-clamped, respectively.

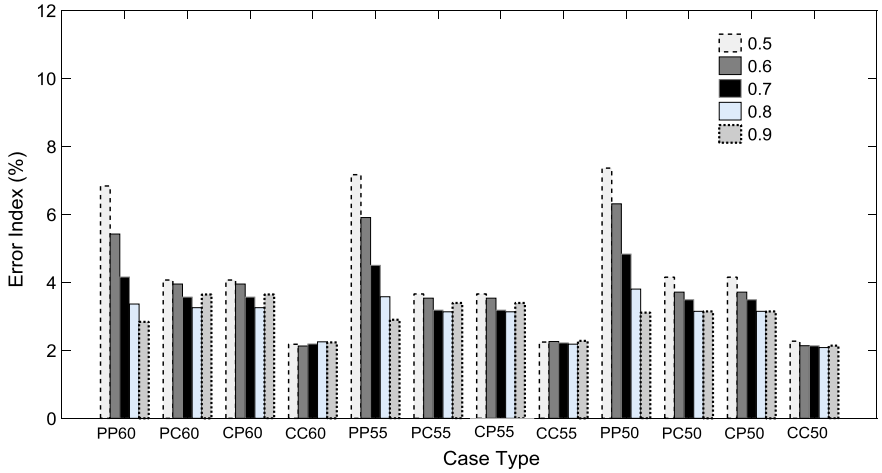

Figure 4-5. Set 2 under different weighting factors. PP, PC, CP, and CC denote pinned-pinned, pinned-clamped, clamped-pinned and clamped-clamped, respectively.

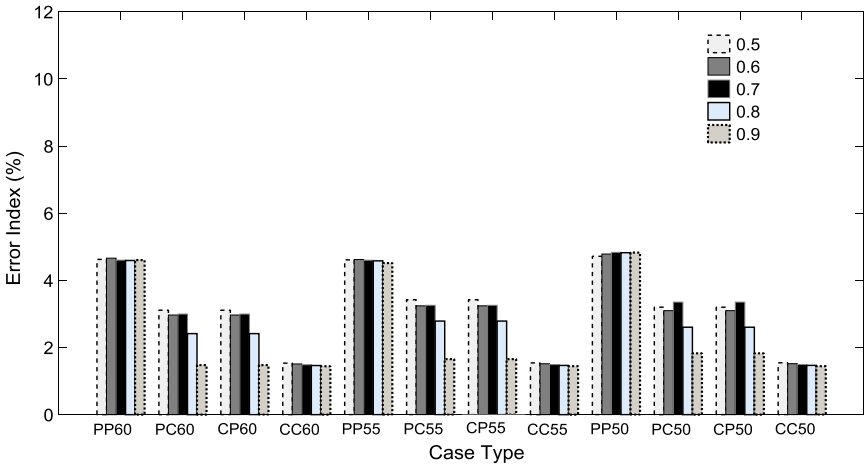

Figure 4-6. Set 3 under different weighting factors. PP, PC, CP, and CC denote pinned-pinned, pinned-clamped, clamped-pinned and clamped-clamped, respectively.

4.3.3 Identification of impact factor by decision tree learning algorithm

The CART is applied to the 180 scenarios, obtaining the decision tree model shown in Figure 4-7 whose node characteristics are indicated in Table 4-2. Therefore, the decision tree considers four explanatory variables: layout, span length, measurement set, and weighting factor, W_λ. Although the decision tree can be pruned to remove those branches that provide little classification power, the entire decision tree has been presented to allow the interpretation of the results and the explanation of the tree itself. The response variable (error-index γ) of the 180 total cases has value of 3.97% for the mean and 2.59% for the standard deviation (see Node 1).

From Figure 4-7, it is clear that the structural layout is the first factor to draw the tree at the first level, which means the influence of the layout on the error-index γ is essential compared to the other three explanatory variables. The layouts of 2|pinned-clamped and 3|clamped-pinned belong to the left branch, and 1|pinned-pinned and 4|clamped-clamped belong to the right branch. Besides, it seems that the error-index is smaller when the boundary conditions of the bridge are asymmetric (left branch). This may be because asymmetric conditions can decompose by symmetric and anti-symmetric conditions. The two conditions exhibit some offsetting behaviors in the parameter evaluation process. That is why the values of PP60 and CC60 in Figure 4-4 are larger than the other two. After this, the next important factor is the selection of the measurement set as indicated by the second level of the tree. The values of measurement Set 1 are classified

separately from the ones of measurement Sets 2 and 3. The selection of both pinned-clamped or clamped-pinned support conditions and measurement Set 1 yields a mean value of the error-index γ of 1.93% with 0.12% of standard deviation (see Node 4 in Table 4-2), whereas selecting measurement Sets 2 and 3 for these types of support almost doubles the error, with 3.17% of mean (see Node 5 in Table 4-2).

For the cases of Layout 2|pinned-clamped and 3|clamped-pinned and measurement Set 1, either the weighting factor, W_λ, or the span length does not pose a big influence, as shown by the small value of the coefficient of variation at Node 4 (0.12/1.93=0.06). However, in other cases, such as the case of Nodes 11 (Layout 2| pinned-clamped or 3| clamped-pinned and measurement Set 3) and 14 (Layout 1|pinned-pinned and measurement Set 2), the adequate selection of the weighting factor ($W_\lambda \geq 0.85$ for the first and $W_\lambda \geq 0.65$ for the second) can almost double the accuracy of the results.

It is noted that the effect of the span length does not appear in the right side of the tree (Layouts 1|pinned-pinned and 4|clamped-clamped), and only appears at Node 8 (cv=0.08/1.88=0.04), meaning that the span length has a residual influence on the results, at least in the studied range (50 to 60 m). This is consistent with the outcome of Section 4.3.2.

Table 4-2. Node characteristics of the decision tree shown in Figure 4-7

Node	Explanatory Variables	Left	Right	Mean (%)	St. Dev (%)
1	Layout	[2 3]	[1 4]	3.97	2.59
2	M. Set	[1]	[2 3]	2.76	0.80
3	M. Set	[1]	[2 3]	5.2	3.14
4	W	<0.85	≥0.85	1.93	0.12
5	M. Set	[2]	[3]	3.17	0.66
6	Layout	[1]	[4]	9.00	1.44
7	Layout	[1]	[4]	3.29	1.67
8	L. span	<52.50	≥52.50	1.88	0.08
9	end node			2.13	0.07
10	W	<0.75	≥0.75	3.58	0.40
11	W	<0.85	≥.85	2.76	0.62

12	W	<0.65	≥0.65	7.76	0.67
13	W	<0.75	≥0.75	10.26	0.70
14	W	<0.65	≥0.65	4.74	1.11
15	M. Set	[2]	[3]	1.84	0.36
16	end node			1.79	0.04
17	end node			1.93	0.02
18	end node			3.78	0.39
19	end node			3.29	0.19
20	end node			3.03	0.29
21	end node			1.65	0.16
22	end node			7.08	0.42
23	end node			8.20	0.31
24	end node			9.79	0.41
25	end node			10.95	0.41
26	M. Set	[2]	[3]	5.59	1.08
27	M. Set	[2]	[3]	4.17	0.71
28	end node			2.19	0.06
29	end node			1.49	0.04
30	end node			6.50	0.75
31	end node			4.66	0.06
32	end node			3.67	0.70
33	end node			4.66	0.13

The performance of an SHM+SSI strategy for the structural Layout 1|pinned-pinned or 4|clamped-clamped using the measurement Set 1 is really poor due to the high values of the error-index γ compared to the other cases. In the case of structural Layout 4|clamped-clamped, it is recommended to choose the measurement Set 3 if possible (yielding a mean error-index γ of 1.49%, Node 29), or measurement Set 2 otherwise, resulting in a very acceptable mean value of the error-index γ of 2.19% (Node 28).

From this decision tree, the best decisions are obtained by comparing the classifications. Some best choices can be drawn. Firstly, measurement Set 1 is the best choice for Layouts 2|pinned-clamped and 3|clamped-pinned. In this case, the role that the weighting factor, W_λ, has on the

accuracy of the estimated $\widetilde{EI_2}$ and $\widetilde{EI_3}$ is negligible. Secondly, a weighting factor of 0.9 is the best choice for Layouts 2|pinned-clamped or 3|clamped-pinned and measurement Set 3. In this case, the weighting factor plays a relevant role in improving the accuracy of the estimation. Thirdly, the optimal measurement choices for the Layout 4|clamped-clamped are Sets 2 and 3. Finally, the combination of the Layout 1|pinned-pinned or 4|clamped-clamped and measurement Set 1 should be avoided due to the resulting large error-index γ, no matter the assumed value of the weighting factor, W_λ.

It is noted that these values correspond to the training set, so different values can be observed in real practice.

4.3.4 Discussion on the optimal SHM+SSI strategy

This part is to investigate the sensitivity of the outcomes to the effects encompassed by each scenario. Using the analysis result in Section 4.3.3, the influence of each factor is found by the control variable method. After removal of one of the four variables (Table 4-1), DT is used to analyze the remaining three ones. Table 4-3 demonstrates the corresponding optimal SHM+SSI strategy when considering the remaining three factors.

Table 4-3. Sensitivity analysis: Strategy comparison when considering three factors

Remove Variables	**Optimal SHM+SSI Strategy**
Layout	Set 2 and 3 & $W_\lambda \geq 0.75$;
Measurement Set	Layout 2| and 3| &$W_\lambda \geq 0.75$;
Span Length	Layout 2| and 3| & Set 1; Layout 4| & Set 2 and 3;
Weighting factor	Layout 4| & Set3; Layout 2| and 3| & Set1;

From the result of Table 4-3, the optimal SHM+SSI strategy corresponds to the choice in Section 4.3.3. For this particular structural analysis, it is clear that the span length of the bridge is not a

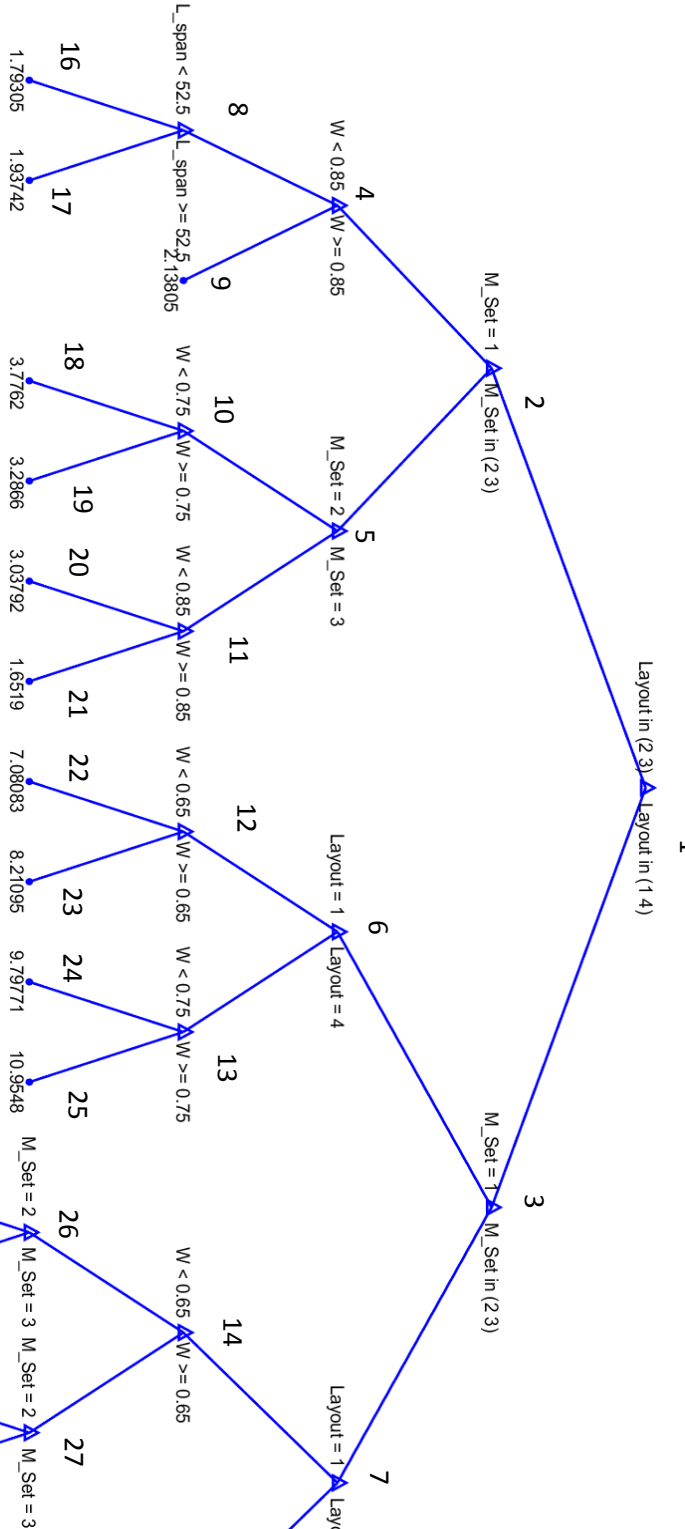

Figure 4-7. Overall structure of the obtained decision tree model. The value of the end nodes refers to the mean error-index ρ of the split.

relevant variable to consider in any optimal strategy, at least in the studied range for the reason that no strategy about the span length appears in Table 4-3. This is a sound result that validates the rationality of the method. Regarding the other studied variables, the layout, measurement set and error frequency-related weighting factor, are the more complex cases when applying the observability method with COM. Although the structural layout is not a decision variable as it cannot be selected, it is the most important input when deciding the optimal SHM+SSI strategy which can be seen in the last three rows of Table 4-3. Besides, the second important decision is the selection of the measurement set. Thirdly, the selection of an adequate value of the weighting factor can significantly increase the quality of the estimation in some cases when ignoring the influence of layout and measurement. Whether low or high values of the weighting factor perform better will depend on the specific case. Decision trees can be used to derive this value. It is highlighted that these results are case-specific but the process of choosing a strategy can be followed in a similar way.

The next section analyses to which extent the information provided by the decision trees based on the assumption of undamaged structure can be useful to support decisions on the optimal SHM+SSI strategy for damage detection in a real case.

4.4 Applicability to best SHM+SSI methodology for damage detection

4.4.1 Bridge description

The Hollandse Brug (Figure 4-8), located in the center part of the Netherlands, belongs to one of the main highway connections between Amsterdam and the Northeast of the Netherlands. The bridge is a pre-stressed concrete bridge composed of precast beams and an upper concrete slab poured in situ and was opened for traffic in 1969. The bridge has seven spans of 50.55 meters. A dilatation joint was placed between each span, which causes that the bending moments cannot be transferred from one span to another. Thus, each span can be considered separately. To extend its service life renovations and strengthening were conducted in 2008.

SHM data collection was conducted to understand the service-life assessment of this renovation bridge by the Infra-Watch research project. The SHM system consists of sensors positioned on three cross-sections of the first span (Figure 4-9 a)).

Figure 4-8. Overview of Hollandse Brug

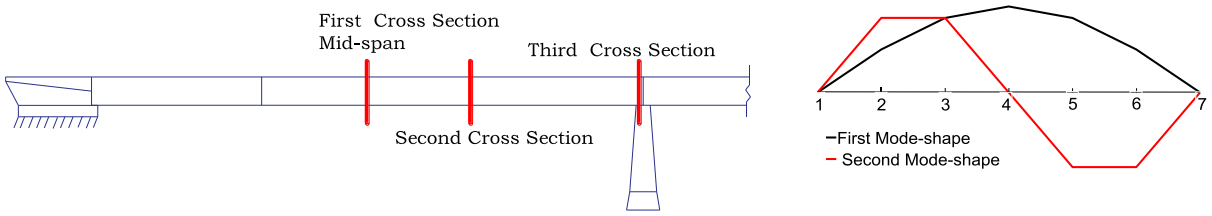

a) b）

Figure 4-9. a) Locations of the sensors (Miao. S.f. 2014); b) The first two mode shape of Hollandse Brug

Based on the vibration data gathered with accelerometers (geo-phones), located at various intervals along and across the bridge, detailed information about the mode shapes (Figure 4-9 b)) and natural frequencies ($f_1 = 2.51\ Hz, f_2 = 10.09\ Hz$) could be obtained (Miao, S.f. et al 2013 & 2014, Veerman, R. 2017) by Peak-Picking method and Stochastic Subspace Identification. It is worth mentioning that the previous studies on this bridge focus on the data collection, processing, and the comparison of the FEM model results instead of the identification of structural health. The next analysis can fill this gap.

4.4.2 Decision tree for the Hollandse Brug (original bridge un-damaged)

The goal is to define the best SHM+SSI strategy to assess the unknown parameters EI_2 and EI_3 according to Figure 4-2. The layout of each span of the bridge can be assumed as pinned-pinned

due to the dilatation joint. Through the model calibration, based on the two natural frequencies, the simplified model could be identified as corresponding to Figure 4-2, Layout 1. The parameters of each element are shown in Table 4-4.

Table 4-4. Parameter of each element of Hollandse Brug

Section Types	**Mode value**		
	Length (m/each)	EI ($N \cdot m^2$)	Mass(kg/m)
①, ②, ③	8.425	8.15e11	49000

The errors of the measured frequencies, vertical displacement, and rotation are assumed to follow uniform distributions bounded between 1%~3%, 2%~6%, and 10%~30%, respectively. A total number of 1000 samples are analysed by dynamic COM under 6 different measurement sets. The six sets are shown in Figure 4-10.

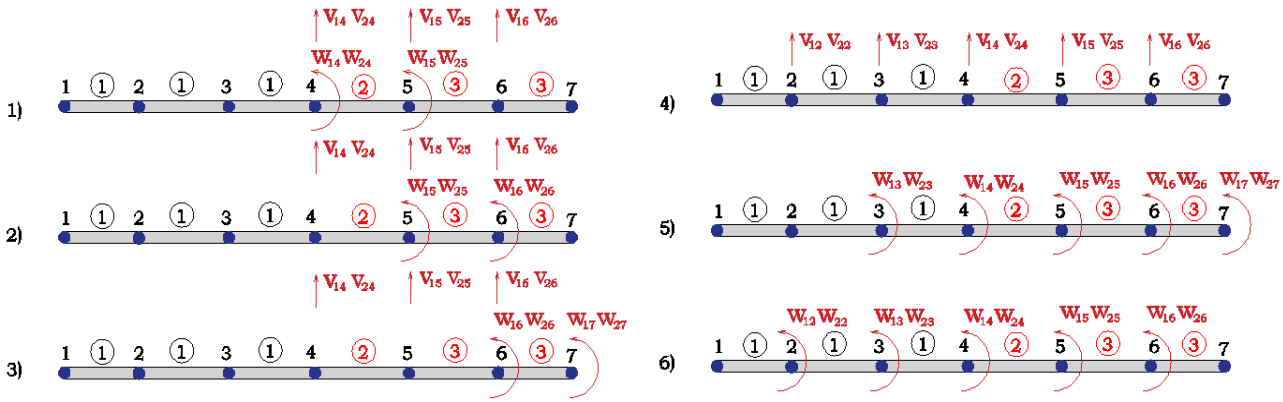

Figure 4-10. Six measurement sets of Hollandse Brug

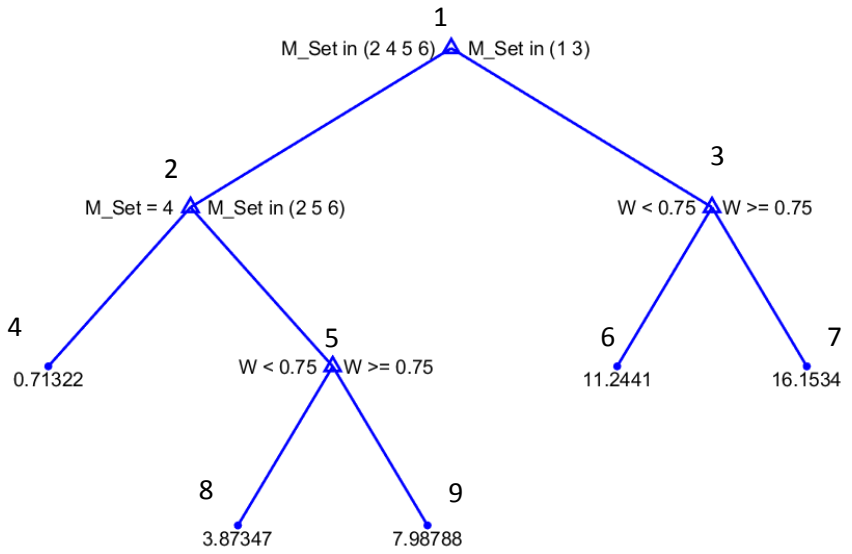

Figure 4-11. Decision tree model for the SHM+SSI of Hollandse Brug

An initial decision tree with no information on the level of damage of the structure (undamaged bridge with all cross-sections with properties as presented in Table 4-4) can be drawn according to Section 4.2.2, see Figure 4-11. From this decision tree, it is clear that the best decision is to select Set 4 (see Node 4). The results of Set 2, 5, and 6 are significantly better than the ones of Set 1 and 3. This clear difference cannot be easily foreseen without the decision tree, showing that the obtained results are not trivial at all. When considering the effect of the weighting factor, W_λ, the performance of lower weighting factors ($W_\lambda < 0.75$) is better than the case of higher weighting factors ($W_\lambda > 0.75$), being a relevant aspect to consider to reduce the error-index γ in most of the cases (compare Nodes 8 and 9). The detailed information of each node is shown in Table 4-4. In the last column of the table, the coefficient of variation, i.e., standard deviation normalized by the mean, exhibits a maximum value of 0.41 for an end node, which shows the robustness of the tree.

Table 4-5. Node characteristics of decision tree shown in Figure 4-11

Node	Explan. Vble	Left	Right	Mean (%)	St. Dev (%)	St. Dev/ Mean
1	M. Set	[2 4 5 6]	[1 3]	7.28	5.48	0.75
2	M. Set	[4]	[2 5 6]	4.31	3.09	0.72
3	W_λ	< 0.75	> 0.75	13.2	4.26	0.32

4	end node			0.71	0.26	0.37
5	W_λ	< 0.75	> 0.75	5.51	2.60	0.47
6	end node			11.2	2.30	0.21
7	end node			16.1	5.15	0.32
8	end node			3.87	1.60	0.41
9	end node			7.98	1.64	0.21

4.4.3 Damaged bridge

Once the theoretical decision tree is obtained for the undamaged bridge, two damage scenarios are analyzed in this section. The bridge mid-span is assumed to be damaged considering 5% and 30% of reduction of EI_2, as shown in Figure 4-12. The damage patterns have been assumed to create the scenarios needed to validate the approach. Nevertheless, this knowledge is not introduced as an input of the model. Therefore, knowing the damage patterns is not required for its application.

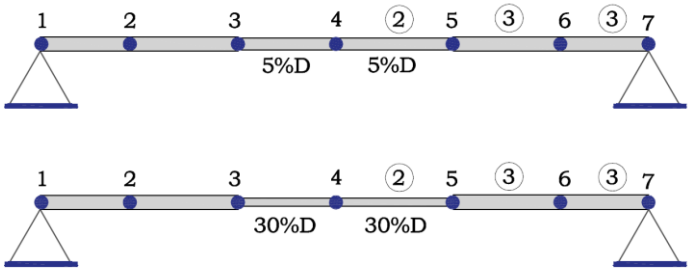

Figure 4-12. 5% and 30% of stiffness reduction at mid-span of Hollandse Brug

The COM is used to obtain the estimated $\widetilde{EI}_2$ and $\widetilde{EI}_3$, with the parameters in Table 4-4 and the two damage levels. The errors of frequencies and vertical displacements are the ones indicated in Section 4.4.2. To account for the measurement error, the average value of 1000 simulations has been considered. Finally, the parameters have been estimated for W_λ= 0.5, 0.6, 0.7, 0.8 and 0.9.

Table 4-6 summarizes the error-index γ comparison between the values given by the decision tree (undamaged structure) and the estimation of the damaged structure. According to the analysis in Section 4.4.2, the largest estimation error occurs with measurement Sets 1 and 3

(Nodes 6 and 7), whereas the best estimation is obtained with measurement Set 4 (Node 4). These two scenarios are used to validate the decision tree.

Table 4-6. Error-index comparison between the original (undamaged) and damaged values. DT stands for decision tree

	Case	**W_λ**	**Mean (%)**	**St. Dev (%)**
DT: Node 6	Undamaged	<0.75	11.20	2.30
DT: Node 7	Undamaged	≥0.75	16.10	5.15
	5% damaged	<0.75	12.70	7.34
Obtained values:	5% damaged	≥0.75	17.22	3.92
Sets 1 and 3	30% damaged	<0.75	11.73	6.50
	30% damaged	≥0.75	18.39	3.96
DT: Node 4	Undamaged		0.71	0.26
Obtained values:	5% damaged		0.59	0.01
Set 4	30% damaged		2.38	0.01

When comparing the values yielded by Nodes 6 and 7 to the obtained ones in case of damage is present, the results are fully consistent for both damage levels. Note that the influence of W_λ indicated by the decision tree remains in the damaged bridge, showing a larger standard deviation for $W_\lambda < 0.75$ in the case of the damaged bridge.

Regarding the values given by Node 4, they are consistent with the results of 5% of damage, however, a larger mean of error-index γ is found for the case of 30% of damage. This can be related to the small value of the error-index γ obtained in the case of the undamaged structure (0.71%). Nonetheless, the values of the error-index γ obtained for the measurement Set 4 are clearly better than the ones of Set 1 and 3. The small value of the standard deviation obtained for the damaged bridge denotes the low influence of the weighting factor, which is consistent with the left branch of the decision tree (the weighting factor is not included in this branch).

Based on these results, for the Hollandse Brug, the optimal measurement set is Set 4, the second choice is Set 2, 5, and 6, the worst set is Set 1 and Set 3 no matter the bridge is undamaged or not. It could be seen that decision trees in combination with the COM method seem to be a useful

tool to plan the best strategy of SHM+SSI, providing information that is not trivial and highly reliable.

4.4.4 Discussion

This section is used to verify the efficiency of the combined method of COM and decision tree. The effective independence method (EIF), as one of the most reliable methods for optimal sensor placement of engineering structures, could provide efficient solutions (Sunca, F. et al. 2020). This method aims to maximize of the linear independence of target modes. But this method is only used to choose the optimal sensor placement and cannot work on SHM+SSI strategies (such as choosing a layout, weighting factors) and the worse optimal sensor placement. But it can be used to verify node 4 in Figure 4-11.

The effective independence method was proposed by Kammer (1991). It attempts to maximize the linear independence between the m target mode shapes through the following Equation (4.5):

$$EIF=[\emptyset]^T_{\mathrm{q}\times np}[\emptyset]_{np\times \mathrm{q}}=\sum_{i=1}^{np}([\emptyset]_i^T[\emptyset]_i) \tag{4.5}$$

Where $[\emptyset]_{\mathrm{np}\times \mathrm{q}}$is a matrix containing the eigenvector, np is the total number of measurement point and q is the number of mode shapes of interest that are used for the analysis, $[\emptyset]_{\mathrm{i}}=\left[\emptyset_{\mathrm{i}1},\emptyset_{\mathrm{i}2},\dots,\emptyset_{\mathrm{iq}}\right]$ is a row vector of vibration shade shapes corresponding to the ith DOF.

E_d is using to represent the effective independence distribution vector of the candidate sensor set. The DOF corresponding to the largest element of E_d is the DOF that contributes most to the rank of EIF. And thus that DOF should be retained. $\mathrm{E_d}$ can be expressed as Equation (4.6),

$$E_d=\emptyset_s[\emptyset_s^T\emptyset_s]^{-1}\emptyset_s^T \tag{4.6}$$

By repeating the process of removing the DOF with the smallest contribution to the rank of EIF until the desired number of sensor is achieved, the sensor locations are determined.

For the case in Section 4.4.1, the optimal sensor placement for 5 mode-shapes as input by EIF is Set 4, which is consistent with the conclusion in Section 4.4.3. However, this EIF method cannot obtain the worse set. What is more, if more variables are considered, such as weight factor, the

optimal SHM+SSI Strategy, such as the one in Table 4-3, will not be able to yield. This is to say, compared with the traditional optical sensor placement (OSP), the merit of the proposed method is efficient to consider all the parameters (including all SHM parameters and SSI parameters).

4.5 Conclusions

This chapter proposes a machine learning decision tool to help building the best combined strategy of SHM (proposal of a measurement set) and SSI (proposal of weighing factors in the objective function of dynamic COM) that can result in the most accurate estimations of the structural properties. To this end, the combination of COM method and CART algorithm is used for the first time.

The main concept of the optimal SHM+SSI strategy is given, as shown in roadmap (Figure 4.1). Decision trees (DT) are firstly presented to investigate the influence of the variables involved in the SHM+SSI process on the error estimation in a general structure, including structural layout, measurement set, span length and weighting factor based on the estimated parameters from COM. Through the sensitivity analysis of the COM and DT, the ranking of the four variables are as follows: layout, measurement set, parameters of the COM (weighting factor) and span-length. The analysis of different variables provides a theoretical framework to clarify this method and illustrate the utility of this technique.

Later, the same concept is applied to a specific structure, the Hollande Brug. The decision tree is used as a tool to plan the optimal SHM+SSI strategy, with no initial knowledge of the actual structural state, and the robustness of the results is given for two levels of damage. For this specific bridge, the optimal measurement set is Set 4, and Set 1 and Set 3 should be avoided. This real application shows the merit of this strategy in proposing the best sensor deployment and its potential application in the field of damage identification

It is worth mentioning that the verification of the method with a real bridge with different levels of damage (5% damage and 30% damage) is conducted, which shows that the method is robust even for a high damage degree, showing the SHM+SSI strategy that yields the most accurate estimation. Thus in analyzing other structures, the roadmap in Figure 4.1 can be used as a guide for action.

The application of this work allows making better use of existing sensor devices and SSI methodologies. Also, it can be useful to identify the main sources of inaccuracy or uncertainty of the results, and thus, helping to put the focus on the aspects to be improved within the SHM+SSI strategy. For instance, the role of the weighting factor in the total accuracy of the results has been identified, thus it can be concluded that it is worthy to further investigate this parameter. By using this tool beforehand, erroneous decisions can be avoided.

The approach does not consider the modeling error, such as the error introduced when making wrong assumptions on the support conditions. In some cases these errors can bring large uncertainty regarding the results and they should be addressed before translating the proposed approach into practice. The proposed approach can be extended towards this direction. Also, the decision tree can be extended by adding different SSI methods to select the ones providing the most accurate results in each case. Moreover, the development of the SHM+SSI strategy for more slender structures will be conducted in the future. In addition, the operational effects due to traffic in the bridge on the final results were not considered in the present example and are a future line to be explored.

CHAPTER 5 Uncertainty quantification (UQ) with the dynamic constrained observability method

5.1 Introduction

This chapter aims at understanding how the uncertainty in the model parameters and measured variables affects the uncertainty of the output variables, that is, how the uncertainty propagates in the SSI process by dynamic COM. Moreover, by dividing the source of uncertainty into aleatory and epistemic, important insights can be obtained regarding the extent of uncertainty that can be potentially removed. With this procedure, the gap of uncertainty quantification identified in section 2.4.3 can be filled by the dynamic COM.

A probabilistic UQ approach is proposed to analyze the SSI through the dynamic Constrained Observability Method, by considering both the epistemic uncertainty modeling and the aleatory uncertainty. To overcome some of the drawbacks mentioned above, different modal orders are considered separately, after that, all involved mode orders are put together to estimate the output parameters in an objective function. The method of simultaneous evaluation can appropriately take into account the dependence between various parameters.

The objective of this chapter is to check the possibility of having some insight in the uncertainty quantification and error propagation before the actual monitoring of a structure. The Dutch bridge known as 'Hollandse Brug' is used as an example. The background of 'Hollandse Brug' is described in Section 4.4.1. This bridge was monitored without a previous evaluation and after its monitoring, the conclusion was that uncertainty was too big to make any conclusive assessment.

The dynamic SSI by COM is explained in Chapter 3. The effect of weighting factor is ignored in the present analysis so $W_\lambda = W_\delta = 0.5$ (Boris Zárate, A. et al 2008, Brownjohn, J. et al 2000) in Eq. (3.5).

5.2 Model calibration

The unidimensional model of the span of Hollandse Brug is divided into 6 elements, as shown in Figure 5-1 a). The background of Hollandse Brug is described in Section 4.4.1. According to the parameters estimated in refences (Miao. s.f. et al 2013 & 2014, Veerman, R. 2017) and model calibration, the simplified model uses the following parameters (Table 5-1), obtaining estimations of the frequencies and mode shapes (Figure 5-1 b)) close to the experimental data ($f_1 = 2.51$ Hz, $f_2 = 10.09$ Hz). The first and second frequencies match the experimental data correctly with -0.1% and -0.5% errors respectively.

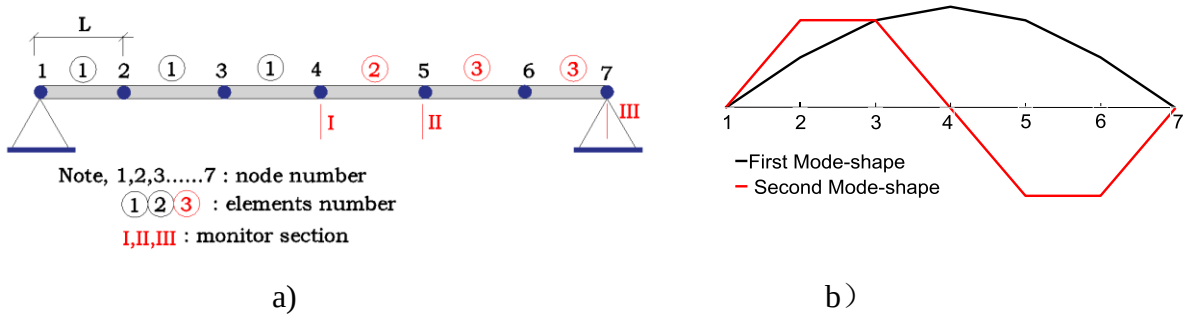

a) b）

Figure 5-1. a) First span of Hollandse Brug; b) First and second mode shape

Table 5-1. Parameter of each element

Element Number	**Mode value**		
	Length (m/each)	EI (N · m^2)	Mass(kg/m)
1-3	8.425	8.15e11	49000

Thus, this model is considered as the exact representation of the real bridge. The estimated values obtained through the SSI will be compared against the parameters of this model, which are referred as the real values. The measure of an error free deflection or rotation refers to the deflection or rotation of this model. Thus, The bridge's stiffness can be derived through modal analysis (Drygala, Izabela J. et al 2020).

5.3 UQ analysis

The goal of this section is to assess the uncertainty regarding the estimation of EI_2 and EI_3 of the Hollandse Brug when EI_1 and m are known with some degree of uncertainty.

To assess the uncertainty associated with the output of the structural system identification, the epistemic uncertainty involved in the assumption of the input-parameters (error incurred during the modelling process) and the aleatory uncertainty involved in the measurement error (inaccuracy of sensors) are independently considered. In that way, insights into the contribution of each type of error to the total uncertainty can be obtained. Then, the combined effect is analysed to determine the total uncertainty of each estimated parameter.

5.3.1 Epistemic uncertainty: input-parameter errors

The contribution of the errors in the input parameters of the structural model, sometimes, referred as model errors are first analyzed. Here, the effect of boundary conditions are not considered as it is assumed that they have been perfectly determined through the model calibration carried out in Section 5.3. In fact, the calibration using the first 2 modal frequencies has identified that a pin connection is the correct assumption. In addition, the shear deformation is ignored based on the low value of the ratio cross-section depth to span length.

Table 5-2 shows the input parameters considered in this analysis, namely, the mass of the bridge, m, assumed as constant for the entire bridge, the Young modulus of element type 1, E_1 and its flexural inertia, I_1 (see Figure 5-1 a)). The probabilistic distributions assumed to introduce the uncertainty regarding those parameters are also indicated.

Table 5-2. Statistical definition of input variables

List of Variables (Units)	Sampling Size	Probabilistic Distribution	95% Confidence Interval
$m_1 = m_2 = m_3 = m$ (kg/m)	10^3	$N(49000, 49000 * 0.05)$	$49000\ (1 \pm 0.1)$
E_1 (N/m^2)		$N(4e10, 4e10 * 0.25)$	$4e10(1 \pm 0.5)$
I_1 (m^4)		$N(20.4, 20.4 * 0.02)$	$20.4\ (1 \pm 0.04)$

They are assumed to follow a normal distribution $N(u, \delta)$, where u is the mean corresponding to the expected value of the variable. The standard deviation, δ, has been chosen to guarantee that the 95% of the distributions falls over the interval $[0.9u\ \ 1.1u], [0.5u\ 1.5u]\ and\ [0.96u\ 1.04u]$, respectively. The variability in the Young modulus was chosen according to the reference

(Bungey, H.B. et al 1995). All the input parameters are assumed to be statistically independent. It is noted that the uncertainty of the three input parameters of the model can be reduced by conducting non-destructive tests in the bridge.

In order to propagate the uncertainty, Monte Carlo simulation (MCS) is used. MCS requires an input sample made of combinations of realizations of each parameter upon which a model will be evaluated to obtain a sample of the model response. However, this approach may be very time-consuming and for large dimensional problems and some reliability problems, the selected combinations might not yield a response sample that can be considered as a good representation of the population. In other words, relevant information can be dismissed if the input sample is not large enough or not adequately selected. To overcome this issue, several sampling methods have been developed. In this research, the Fast Optimal Latin Hypercube (FOLH) sampling is preferred for its sampling strategy, which can achieve higher sampling accuracy with a smaller sampling scale (Viana, F. et al 2009).

The FOLH, as the common Latin hypercube method, requires of the selection of the individual realizations of the input parameters according to their probability distribution. To do that, the Cumulative Distribution Function (CDF) of each input parameter is equally divided into the number of required realizations, and then, the corresponding percentile is obtained. By doing so, the set of selected realizations will follow the required probability distribution. The main contribution of FOLH with respect to LH is the way that the realizations are combined (pairing process). To illustrate this process, Figure 5-2 shows an example considering only two random variables, for instance m and E_1. Figure 5-2 a) depicts the equal division of the CDFs to obtain 10^3 realizations of each variable. Then the realizations are paired into 10^3 combinations. Figure 5-2 b) shows the resulting sample points. In the case of the variables shown in Table 5-2, combinations of the three variables should be generated. In this case, a total of 10^3 sampling points are selected to statistically represent the 3-dimensional space. It is noted that the benefit of the FOLH method is not so obvious in this case, as only 3 variables are combined. Nevertheless, in the following sections, the number of the involved variables is significantly larger, thus, the FOLH method is required to reduce the computational time without a loss of representation of the input space.

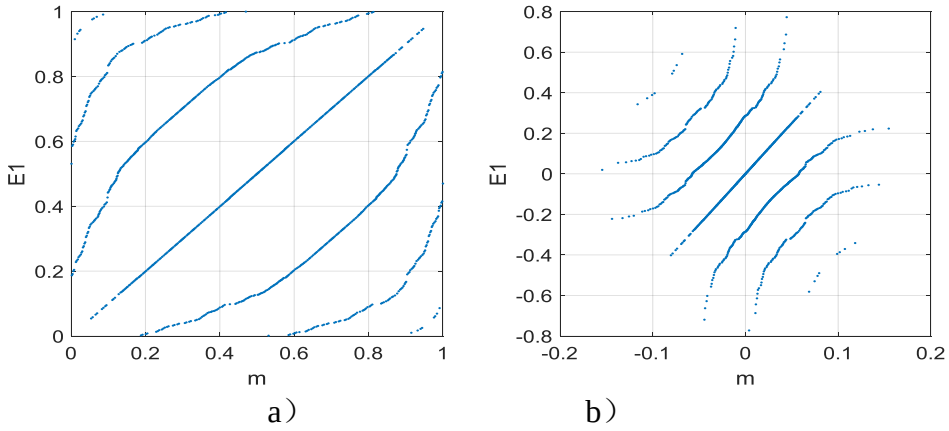

Figure 5-2. a) Division of the CDFs equally and pairing process; b) Resulting sample points

The sample points are studied for three scenarios that differ in the considered measurement sets. It is noted that in this stage the measurements are assumed error free. The three measurement sets are shown in Figure 5-3. v_{ik} and w_{ik} denote the vertical and rotation mode-shapes of the k^{th} node in the i^{th}mode. Thus, measurement Set A mainly focuses on the estimation of element type 2, the distribution of measurement Set B aims at both element types, 2 and 3, and measurement Set C includes all the possible measures as it is expected to improve the estimation accuracy of EI_2 and EI_3. Given that the corresponding raw row of $[V]$ to EI_2 and EI_3 is equal to 0 under these three sets, EI_2 and EI_3 can be directly identified by Eq. (2.4), with no need of conducting the optimization step.

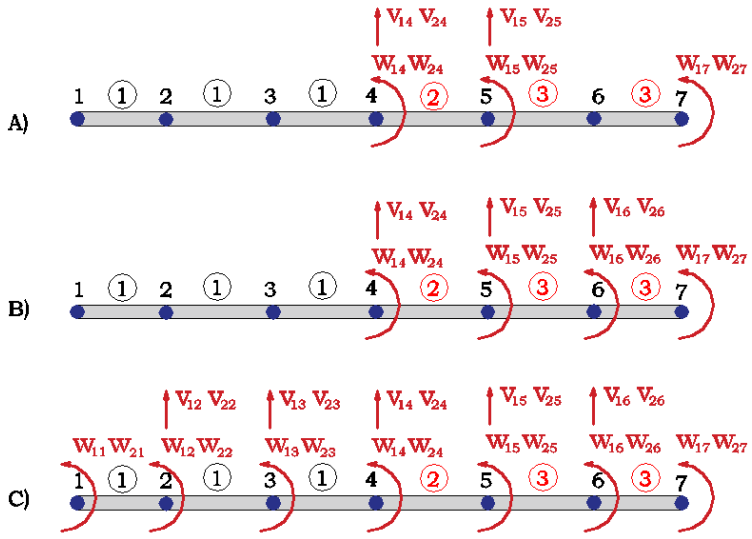

Figure 5-3. Three measurement sets

The results corresponding to the three measurement sets are depicted by their empirical cumulative distribution functions (ECDF) to avoid making any assumption on the probability distribution of the results. The obtained values, shown in Figure 5-4, are normalized with respect to the real values. In all the cases, the distributions are almost unbiased and symmetric, which is reflected in the mean and probability of overestimated rows in Table 5-3.

More precisely, for the measurement Set A, the expected values of the estimated parameters (EI_2, EI_3) have 0.0% and 0.3% skewness with respect to the real values, respectively. The 5% and 95% percentages of the normalized values of EI_2 and EI_3 are [0.684,1.312] and [0.608, 1.383], respectively. In absolute terms, EI_2 will be in the range of [5.57, 10.68]$*$ 10^{11} and EI_3 in [4.96, 11.27]$*$ 10^{11} within 95% confidence interval. It can be seen that the output variable EI_2 exhibits less uncertainty. This can be explained by the amount of information provided per unit length, which in the case of EI_2 is bigger than in the case of EI_3 (see Figure 5-4).

For the case of the measurement Set B, the skewness and 90% confidence intervals of the normalized EI_2 and EI_3 are -0.1%, -0.1% and [0.879, 1.117], [0.884, 1.113], respectively. In this case, both estimations exhibit the same level of uncertainty. For the measurement Set C, the 90% confidence intervals of the normalized EI_2 and EI_3 are [0.770, 1.228] and [0.782, 1.217], which are surprisingly wider than in the case of the Set B even though the Set C contains more information than Set B. This is because of the introduction of redundant information that may derive in some lack of consistency between the mechanical properties of Section ① and the observed displacement and rotation in this part of the structure. In fact, the model is assuming the same mass per unit length all along the span, but not for the stiffness. As no error is assumed in the measurements and those are obtained assuming both mass and stiffness uniformly distributed along the span, this produces an inconsistency with the introduction of additional information in Set C.

Therefore, it seems that the best measurement set is B. Table 4 summarizes the discussed results. It is noted that the observed errors can also be affected by the unavoidable computational inaccuracies. As seen in Table 4, the probability of over/underestimation is similar and roughly about 50 % in all the cases.

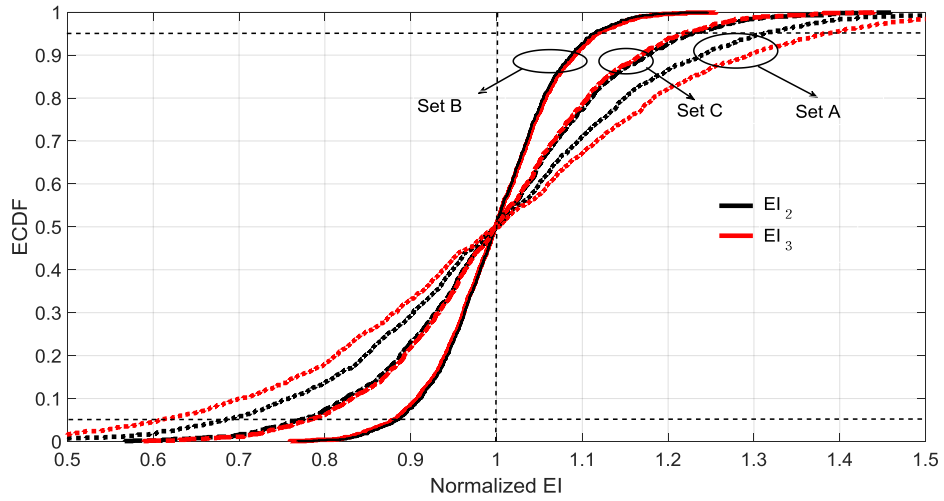

Figure 5-4. ECDF of estimated under different sets considering epistemic uncertainty. The vertical dotted line represents the correct value, and the 5 and 95 percentiles are indicated with horizontal dotted lines.

Table 5-3. Statistical data of the estimated EI_2 and EI_3 under different measurement sets (normalized)

	EI_2			EI_3		
Measurement Set	A	B	C	A	B	C
p5	0.684	0.879	0.77	0.608	0.884	0.782
p95	1.312	1.117	1.228	1.383	1.113	1.217
p50	1.000	0.999	0.999	1.003	0.999	0.999
Range	0.628	0.238	0.458	0.775	0.229	0.435
Skewness	0.000	-0.001	-0.001	0.003	-0.001	-0.001
Mean (Bias)	0.999	0.999	1.000	0.999	0.999	1.000
Standard Deviation	0.257	0.096	0.185	0.319	0.092	0.176
Probability of Overestimated	49.8%	49.8%	49.8%	49.9%	49.6%	49.8%

5.3.2 Aleatory uncertainty: measurement errors from sensors

This part considers the error caused by the accuracy of measurement devices, although the effect of other factors, such as the computational error and the accuracy of the data-extraction method are implicitly included as part of the data processing.

The error assumed for the analysis of this section adopts the values indicated in Table 5-4. Following the same method as the previous section, 10^4 samples are generated for each set with

a frequency error level of 3%, a vertical displacement error level of 6% and a rotation displacement error level of 30%. Normally, the frequency error is small according to the relevant literature (Li, Z. 2016, Hou, R. 2018 & Chen, J. 2015), the vertical displacement error range was chosen following Li, Z. (2016), who identifies the first vertical displacement with accuracies of about 3%. Given that the accuracy of rotations is lower than the accuracy of vertical displacements (Mares, C. et al, 2002), 30% was chosen for this purpose.

Table 5-4. Measurement input variables

	List of variables	Sampling size	Probabilistic Distribution	95% Confidence Interval
Main bridge	Frequencies ($f_i, i = \{1,2\}$)	10^4	$N(f_i,\ f_i * 0.015)$	$f_i\ (1 \pm 0.03)$
	Vertical displacements (v_{ik})		$N(v_{ik}, v_{ik} * 0.03)$	$v_{ik}\ (1 \pm 0.06)$
	Rotation displacements (w_{ik})		$N(w_{ik},\ w_{ik} * 0.15)$	$w_{ik}\ (1 \pm 0.3)$

The choice of the sampling size is because the number of actual optimization parameters in Eq. (3.5) is 4 when the information of two mode-shapes is used, two frequencies and two MAC. To further check the rationale of this sample size, the MAC_1 and MAC_2 are analyzed under different sample sizes and measurement sets. Figure 5-5 shows an example of the corresponding ECDF under different sample sizes. It shows how the quality of the ECDF for different sample sizes significantly improves till the case of 10^4 . After this, there is not a significant improvement. See how the sample size of 10^4 is extremely close to the ECDF of 10^5 in Figure 5-5.

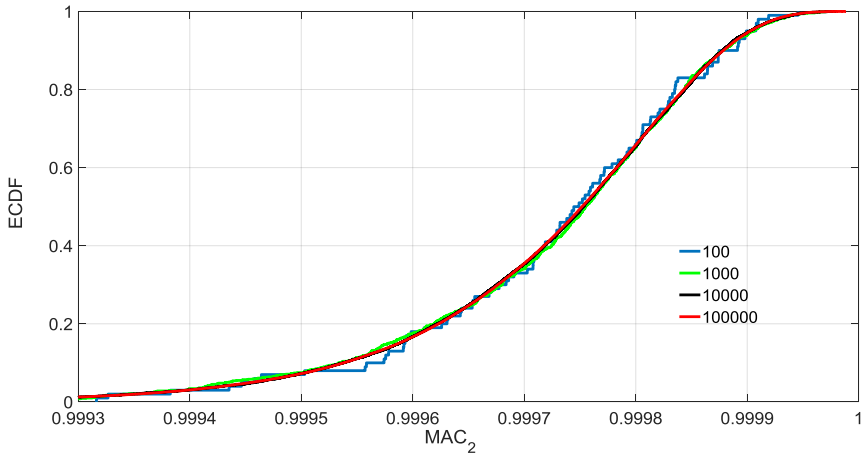

Figure 5-5. ECDF of MAC_2 under Set C and different sample sizes

Figure 5-6 shows the ECDF of the estimated EI_2 and EI_3 under the three measurement sets considering the aleatory uncertainty of the sensor measurements. Table 5-5 shows 5%, 95% percentages, the bias, standard deviation and skewness of the estimated data. Here, again, the obtained results show that Set B is the best among the three original sets because it presents the smallest confidence interval, which is un-skewed in the case of EI_2 and slightly skewed in the case EI_3 towards conservative values (i.e., underestimate the structural stiffness). Sets A and C exhibit comparable results in terms of confidence intervals. However, the results yielded by Set A are clearly skewed; EI_3 towards conservative values compensated by EI_2, which tends to be overestimated under this measurement set. It is recalled that, similarly, Set B presented the most reliable results in terms of epistemic uncertainty, whereas Set A presented the worst estimation. As in the case of epistemic uncertainty, it seems illogical that Set C, which provides more measured data into the system than Set B, provides worse results than Set B.

In Set C, more measurements corresponding to the left part of the beam are introduced. Error level of the measurements taken from the left and right part of the beam is the same. However, the measurement errors from the left part of the beam have a worse effect on the observed values (corresponding to parameters from the right part of the beam) than the measurement errors from the right part of the beam. In this sense, on the one hand, adding more information should improve the results but on the other hand the errors of this new information are impacting much more the variability and values of the targeted parameters, in such a way that the overall result is worse. This is an interesting and non-intuitive result, as it can be thought that, with the same error level the more measurements, the better and it is not always the case. It is always interesting to add more measurement points, but in the vicinity of the structural part whose mechanical properties are to be identified. This aligns with the fact that where new information without error is introduced (Set D, Figure 5-7) results from Set B are improved. The most important conclusion of this example is that when the model error is supposed to be low, to decide the sensor locations and, therefore, where to obtain information, it should be taken into account not only the measurement number, but also the structural part whose properties need to be identified. Only in this way, the optimum sensor deployment will be achieved in order to get the maximum of information (not being redundant) with the minimum uncertainty.

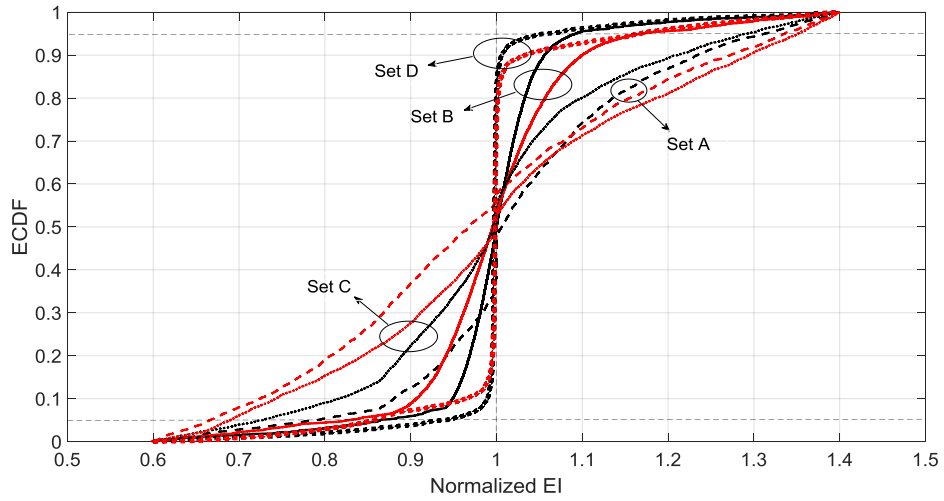

Figure 5-6. ECDF of estimated under different set considering aleatory uncertainty. The vertical dotted line represents the correct value, and the 5 and 95 percentiles are indicated with horizontal dotted lines.

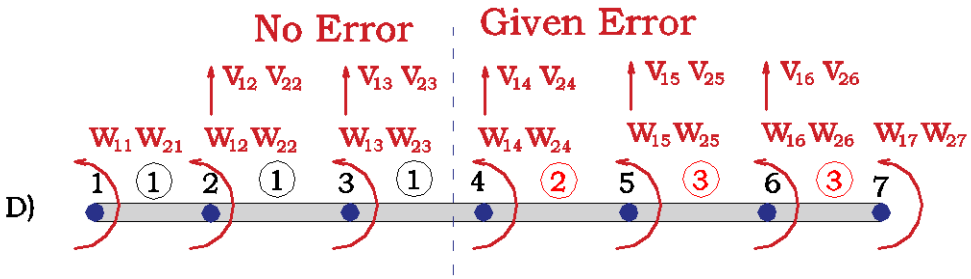

Figure 5-7. Measurement Set D

Table 5-5. Statistical data of the estimated EI_2 and EI_3 under different measurement sets

	EI_2				EI_3			
Measurement Set	A	B	C	D	A	B	C	D
p5	0.788	0.865	0.728	0.936	0.666	0.827	0.670	0.857
p95	1.313	1.092	1.292	1.060	1.336	1.169	1.352	1.165
p50	1.006	1.000	0.997	0.998	0.968	0.995	1.000	0.999
Range	0.525	0.227	0.564	0.124	0.67	0.342	0.682	0.308
Skewness	0.006	0.000	0.003	0.002	-0.032	-0.005	0.000	0.001
Mean (Bias)	1.032	1.003	0.980	0.998	0.997	1.000	1.007	0.997
Standard Deviation	0.144	0.064	0.195	0.053	0.152	0.099	0.191	0.087
Probability of Overestimated	56.8%	50.1%	49.8%	50.2%	45.7%	49.8%	49.5%	51.2%

5.3.3 Combination of epistemic uncertainty and aleatory uncertainty

The combination of the two types of errors, i.e., input-parameter error and measurement error, are considered, as well as the three measurement sets shown in Figure 5-3. The total calculation sample is 10^4 for each set by the fast optimal Latin hypercube (FOLH) sampling to produce the independent and representative samples and ensure the accuracy of MAC. The ECDF under this combination is shown in Figure 5-8, and the related numerical information is illustrated in Table 5-6.

When both aleatory and epistemic uncertainties are considered, the best measurement set in terms of the uncertainty range is Set C, which includes all the measurement information, instead of Set B that was identified as the best measurement set when considered the uncertainties individually. However, the results from Set C produce some skewness compared with the corresponding value in Tables 5-3 and 5-5, especially for EI_3, where a overestimation probability of 81.6% is observed. While in terms of structural safety, compared with the huge overestimation estimated of Set C, the results by Set A and Set B tend to be safer with lower percentage of overestimated, the former one performs better on the range and the latter one on the standard deviation. Set B results in the least skewed estimation when compared to the other two sets, while the values of the 5% and 95% percentiles are worse than the ones under Set C. Compared to Figures 5-4 and 5-6, the best measurement set in terms of accuracy is Set C rather than Set B, which highlights the importance of understanding the error source when trying to improve the quality of the estimation. When both model and measurement errors play an important role in the identification process, introducing as many measurements as possible is the best strategy because the information provided by them is not redundant in this case to improve the estimated accuracy. The result for Set C is slightly more biased (compared with the normalized value 1), however, with less uncertainty, as clearly shown by the rows of standard deviation and probability of overestimation in Table 5-6.

As a summary it can be concluded that both error sources, epistemic and measurement, interacts in a non-linear way due to the dynamic effects, in such a way that from the results of their individual effects it cannot be concluded what will happen when both sources act in a combined way. Hence, to study this, it is necessary to tackle both effects jointly and not in a disaggregate manner.

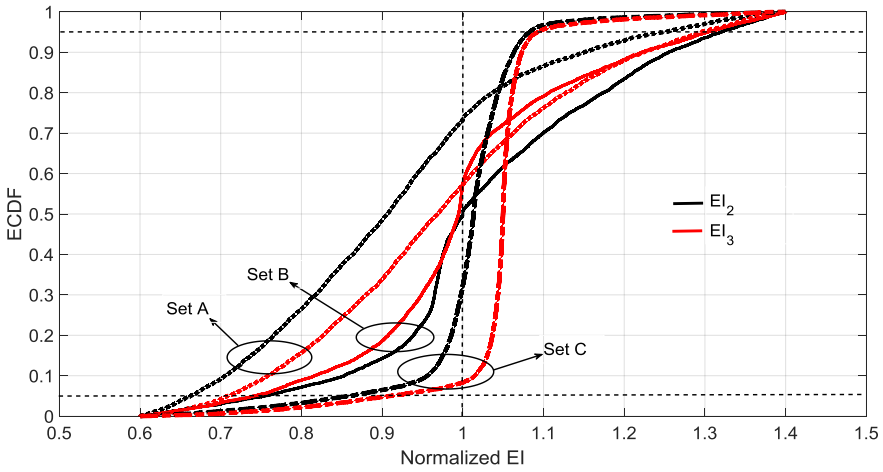

Figure 5-8. ECDF of estimated under different set considering aleatory and epistemic uncertainties. The vertical dotted line represents the correct value, and the 5 and 95 percentiles are indicated with horizontal dotted lines.

Table 5-6. Statistical data of the estimated EI_2 and EI_3 under different measurement sets

	EI_2			EI_3		
Measurement Set	A	B	C	A	B	C
p5	0.663	0.754	0.860	0.709	0.742	0.911
p95	1.250	1.320	1.080	1.295	1.304	1.094
p50	0.906	1.000	1.013	0.9691	0.9946	1.050
Range	0.587	0.566	0.222	0.586	0.562	0.183
Skewness	-0.094	0.000	0.013	-0.031	-0.005	0.050
Mean (Bias)	0.915	1.032	1.006	0.979	1.003	1.042
Standard Deviation	0.168	0.158	0.079	0.172	0.152	0.072
Probability of Overestimated	26.6%	49.9%	67.8%	42.8%	42.8%	81.6%

5.4 Discussion

Hollandse bridge was studied in InfraWatch project (Miao. s.f. et al 2013 & 2014, Veerman, R. 2017). After much effort in collecting and analysing data, no conclusive results were obtained in the structural identification process due to the large level of uncertainty. This fact has motivated the present work, because it is important to know in advance if the uncertainty related to a given SSI approach when applied to a specific structural setup is acceptable or not in real practice.

With proper sensor placement, the 90% confidence interval range of the estimated stiffness is found as small as 0.222 for EI_2 and 0.183 for EI_3 when considering both sources of uncertainty (Table 5-6). This means that the estimated stiffness presents around 10% of uncertainty to each direction given that the range is sensibly unbiased. This uncertainty range seems very reasonable if we consider the high level of uncertainty of the input variables (e.g., 50% in the case of the Young modulus or 30% in the rotation displacements).

To assess to which extent the dynamic COM provides acceptable results in terms of uncertainty when compared with other SSI methods in the literature, the example proposed by Simoen, E. et al. 2015, and further investigated in Peng, T. et al., 2020 and presented in Chapter 3.3.2 is used (see Figure 3-12). This is a reinforced concrete beam with a length of 6m divided into 10 substructures with a uniform stiffness value, as shown in Figure 3-13. The measured transverse mode shape displacements are observed at equidistant positions along the beam at 31 points. The resulting mode shape measurements are shown in Figure 3-13 with their corresponding natural frequencies. The stiffness of these 10 elements given in Reference (Simoen, E. et al. 2015), are taken as the real values for this beam. The considered measurement set includes the frequencies and vertical displacement at the 31 points given by the same reference. Regarding the errors considered, to introduce the epistemic uncertainty, given that it is a free-free vibration beam with unknown stiffness, only the input parameter, m is considered. It takes the common density of reinforced concrete $\rho = 2551\text{kg/m}^3$ (probabilistic distribution $N(1, 1 * 0.05)$, the same as in Table 5-2). The aleatory uncertainty has been calculated through the difference between the experimental bending modes and frequencies and the corresponding theoretical data at each of these 31 points. The average values of the obtained uncertainty are given in Table 5-7.

Table 5-7. Measurement input variables (averaged values for the 31 measured points)

	List of variables	Probabilistic Distribution	95% Confidence Interval
Structure in Figure 3-12	Frequencies ($f_i, i = \{1,4\}$)	$N(f_i,\ f_i * 0.005)$	$f_i\ (1 \pm 0.01)$
	Vertical displacements (v_{ik})	$N(v_{ik}, v_{ik} * 0.03)$	$v_{ik}\ (1 \pm 0.06)$

Considering the epistemic and aleatory uncertainty together, the sample size is determined based on the ECDF of MAC_i, as shown in Figure 5-9. The MAC_i distributions obtained for sample sizes of 10^3 and 10^4 are very close to each other, which implies that a sample size of 10^3 is enough to

guarantee the accuracy of MAC_i. Figure 5-10 shows the estimated unknown stiffnesses EI_i, $i = 1{\sim}10$, as well as their standard deviation. The COM tends to slightly underestimate the mean values of the stiffness when all mode-shape information is used. The stiffness range associated with the 99% confidence interval obtained by COM is shown in red colour in Figure 5-11, in comparison with the results reported by Simoen when using a Bayesian approach for the SSI (grey shadow). The real values are indicated with a thick black line. For all the elements, COM provides less uncertain estimations. All in all, this figure shows how the UQ associated with COM provides reasonable and acceptable results, and slightly better than the Bayesian approach. Figure 5-12 depicts the distribution of Young's moduli E_2 and E_8 by UQ analysis of COM (red line) and the distributions obtained by the Bayesian approach (grey line). It is shown that the proposed approach does not require a prior joint PDF to obtain an accurate stiffness probability distribution.

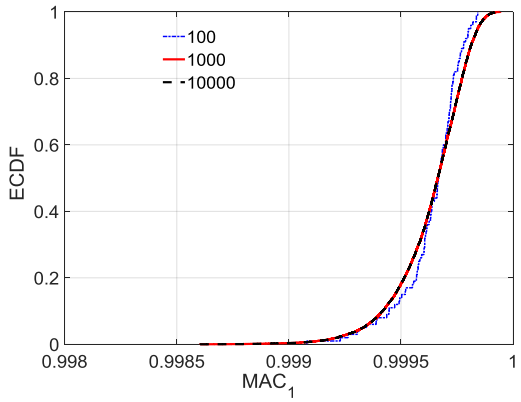

Figure 5-9. ECDF of MAC_1 under different sample sizes of RC beam

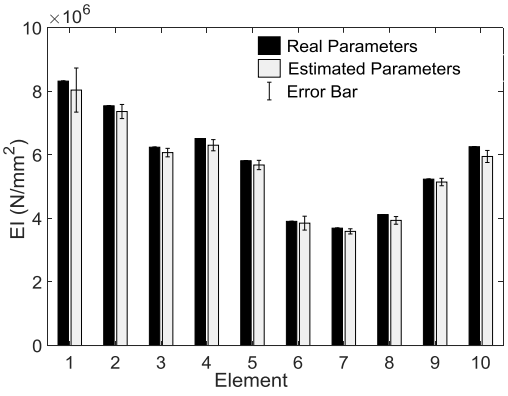

Figure 5-10. Uncertainty of $EI_i, i = 1{\sim}10$ given by the mean value and the standard deviation

Even when the obtained uncertainty is acceptable, it is always desirable to minimise such an uncertainty. The analysis of the two sources of uncertainty takes relevance in this context. For instance, it is appreciated that there is no bias and skewness in Table 5-3 (epistemic uncertainty), whereas obvious bias and skewness is presented in Tables 5-5 and 5-6, which mean these are caused by the sensor error. Thus, increasing the sensor accuracy might reduce the bias and skewness effects. Besides, compared to the estimated data of Sets A, B and C in Tables5-3, 5-5, and 5-6, the optimal sensor set shifts from Set B under a single source of uncertainty to Set C when considering both uncertainties. This means that selecting the optimal placement of the sensor sets is also an effective method to lower uncertainty of the output in addition to increase

the sensor accuracy. However, because the aleatory uncertainty is hard to remove, efforts must be made in minimizing the epistemic uncertainty involved in the problem. The more information about the structural setup, the closer the UQ of the SSI will be to the analysis of Section 5.4.2.

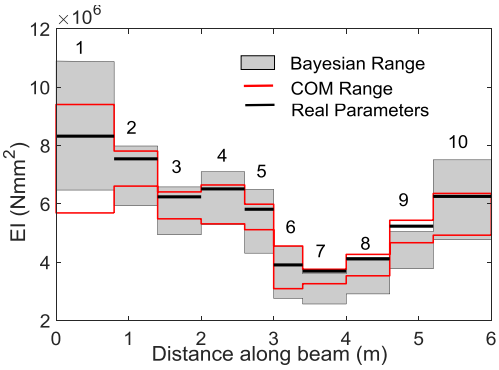

Figure 5-11. The stiffness range associated with the 99% confidence interval along the beam (the grey shadow represents the result by Bayesian analysis given in [4], the red line represents the range obtained by COM)

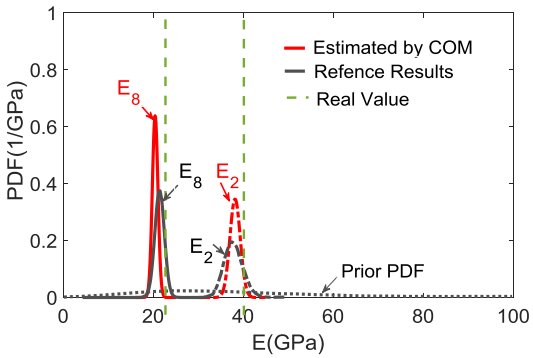

Figure 5-12. Uncertainty distribution of Young's modulus E_2 and E_8, prior and posterior PDF (grey line) of element Young's modulus according to [4], the red PDF by COM UQ analysis

5.5 Conclusions

The UQ analysis of the proposed dynamic COM method is carried out in this chapter. Two sources of uncertainty, that is, epistemic and aleatory, are studied separately and also together to better understand the role of modelling error and measurement error when dynamic COM is used. The following conclusions can be drawn:

The analysis of the error propagation in the case of the Hollandse bridge has made evident that when the epistemic uncertainty is low (i.e., when very accurate models are used in the identification process), the sensor deployment should take into account not only the measurement accuracy but also the location of unknown structural part. Only in this way, the optimum sensor placement will be achieved in order to get the maximum of information (not being redundant) with the minimum uncertainty. Feeding the model with redundant information (if, for instance the location of sensors is not conveniently chosen) can produce worse results, although more measurement points (more sensors) are deployed.

When both epistemic and aleatory uncertainties are relevant, the error propagation decreases with the increase of the measurement points. In this case, the results show that Set B, which includes 2 additional sensors, is biased to the overestimation side when compared to Set A. If the objective of the identification process is to detect damage, as damage will produce a reduction of the stiffness (due to cracking, for instance), it will be a better solution the use of fewer sensors, as the trend to the overestimation of the stiffness in the identified elements could hide the existence of damage. This appears as a contradictory conclusion, where the use of an increasing number of sensors derives on decreasing the potentiality of damage detection. However, this result is well in line with the result obtained in the case when only aleatory uncertainty is considered and stated in the previous paragraph, where the addition of more data measurements (Set C compared to Set B) resulted in a worse identification due to the redundancy in the information and the increase in the global measurement error introduced by the additional measurements.

The analysis of Hollandse bridge shows that the best measurement set will change from Set B to Set C in terms of range depending whether the epistemic uncertainty is involved or not. Therefore, before the field test execution, when deciding the optimal sensor deployment, it is important to consider the effect of epistemic uncertainty in the sense of trying to gather information from the test that is compatible and non-contradictory with the proposed model. The calculated mode shapes can help on this objective.

The correct performance of the UQ analysis by COM is verified by an example where the results from the Bayesian method are compared. The performance of the proposed approach is better despite the modelling error in the mass of the structure is considered. The results show the robustness of the method in terms of propagated uncertainty.

CHAPTER 6 Conclusions and future research

6.1 Conclusions

The major contributions of this work might be summarised as follows:

1) The first application of constrained observability techniques for parametric estimation of structures using dynamic information such as frequencies and mode-shapes is proposed.

2) A new algorithm is introduced based on the dynamic eigenvalue equation. One step by step example is used to illustrate the functioning of constrained observability techniques. In addition, the merit of the dynamic constrained observability analysis is demonstrated as a good solution to the fully observability which OM cannot achieve.

3) Two examples using experimental data are used as a proof of concept to verify the feasibility and accuracy of the proposed COM method.

4) A large frame structure is used to show the potential of this new application, whose structural properties can be obtain satisfactorily even if the real mechanical parameters are perturbed by random numbers in order to simulate measurement errors. The results show that the flexural stiffness of all elements can be estimated with errors smaller than 8%.

5) A machine learning decision tool, based on Decision Trees, to help building the best-combined strategy of SHM and SSI that can result in the most accurate estimations of the structural properties is proposed, and a combination of COM and CART algorithm is used for the first time.

6) Decision trees are firstly applied to investigate the influence of several variables (bridge layout, span length, measurement set, and weight factor) involved in the SHM+SSI process on the error estimation of the parameters in a general structure. This helps in the identification of the best sensor deployment and weight factors to be used in the objective function

7) The verification of the method with a real bridge with different levels of damage shows that the method is robust even in the case of identification of the structure with a high damage level, showing the SHM+SSI strategy that yields the most accurate parameter estimation.

8) In order to get the minimum uncertainty in the identified parameters, the sensor deployment should take into account the measurement accuracy and the location of the unknown structural parts to get the maximum of information with minimum uncertainty from the input parameters, thus avoiding redundant information from the measurement set, what in some cases can derive in more uncertain results.

9) The best measurement set is not a stable set and it depends on whether the epistemic uncertainty is involved or not. The effect of epistemic uncertainty in the objective of trying to gather maximum information from the test cannot be ignored when defining the experimental campaign

10) The UQ analysis by COM is verified by a reinforced concrete beam and compared with the Bayesian method. The COM approach is better than the Bayesian method, even considering that the epistemic uncertainty is involved.

6.2 Future research

The future research lines are summarized as follows.

1. The approach of COM (Constrained Observability Method) as formulated in this thesis does not consider the modeling error, such as the error introduced when making wrong assumptions on the support conditions. The future research can be extended towards this direction.

2. The decision tree algorithm proposed in Chapter 4 can be extended by adding different SSI methods to select the ones providing the most accurate results in each case. In addition, the operational effects due to traffic in the bridge on the final results were not considered in the present example and are a future line to be explored. The development of the SHM+SSI strategy for more slender structures is also worth of further investigation.

3. The implementation of the observability technique to the dynamic eigenvalue equation may not provide enough accurate results when dealing with real structures, either because of the

existence of damping or torsion, which have not been considered in this work. To do so, the general dynamic equation should be used and its applicability studied.

4. The identification of the structures presented in this work is based on measurements obtained numerically with a Matlab program. However, to further check the reliability of the proposed method in real structures, more cases using dynamic measurements taken on site should be analysed.

5. The sensor optimal placement based on the dynamic Constrained Observability Method (COM) needs to develop further based on some sensor placement guidance in this thesis.

6.3 Related works and publications

1. T. Peng, M. Nogal, J.R. Casas, J.A. Lozano-Galant and J. Turmo*, Constrained observability techniques for structural system identification using modal analysis. *Journal of Sound and Vibration*, 479, p.115368 (2020). https://doi.org/10.1016/j.jsv.2020.115368.

2. T. Peng, M. Nogal*, J.R. Casas, J. Turmo. Planning low-error SHM strategy by Constrained Observability Method. *Automation in Construction*. (Accepted).

3. T. Peng, M. Nogal*, J.R. Casas, J. Turmo. Role of sensors in error propagation with the dynamic constrained observability method: Application to the Hollandse Brug. *Sensors*. (Under review).

4. T. Peng*, J.R. Casas, J. Turmo. Dynamic Observability Method for Durability Assessment Considering Measurement Noise. *DBMC 2020*, Barcelona, Oct, 23-24, 2020.

5. T. Peng*, J.R. Casas, J. Turmo. Analysis using modal information in SSI by dynamic observability method. *IABMAS 2020*. Hokkaido, April 11-15, 2021

6. T. Peng*, J.R. Casas, J. Turmo. The Dynamic Assessment of Structural condition by Measurement Error-Minimizing Observability Method. *IALCCE2020*. Shanghai, 27th,Oct. 2020.

References

1. Abdeljaber, O., Avci, O., Kiranyaz, S., Gabbouj, M., & Inman, D. (2017). Real-time vibration-based structural damage detection using one-dimensional convolutional neural networks. *Journal of Sound And Vibration*, 388, 154-170. https://doi.org/10.1016/j.jsv.2016.10.043.
2. Al-Wazeer, A. (2007). Risk-based Bridge Maintenance Strategies, *Ph.D. Dissertation*, University of Maryland.
3. ASCE (2013). Report Card for America's Infrastructure. Retrieved September 23, 2014, from http://www.infrastructurereportcard.org/a/#p/bridges/overview.
4. Baudrit, C., Dubois, D., & Perrot, N. (2008). Representing parametric probabilistic models tainted with imprecision. *Fuzzy Sets And Systems*, 159(15), 1913-1928. https://doi.org/10.1016/j.fss.2008.02.013
5. Bel, L., Allard, D., Laurent, J., Cheddadi, R., & Bar-Hen, A. (2009). CART algorithm for spatial data: Application to environmental and ecological data. *Computational Statistics & Data Analysis*, 53(8), 3082-3093. https://doi.org/10.1016/j.csda.2008.09.012
6. Ben-Haim, Y., Cogan, S., & Sanseigne, L. (1998). Usability of mathematical models in mechanical decision processes. *Mechanical Systems And Signal Processing*, 12(1), 121-134. https://doi.org/10.1006/mssp.1996.0137
7. Bentz, E., & Hoult, N. (2017). Bridge model updating using distributed sensor data. *Proceedings of The Institution of Civil Engineers - Bridge Engineering*, 170(1), 74-86. https://doi.org/10.1680/jbren.15.00030.
8. Breiman, L. (1984). Classification and regression trees. *Wadsworth Int Group*.
9. Brincker, R., Ventura, C. (2015).Introduction to operational modal analysis. *John Wiley & Sons*.
10. Brownjohn, J., & Xia, P. (2000). Dynamic Assessment of Curved Cable-Stayed Bridge by Model Updating. *Journal of Structural Engineering*, 126(2), 252-260. https://doi.org/10.1061/(asce)0733-9445(2000)126:2(252)
11. Bungey, H.B., Millard, G.M., & Grantham G.M. (1995). Testing of concrete in structures, *CRC Press*.
12. Cao, J., Xiong, H., Chen, J., & Huynh, A. (2019). Bayesian parameter identification for empirical model of CLT connections. *Construction And Building Materials*, 218, 254-269. https://doi.org/10.1016/j.conbuildmat.2019.05.051
13. Cao, L., Liu, J., Xie, L., Jiang, C., & Bi, R. (2021). Non-probabilistic polygonal convex set model for structural uncertainty quantification. *Applied Mathematical Modelling*, 89, 504-518. https://doi.org/10.1016/j.apm.2020.07.025
14. Cao, M., Pan, L., Gao, Y., Novák, D., Ding, Z., Lehký, D., & Li, X. (2015). Neural network ensemble-based parameter sensitivity analysis in civil engineering systems. *Neural Computing And Applications*, 28(7), 1583-1590. https://doi.org/10.1007/s00521-015-2132-4

15. Castillo, E., Conejo, A., Eva Pruneda, R., & Solares, C. (2007). Observability in linear systems of equations and inequalities: Applications. *Computers & Operations Research*, 34(6), 1708-1720. https://doi.org/10.1016/j.cor.2005.05.035.
16. Castillo, E., Conejo, A., Pruneda, R., & Solares, C. (2006). Observability Analysis in State Estimation: A Unified Numerical Approach. *IEEE Transactions On Power Systems*, 21(2), 877-886. https://doi.org/10.1109/tpwrs.2006.873418
17. Castillo, E., Jimenez, P., Menendez, J., & Conejo, A. (2008). The Observability Problem in Traffic Models: Algebraic and Topological Methods. *IEEE Transactions On Intelligent Transportation Systems*, 9(2), 275-287. https://doi.org/10.1109/tits.2008.922929
18. Castillo, E., Nogal, M., Rivas, A., & Sánchez-Cambronero, S. (2013). Observability of traffic networks. Optimal location of counting and scanning devices. *Transportmetrica B: Transport Dynamics*, 1(1), 68-102. https://doi.org/10.1080/21680566.2013.780987
19. Castillo, E., Lozano-Galant, J., Nogal, M., & Turmo, J. (2015). New tool to help decision making in civil engineering. *Journal of Civil Engineering And Management*, 21(6), 689-697. https://doi.org/10.3846/13923730.2014.893904.
20. Castillo, E., Nogal, M., Lozano-Galant, J., & Turmo, J. (2016). Solving Some Special Cases of Monomial Ratio Equations Appearing Frequently in Physical and Engineering Problems. *Mathematical Problems In Engineering*, 2016, 1-25. https://doi.org/10.1155/2016/9764913
21. Chandra, B., & Varghese, P. (2008). Fuzzy SLIQ Decision Tree Algorithm. *IEEE Transactions On Systems, Man, And Cybernetics, Part B (Cybernetics)*, 38(5), 1294-1301. https://doi.org/10.1109/tsmcb.2008.923529
22. Chee, C. (2017). A mixture model-based nonparametric approach to estimating a count distribution. *Computational Statistics & Data Analysis*, 109, 34-44. https://doi.org/10.1016/j.csda.2016.11.012
23. Chen, J., Wadhwa, N., Cha, Y., Durand, F., Freeman, W., & Buyukozturk, O. (2015). Modal identification of simple structures with high-speed video using motion magnification. *Journal of Sound And Vibration*, 345, 58-71. https://doi.org/10.1016/j.jsv.2015.01.024
24. Choi, C., & Yoo, H. (2016). Stochastic inverse method to identify parameter random fields in a structure. *Structural And Multidisciplinary Optimization*, 54(6), 1557-1571. https://doi.org/10.1007/s00158-016-1534-y
25. Christodoulou, K., & Papadimitriou, C. (2007). Structural identification based on optimally weighted modal residuals. *Mechanical Systems And Signal Processing*, 21(1), 4-23. https://doi.org/10.1016/j.ymssp.2006.05.011
26. Der Kiureghian, A., & Ditlevsen, O. (2009). Aleatory or epistemic? Does it matter?. *Structural safety*, 31(2), 105-112. https://doi.org/10.1016/j.strusafe.2008.06.020
27. Drygala, Izabela J., Dulinska, Joanna M., & Polak, Maria A. (2020). Seismic Assessment of Footbridges under Spatial Variation of Earthquake Ground Motion (SVEGM): Experimental Testing and Finite Element Analyses, *Sensors*, 20, no. 4: 1227. https://doi.org/10.3390/s20041227

28. Emadi, S., Lozano-Galant, J., & Xia, Y.. (2019). Structural system identification including shear deformation of composite bridges from vertical deflections. *Steel and Composite Structures.* 32(6), pp.731–741. https://doi.org/10.12989/SCS.2019.32.6.731.
29. Eskew, E., & Jang, S. (2016). Remaining stiffness estimation of buildings using incomplete measurements. *Structural Control And Health Monitoring*, 24(4), e1899. https://doi.org/10.1002/stc.1899
30. Ewins, D. (2000). Modal testing. Research Studies Press.
31. Faes, M., & Moens, D. (2019). Recent Trends in the Modeling and Quantification of Non-probabilistic Uncertainty. *Archives of Computational Methods In Engineering*, 27(3), 633-671. https://doi.org/10.1007/s11831-019-09327-x
32. Farhat, C., & Hemez, F. (1993). Updating finite element dynamic models using an element-by-element sensitivity methodology. *AIAA Journal*, 31(9), 1702-1711. https://doi.org/10.2514/3.11833
33. Farhey, D. (2018). Material Structural Deficiencies of Road Bridges in the U.S. *Infrastructures*, 3, 2. https://doi.org/10.3390/infrastructures3010002
34. FHWA (2018). Bridge Deck Preservation Guide. Publication No. FHWA-HIF-18-022. Washington, D.C.
35. Garc á, O., Veh í J., Matos, J., Henriques, A., Casas, J.R. (2008). Structural assessment under uncertain parameters via interval analysis. *Journal of Computational and Applied Mathematics* 218, 43 – 52. https://doi.org/10.1016/j.cam.2007.04.047
36. Guo, Y., Ni, Y., & Chen, S. (2016) . Optimal sensor placement for damage detection of bridges subject to ship collision. *Structural Control And Health Monitoring*. 24(9), e1963. https://doi.org/10.1002/stc.1963
37. Haag, T., Carvajal Gonz ález, S., & Hanss, M. (2012). Model validation and selection based on inverse fuzzy arithmetic. *Mechanical Systems And Signal Processing*, 32, 116-134. https://doi.org/10.1016/j.ymssp.2011.09.028
38. Hajela, P., & Soeiro, F. (1990). Structural damage detection based on static and modal analysis. *AIAA Journal*, 28(6), 1110-1115. https://doi.org/10.2514/3.25174
39. Han, L., Zhang, J., & Yang, Y. (2014). Optimal Placement of Sensors for Monitoring Systems on Suspension Bridges Using Genetic Algorithms. *Applied Mechanics And* Materials, 530-531, 320-331. https://doi.org/10.4028/www.scientific.net/amm.530-531.320
40. Hanss, M. (2005). Applied fuzzy arithmetic: an introduction with engineering applications. *Springer*, Berlin.
41. Haralampidis, Y., Papadimitriou, C., & Pavlidou, M. (2005). Multi-objective framework for structural model identification. *Earthquake Engineering & Structural Dynamics*, 34(6), 665-685. https://doi.org/10.1002/eqe.449
42. Harrington, P. (2012). Machine Learning in Action. Manning Publications Co.
43. Hasni, H., Jiao, P., Alavi, A., Lajnef, N., & Masri, S. (2018). Structural health monitoring of steel frames using a network of self-powered strain and acceleration sensors: A numerical study. *Automation In Construction*, 85, 344-357. https://doi.org/10.1016/j.autcon.2017.10.022
44. Hjelmstad, K., Banan, M., & Banan, M. (1995). On building finite element models of structures from modal response. *Earthquake Engineering & Structural Dynamics*, 24(1), 53-67. https://doi.org/10.1002/eqe.4290240105

45. Hjelmstad, K., & Shin, S. (1997). Damage Detection and Assessment of Structures from Static Response. *Journal of Engineering Mechanics*, 123(6), 568-576. https://doi.org/10.1061/(asce)0733-9399(1997)123:6(568)

46. Hosoya, N., Ozawa, S., & Kajiwara, I. (2019). Frequency response function measurements of rotational degrees of freedom using a non-contact moment excitation based on nanosecond laser ablation. *Journal of Sound And Vibration*, 456, 239-253. https://doi.org/10.1016/j.jsv.2019.05.024

47. Hou, R., Xia, Y., Xia, Q., & Zhou, X. (2018). Genetic algorithm based optimal sensor placement forL1-regularized damage detection. *Structural Control And Health Monitoring*, 26(1), e2274. https://doi.org/10.1002/stc.2274

48. Huang, C., Hung, S., Lin, C., & Su, W. (2005). A Wavelet-Based Approach to Identifying Structural Modal Parameters from Seismic Response and Free Vibration Data. *Computer-Aided Civil And Infrastructure Engineering*, 20(6), 408-423. https://doi.org/10.1111/j.1467-8667.2005.00406.x

49. Hu, Z., Ao, D., & Mahadevan, S. (2017). Calibration experimental design considering field response and model uncertainty. *Computer Methods In Applied Mechanics And Engineering*, 318, 92-119. https://doi.org/10.1016/j.cma.2017.01.007

50. Huang, T., & Schröder, K. (2021). A Bayesian probabilistic approach for damage identification in plate structures using responses at vibration nodes. *Mechanical Systems And Signal Processing*, 146, 106998. https://doi.org/10.1016/j.ymssp.2020.106998

51. Jaishi, B., & Ren, W. (2005). Structural Finite Element Model Updating Using Ambient Vibration Test Results. *Journal of Structural Engineering*, 131(4), 617-628. https://doi.org/10.1061/(asce)0733-9445(2005)131:4(617)

52. Jang, J., & Smyth, A. (2017). Bayesian model updating of a full-scale finite element model with sensitivity-based clustering. *Structural Control And Health Monitoring*, 24(11), e2004. https://doi.org/10.1002/stc.2004

53. Jena, S., Chakraverty, S., & Malikan, M. (2020). Implementation of non-probabilistic methods for stability analysis of nonlocal beam with structural uncertainties. *Engineering With Computers*. https://doi.org/10.1007/s00366-020-00987-z

54. Josa, I. (2017). Dynamic structural system identification, *Master Thesis*, Universidad Politécnica de Catalunya.

55. Juang, J. & Phan, M. (1994). Linear system identification via backward-time observer models. *Journal of Guidance, Control, And Dynamics*, 17(3), 505-512. https://doi.org/10.2514/3.21227

56. Kammer, D. (1991). Sensor Placement for On-Orbit Modal Identification and Correlation of LargeSpace Structures. *Journal of Guidance, Control, and Dynamics*, 14(2):251–9. https://doi.org/ 10.2514/3.20635

57. Kijewski, T., & Kareem, A. (2003). Wavelet Transforms for System Identification in Civil Engineering. *Computer-Aided Civil And Infrastructure Engineering*, 18(5), 339-355. https://doi.org/10.1111/1467-8667.t01-1-00312

58. Lam, H., & Yang, J. (2015). Bayesian structural damage detection of steel towers using measured modal parameters. *Earthquakes And Structures*, 8(4), 935-956. https://doi.org/10.12989/eas.2015.8.4.935
59. Lam, H.F. (1998). Structural model updating and health monitoring in the presence of modeling uncertainties, *P.h. D thesis*, Department of Civil Engineering, Hong Kong University of Science and Technology, Hong Kong.
60. Legault, J., Langley, R., & Woodhouse, J. (2012). Physical consequences of a nonparametric uncertainty model in structural dynamics. *Journal of Sound And Vibration*, 331(25), 5469-5487. https://doi.org/10.1016/j.jsv.2012.07.017
61. Lei, J., Lozano-Galant, J., Nogal, M., Xu, D., & Turmo, J. (2016). Analysis of measurement and simulation errors in structural system identification by observability techniques. *Structural Control And Health Monitoring*, 24(6), e1923. https://doi.org/10.1002/stc.1923
62. Lei, J., Lozano‐Galant, J., Xu, D., & Turmo, J. (2019). Structural system identification by measurement error‐minimizing observability method. *Structural Control And Health Monitoring*, 26(10). https://doi.org/10.1002/stc.2425
63. Lei, J., Nogal, M., Lozano-Galant, J., Xu, D., & Turmo, J. (2017). Constrained observability method in static structural system identification. *Structural Control And Health Monitoring*, 25(1), e2040. https://doi.org/10.1002/stc.2040
64. Lei, J., Xu, D., & Turmo, J. (2017). Static structural system identification for beam-like structures using compatibility conditions. *Structural Control And Health Monitoring*, 25(1), e2062. https://doi.org/10.1002/stc.2062
65. Li, H., Ke, L., Yang, J., Kitipornchai, S., & Wang, Y. (2020). Free vibration of variable thickness FGM beam submerged in fluid. *Composite Structures*, 233, 111582. https://doi.org/10.1016/j.compstruct.2019.111582
66. Li, S., Laima, S., & Li, H. (2018). Data-driven modeling of vortex-induced vibration of a long-span suspension bridge using decision tree learning and support vector regression. J*ournal of Wind Engineering And Industrial Aerodynamics*, 172, 196-211. https://doi.org/10.1016/j.jweia.2017.10.022
67. Li, S., Laima, S., & Li, H. (2018). Data-driven modeling of vortex-induced vibration of a long-span suspension bridge using decision tree learning and support vector regression. *Journal of Wind Engineering And Industrial Aerodynamics*, 172, 196-211. https://doi.org/10.1016/j.jweia.2017.10.022
68. Li, Z., Park, H., & Adeli, H. (2016). New method for modal identification of super high-rise building structures using discretized synchrosqueezed wavelet and Hilbert transforms. *The Structural Design of Tall And Special Buildings*, 26(3), e1312. https://doi.org/10.1002/tal.1312
69. Liu, W., Gao, W., Sun, Y., & Xu, M. (2008). Optimal sensor placement for spatial lattice structure based on genetic algorithms. *Journal of Sound And Vibration*, 317(1-2), 175-189. https://doi.org/10.1016/j.jsv.2008.03.026

70. Lozano-Galant, J., Nogal, M., Castillo, E., & Turmo, J. (2013). Application of Observability Techniques to Structural System Identification. *Computer-Aided Civil And Infrastructure Engineering*, 28(6), 434-450. https://doi.org/10.1111/mice.12004

71. Lozano-Galant, J., Nogal, M., Paya-Zaforteza, I., & Turmo, J. (2014). Structural system identification of cable-stayed bridges with observability techniques. *Structure And Infrastructure Engineering*, 10(11), 1331-1344. https://doi.org/10.1080/15732479.2013.807292

72. Lozano-Galant, J, Nogal, M., & Turmo, J. (2015). Selection of measurement sets in static structural identification of bridges using observability trees. *Computers And Concrete*. 15(5). https://doi.org/10.12989/cac.2015.15.5.771

73. Maes, K., Peeters, J., Reynders, E., Lombaert, G., & De Roeck, G. (2013). Identification of axial forces in beam members by local vibration measurements. *Journal of Sound And Vibration*, 332(21), 5417-5432. https://doi.org/10.1016/j.jsv.2013.05.017

74. Mares, C., Friswell, M., & Mottershead, J. (2002). Model updating using robust estimation. *Mechanical Systems And Signal Processing*, 16(1), 169-183. https://doi.org/10.1006/mssp.2000.1375

75. Melhem, H., Cheng, Y., Kossler, D., & Scherschligt, D. (2003). Wrapper Methods for Inductive Learning: Example Application to Bridge Decks. *Journal of Computing In Civil Engineering*, 17(1), 46-57. https://doi.org/10.1061/(asce)0887-3801(2003)17:1(46)

76. Miao, Sf. (2014). Structural health monitoring meets data mining. *P.h. D thesis*. Delft University of Technology.

77. Meo, M., & Zumpano, G. (2005). On the optimal sensor placement techniques for a bridge structure. *Engineering Structures*, 27(10), 1488-1497. https://doi.org/10.1016/j.engstruct.2005.03.015

78. Miao S, Veerman R, Koenders E. Modal analysis of a concrete highway bridge-structural calculations and vibration-based results. *The 6th International Conference on Structural Health Monitoring of Intelligent Infrastructure*. Hong Kong, China, Dec 9-11, 2013.

79. Moens, D., & Hanss, M. (2011). Non-probabilistic finite element analysis for parametric uncertainty treatment in applied mechanics: Recent advances. *Finite Elements In Analysis And Design*, 47(1), 4-16. https://doi.org/10.1016/j.finel.2010.07.010

80. Möller, B., & Beer, M. (2008). Engineering computation under uncertainty – Capabilities of non-traditional models. *Computers & Structures*, 86(10), 1024-1041. https://doi.org/10.1016/j.compstruc.2007.05.041

81. Nie, Z., Guo, E., Li, J., Hao, H., Ma, H., & Jiang, H. (2020). Bridge condition monitoring using fixed moving principal component analysis. *Structural Control And Health Monitoring*, 27(6). https://doi.org/10.1002/stc.2535

82. Ni, Y., Alamdari, M., Ye, X., & Zhang, F. (2021). Fast operational modal analysis of a single-tower cable-stayed bridge by a Bayesian method. *Measurement*, 174, 109048. https://doi.org/10.1016/j.measurement.2021.109048

83. Nogal, M., Lozano-Galant, J., Turmo, J., & Castillo, E. (2015). Numerical damage identification of structures by observability techniques based on static loading tests. *Structure And Infrastructure Engineering*, 12(9), 1216-1227. https://doi.org/10.1080/15732479.2015.1101143

84. Oberkampf, W., DeLand, S., Rutherford, B., Diegert, K., & Alvin, K. (2002). Error and uncertainty in modeling and simulation. *Reliability Engineering & System Safety*, 75(3), 333-357. https://doi.org/10.1016/S0951-8320(01)00120-X

85. Park, H., & Oh, B. (2018). Real-time structural health monitoring of a supertall building under construction based on visual modal identification strategy. *Automation In Construction*, 85, 273-289. https://doi.org/10.1016/j.autcon.2017.10.025

86. Peng, T., Nogal, M., Casas, J., Lozano-Galant, J., & Turmo, J. (2020). Constrained observability techniques for structural system identification using modal analysis. *Journal of Sound And Vibration*, 479, 115368. https://doi.org/10.1016/j.jsv.2020.115368

87. Perera, R., Marin, R., & Ruiz, A. (2013). Static–dynamic multi-scale structural damage identification in a multi-objective framework. *Journal of Sound And Vibration*, 332(6), 1484-1500. https://doi.org/10.1016/j.jsv.2012.10.033

88. Pimentel, M., & Figueiras, J. (2017). Assessment of an existing fully prestressed box-girder bridge. *Proceedings of The Institution of Civil Engineers - Bridge Engineering*, 170(1), 42-53. https://doi.org/10.1680/jbren.15.00014

89. Proske, D. (2020). Fatalities due to bridge collapse. *Proceedings of The Institution of Civil Engineers - Bridge Engineering*, 1-24. https://doi.org/10.1680/jbren.20.00001

90. Quinlan, J. (1986). Induction of decision trees. *Machine Learning* 1, 81–106. https://doi.org/10.1007/BF00116251

91. Raich, A., & Liszkai, T. (2011). Multi-objective Optimization of Sensor and Excitation Layouts for Frequency Response Function-Based Structural Damage Identification. *Computer-Aided Civil And Infrastructure Engineering*, 27(2), 95-117. https://doi.org/10.1111/j.1467-8667.2011.00726.x

92. Salazar, F., Toledo, M., González, J., & Oñate, E. (2017). Early detection of anomalies in dam performance: A methodology based on boosted regression trees. *Structural Control And Health Monitoring*, 24(11), e2012. https://doi.org/10.1002/stc.2012

93. Salzberg, S. (1995). Locating Protein Coding Regions in Human DNA Using a Decision Tree Algorithm. *Journal of Computational Biology*, 2(3), 473-485. https://doi.org/10.1089/cmb.1995.2.473

94. Sanayei, M., Arya, B., Santini, E., & Wadia-Fascetti, S. (2001). Significance of Modeling Error in Structural Parameter Estimation. *Computer-Aided Civil And Infrastructure Engineering*, 16(1), 12-27. https://doi.org/10.1111/0885-9507.00210

95. Sankararaman, S., Ling, Y., & Mahadevan, S. (2011). Uncertainty quantification and model validation of fatigue crack growth prediction. *Engineering Fracture Mechanics*, 78(7), 1487-1504. https://doi.org/10.1016/j.engfracmech.2011.02.017

96. Saydam, D. (2007). Reliability and Risk of Structural Systems under Progressive and Sudden Damage, *Thesis and Dissertation*, 2007,Paper 1616, Lehigh University, Lehigh Preserver.

97. Simoen, E., Roeck, G.D., & Lombaert, G. (2015). Dealing with uncertainty in model updating for damage assessment:a review, *Mechanical Systems and Signal Processing*. 56(2015), 123-149. https://doi.org/10.1016/j.ymssp.2014.11.001.

98. Soize, C. (2000). A nonparametric model of random uncertainties for reduced matrix models in structural dynamics. *Probabilistic Engineering Mechanics*, 15(3), 277-294. https://doi.org/10.1016/S0266-8920(99)00028-4

99. Soize, C. (2003). Random matrix theory and non-parametric model of random uncertainties in vibration analysis. *Journal of Sound And Vibration*, 263(4), 893-916. https://doi.org/10.1016/S0022-460X(02)01170-7

100. Soize, C. (2005). Random matrix theory for modeling uncertainties in computational mechanics. *Computer Methods In Applied Mechanics And Engineering*, 194(12-16), 1333-1366. https://doi.org/10.1016/j.cma.2004.06.038

101. Soize, C. (2005). A comprehensive overview of a non-parametric probabilistic approach of model uncertainties for predictive models in structural dynamics. *Journal of Sound And Vibration*, 288(3), 623-652. https://doi.org/10.1016/j.jsv.2005.07.009

102. Soize, C. (2009). Generalized probabilistic approach of uncertainties in computational dynamics using random matrices and polynomial chaos decompositions. *International Journal for Numerical Methods In Engineering*, 81(8), 939-970. https://doi.org/10.1002/nme.2712

103. Song, J., Lee, E., & Eun, H. (2021). Optimal sensor placement through expansion of static strain measurements to static displacements. *International Journal of Distributed Sensor Networks*, 17(1), 155014772199171. https://doi.org/10.1177%2F1550147721991712

104. Spiridonakos, M., & Fassois, S. (2009). Parametric identification of a time-varying structure based on vector vibration response measurements. *Mechanical Systems And Signal Processing*, 23(6), 2029-2048. https://doi.org/10.1016/j.ymssp.2008.11.004

105. Stutz, L., Tenenbaum, R., & Corrêa, R. (2015). The Differential Evolution method applied to continuum damage identification via flexibility matrix. Journal of Sound And Vibration, 345, 86-102. https://doi.org 10.1016/j.jsv.2015.01.049

106. Sunca, F., Okur, F., Altunişik, A., & Kahya, V. (2020). Optimal Sensor Placement for Laminated Composite and Steel Cantilever Beams by the Effective Independence Method. *Structural Engineering International*, 31(1), 85-92. https://doi.org10.1080/10168664.2019.1704202

107. Tarinejad, R., & Damadipour, M. (2014). Modal identification of structures by a novel approach based on FDD-wavelet method. Journal of Sound And Vibration, 333(3), 1024-1045. https://doi.org/10.1016/j.jsv.2013.09.038

108. Teughels, A., Maeck, J., Roeck, G.D. (2001). A finite element model updating method using experimental modal parameters applied on a railway bridge. *Proceedings 7th In. Conference on Computer Aided Optimum Design of Structures*, Bologna, Italy, 97–106.

109. Tomàs, D., Lozano-Galant, J., Ramos, G., & Turmo, J. (2018). Structural system identification of thin web bridges by observability techniques considering shear deformation. *Thin-Walled Structures*, 123, 282-293. https://doi.org/10.1016/j.tws.2017.11.017

110. Torres Cedillo, S., & Bonello, P. (2016). An equivalent unbalance identification method for the balancing of nonlinear squeeze-film damped rotordynamic systems. *Journal of Sound And Vibration*, 360, 53-73. https://doi.org/10.1016/j.jsv.2015.08.028

111. Veerman R. (2017). Deflections and Natural Frequencies as Parameters for Structural Health Monitoring. P.h.D thesis. Delft University of Technology.

112. Viana, F., Venter, G., & Balabanov, V. (2009). An algorithm for fast optimal Latin hypercube design of experiments. *International Journal for Numerical Methods In Engineering*, 82(2), 135-156. https://doi.org/10.1002/nme.2750

113. Viola, E., & Bocchini, P. (2013). Non-destructive parametric system identification and damage detection in truss structures by static tests. *Structure And Infrastructure Engineering*, 9(5), 384-402. https://doi.org/10.1080/15732479.2011.560164

114. Wang, C., Qiu, Z., Xu, M., & Li, Y. (2017). Novel reliability-based optimization method for thermal structure with hybrid random, interval and fuzzy parameters. *Applied Mathematical Modelling*, 47, 573-586. https://doi.org/10.1016/j.apm.2017.03.053

115. Wang, Y., & Elhag, T. (2007). A fuzzy group decision making approach for bridge risk assessment. *Computers & Industrial Engineering*, 53(1), 137-148. https://doi.org/10.1016/j.cie.2007.04.009

116. Xiong, H.B ., Cao, J.X. & Zhang, F..L. (2019). Investigation of the SHM-oriented model and dynamic characteristics of a super-tall building, *Smart Structure System*, 23(3): 295-306. https://doi.org/10.12989/sss.2019.23.3.295

117. Yehia, S., Abudayyeh, O., Fazal, I., & Randolph, D. (2008). A decision support system for concrete bridge deck maintenance. *Advances In Engineering Software*, 39(3), 202-210. https://doi.org/10.1016/j.advengsoft.2007.02.002

118. Zadeh, L.A. (1965). Fuzzy sets, *Information and Control*, 8(3):338-353. https://doi.org/10.1016/S0019-9958(65)90241-X

119. Zárate, B., & Caicedo, J. (2008). Finite element model updating: Multiple alternatives. *Engineering Structures*, 30(12), 3724-3730. https://doi.org/10.1016/j.engstruct.2008.06.012

120. Zhang, F., Xiong, H., Shi, W. & Ou, X. (2016). Structural health monitoring of Shanghai Tower during different stages using a Bayesian approach. *Structural Control And Health Monitoring*, 23(11), 1366-1384. https://doi.org/10.1002/stc.1840

121. Zhao, J., & DeWolf, J. (2002). Dynamic Monitoring of Steel Girder Highway Bridge. *Journal of Bridge Engineering*, 7(6), 350-356. https://doi.org/10.1061/(asce)1084-0702(2002)7:6(350)

122. Zhou, S., Sheng, W., Deng, F., Wu, X., & Fu, Z. (2017). A novel passive wireless sensing method for concrete chloride ion concentration monitoring. *Sensors* , 17, 2871. https://doi.org/10.3390/s17122871

123. Zhou, Z., & Adeli, H. (2003). Time-Frequency Signal Analysis of Earthquake Records Using Mexican Hat Wavelets. *Computer-Aided Civil And Infrastructure Engineering*, 18(5), 379-389. https://doi.org/10.1111/1467-8667.t01-1-00315

Appendix 1. List of symbols and notation

Symbol	Significance
$\mathbf{B}$	Total coefficient matrix
$\mathbf{B}_i$	Coefficient matrix of i^{th} mode
$\mathbf{B}_{om}$	Coefficient matrix from the last recursive step by OM
$\mathbf{B}^*$	Coefficient matrix from the last recursive step by COM
$\mathbf{D}$	Total constant vector
$\mathbf{D}_i$	Constant vector of i^{th} mode
$\mathbf{D}_{om}$	Constant vector from the last recursive step by OM
E_{level}	Error level in the measurement
EA_j	Axial stiffness of j^{th} element
EI_j	Flexural stiffness of j^{th} element
$\tilde{f}$	Hypothetical measurement frequencies
$\mathbf{f}$	Vector of forces
$\mathbf{K}$	Stiffness matrix
$\mathbf{K}^*$	Modified stiffness matrices of static analysis
$[\mathbf{K}_i^*]$	Modified stiffness matrices of i^{th} mode
L_j	Length of j^{th} element
m_j	Mass density of j^{th} element
$\mathbf{M}$	Mass matrix
$\mathbf{M}_i^*$	Modified mass matrices of i^{th} mode
N_B	Number of boundary condition
N_N	Number of nodes
$[V]$	Null space of $\mathbf{B}$
R	Total number of modes considered
u_{ik}	Horizontal displacement of k^{th} point and i^{th} mode
v_{ik}	Vertical displacement of k^{th} point and i^{th} mode
w_{ik}	Rotation of k^{th} point under i^{th} mode
W_λ	Weighting factors of squared frequencies
$W_\emptyset$	Weighting factors of mode-shapes
$\mathbf{z}$	Total vector of OM unknowns
$\mathbf{z}_i$	Vector of unknowns of i^{th} mode
$\mathbf{z}_{nh}$	Vector of homogeneous solution
$\mathbf{z}_{om}$	Vector of unknowns from the last recursive step by OM
$\mathbf{z}_p$	Particular solution
$\mathbf{z}^*$	Total vector of COM unknowns
z_c	Coupled variables unknowns
z_n	Subset of new identified singles variable
z_s	Single variables unknowns
$\boldsymbol{\delta}$	Vector of displacements
$\boldsymbol{\delta}^*$	Vector of knowns and unknowns of static analysis
$\boldsymbol{\epsilon}$	Squared sum of the residual
$\emptyset_i$	Mode-shape vector under i^{th} mode

$\emptyset_{mi}$	Measured mode-shape vector under i^{th} mode
$\widetilde{\emptyset_{mi}}$	Estimated mode-shape vector under i^{th} mode corresponded to measured nodes
$\emptyset_{Ki}^{*}$	Modified modal shapes for the part of stiffness and i^{th} mode
$\emptyset_{Mi}^{*}$	Modified modal shapes for the part of mass and i^{th} mode
λ_i	Theoretical circular frequency under i^{th} mode
$\widetilde{\lambda_i}$	Measured frequencies, $\tilde{\lambda}$
$\Delta\lambda_i$	Differences between the measured, $\widetilde{\lambda_i}$, and the estimated
τ	Arbitrary real values that represent the coefficients of all possible linear combinations
$\tilde{\delta}$	Hypothetical measurement
δ	Theoretical values (frequencies/mode shape)
$\mathcal{S}$	A random number following a normal distribution
γ	Error-index
x	Response variable
S	Set of sample indices before splitting
S_t	Set of sample indices for which the split test is true
S_f	Set of sample indices for which the split test is false
$\tilde{\theta}$	Estimated parameters
$[\emptyset]_{np\times q}$	A matrix containing the eigenvector
np	Total number of measurement point
q	Number of mode shapes of interest that are used for the analysis
E_d	Effective independence distribution vector of the candidate sensor set
$N(u,\delta)$	A normal distribution, u is the mean, δ is standard deviation
ρ	Density

Appendix 2. Code of decision tree drawn

```
function DecisionTress_v1
%decision tress serves for both, (a) classification (fit) and (b) prediction
(regression)
clc
close all
clear


%% Generate data
var_lab={'Layout','M_Set','L_span','W'}; %%%%%%%
lay={'pin-pin','pin-fix','fix-pin','fix-fix'}; %%%%%%%
mset={'A','B','C'};
span=[50, 55, 60]; %(m)
weigF=0.5:0.1:0.9;
categ=[1,2]; %categorical variables

% Load data
load('data.mat','data')


%% Fittig Decision tree
DT_fit(data,var_lab,categ,16)

end

%%%%%%%%%%%%%%%%%%%%%%%%%%%%%%%%%%%%%%%%%%%%%%%%%%%%%%%%%%%%%%%%%%%%%%%%%%%%%%%

function DT_fit(data,var_lab,categ,nsplits)
%% Create regression tree (binary type)
%categ is a vector indicating the position of the categoric variables

tree = fitrtree(data(:,1:end-1),data(:,end)/2,...
    'PredictorNames',var_lab,...
    'CategoricalPredictors',categ,... %indicate which are categorical
    'MaxNumSplits',nsplits) % limit the number of branches
Default=10.
view(tree) % text description
view(tree,'Mode','graph')
tr=view(t)
inspect(tr)
allHandles=findall(tr,'Type','text')
set(allHandles,'FontSize',16)
end
```

Appendix 3. Publication

Journal of Sound and Vibration 479 (2020) 115368

Contents lists available at ScienceDirect

Journal of Sound and Vibration

journal homepage: www.elsevier.com/locate/jsvi

Constrained observability techniques for structural system identification using modal analysis

T. Peng [a], M. Nogal [b], J.R. Casas [a], J.A. Lozano-Galant [c], J. Turmo [a, *]

[a] Department of Civil and Environmental Engineering, Universitat Politècnica de Catalunya, Barcelona, 08034, Spain
[b] Dept. of Materials, Mechanics, Management & Design, Faculty of Civil Engineering and Geosciences, Delft University of Technology, Netherlands
[c] Department of Civil Engineering, University of Castilla–La Mancha, Ciudad Real, 13071, Spain

ARTICLE INFO

Article history:
Received 12 March 2019
Received in revised form 26 March 2020
Accepted 2 April 2020
Available online 16 April 2020
Handling Editor: W. Zhu

Keywords:
Structural system identification
Inverse analysis
Constrained observability method
Structural dynamics

ABSTRACT

The characteristics of civil structures inevitably suffer a certain level of damage during its lifetime and cheap, non-destructive and reliable methods to assess their correct performance are of high importance. Structural System Identification (SSI) using measured response is the way to fine why performance is not correct and identify where the problems can be found. Different methods of SSI exist, both using static and vibration experimental data. However, using these methods is not always possible to decide if available measurements are sufficient to uniquely obtain the unknown. A (SSI) method that uses constrained observability method (COM) has already been developed based on the information provided by the monitoring of static non-destructive tests - using deflections and rotations under a known loading case. The method assures that all observable variables can be obtained with the available measured data. In the present paper, the problem of determining the actual characteristics of the members of a structure such as axial stiffness, flexural stiffness and mass using vibration data is analyzed. Subsets of natural frequencies and/or modal shapes are used. To give a better understanding of the proposed method and to demonstrate its potential applicability, several examples of growing complexity are analyzed, and the results show how constrained observability techniques might be efficiently used for the dynamic identification of structural systems using dynamic data. These lead to significant conclusions regarding the functioning of an SSI method based on dynamic behavior.

1. Introduction

The up-dated knowledge of the integrity of in-service structures through its lifetime is a very important objective for owners, end-users and both, construction and maintenance teams, to whom this information might help in decision making [1–3].

Simplified Finite Element Models (FEMs) are often used to simulate the response of civil structures [4]. When this structural response is modeled through computer simulations, mechanical and geometrical properties of the structural

* Corresponding author.
E-mail addresses: tian.peng@upc.edu (T. Peng), M.Nogal@tudelft.nl (M. Nogal), joan.ramon.casas@upc.edu (J.R. Casas), JoseAntonio.Lozano@uclm.es (J.A. Lozano-Galant), jose.turmo@upc.edu (J. Turmo).